1-1-2010

Detection Statistics Of Multiple-Pulse Optical Signals Through Atmospheric Turbulence

Jacob C. Brandenburg
Wayne State University

DETECTION STATISTICS OF MULTIPLE-PULSE OPTICAL SIGNALS THROUGH ATMOSPHERIC TURBULENCE

by

JACOB C. BRANDENBURG

DISSERTATION

Submitted to the Graduate School

of Wayne State University,

Detroit, Michigan

in partial fulfillment of the requirements

for the degree of

DOCTOR OF PHILOSOPHY

2010

MAJOR: ELECTRICAL ENGINEERING

Approved by:

_____

Advisor Date

_____

_____

_____

Acknowledgments

I would like to thank my parents who made it possible for me to begin my education in electrical engineering and for the love and support that they provided along the way. Similarly, I would like to thank my girlfriend who provided me with love and support as I pursued my Ph.D. She gave me much needed emotional support when times were tough, especially before my first conference presentation.

I also thank the professors who served on my committee: Professors Basu, Jiang, Liu and Schreiber. Professor Schreiber provided me with instruction and discussion in probability theory that was useful for my dissertation work. And Professor Liu, as my advisor from our first meeting at OU till now, taught me many important skills that I will use throughout my career.

Table of Contents

Acknowledgments ii

List of Tables v

List of Figures vi

Chapter 1. Introduction 1

Chapter 2. Detection Statistics for Optical Signal Through Weak Turbulence With Chernoff Bound 4

2.1. Introduction 4

2.2. System Model 6

2.3. Chernoff Bound on Lognormal Sum Distribution 11

2.4. Approximation of the Lognormal Sum Distribution 15

2.5. Calculation of Lognormal Sum Distribution using Lognormal characteristic function 18

2.6. Probability of Miss 21

2.7. Conclusions 26

Chapter 3. Detection Statistics for Optical Signal Through Weak Turbulence Using p-i-n Photodiode 27

3.1. Introduction 27

3.2. System Model 30

3.3. Photoelectron Count Statistics 33

3.4. Probabilities of Miss and False Alarm 39

3.5. Determination of Signal Length and Detection Threshold 41

3.6. Conclusions 47

Chapter 4. Detection Statistics for Optical Signal Through Weak Turbulence Using Avalanche Photodiode 50

4.1. Introduction 50
4.2. System Model 52
4.3. Probabilities of Miss and False Alarm 58
4.4. Determination of Signal Length and Detection Threshold 63
4.5. Conclusions 65
Chapter 5. Detection Statistics for Optical Signal Through Strong Turbulence 68
5.1. Introduction 68
5.2. System Model 69
5.3. Probabilities of Miss and False Alarm 73
5.4. Examples 78
5.5. Concluding Remarks 82
Chapter 6. Conclusions 88
References 89
Abstract 94
Autobiographical Statement 96

List of Tables

4.1 APD and Thermal Noise Parameters 64

5.1 OWC Link Parameters 78

List of Figures

2.1 Block diagram for optical communications system through the turbulent atmosphere. 6

2.2 Chernoff bound on the lognormal sum CDF computed using the 2nd and 3rd order Taylor approximation of e^x ($L = 108$). The dashed lines are the bounds computed with the 2nd order approximation and the solid lines are the bounds computed with the 3rd order approximation. 13

2.3 Graph of Eq. (2-29) for four different values of the scintillation index. λ_0 is the parameter which minimizes the Chernoff bound at normalized threshold α_N. 14

2.4 Fenton's approximation of the lognormal sum CDF ($\mu = 0; L = 108$) 18

2.5 Probability of miss calculated using (2-43) for three different values of the scintillation index, SNR = 10 dB and $L = 108$. 19

2.6 CDF of sum of 108 i.i.d. lognormal rv's for $\sigma \in \{0.05, 0.2, 0.4, 0.6, 0.8\}$. The solid lines are calculations and the points are simulations. . 22

2.7 Probability of miss for $L = 108$. As the SNR decreases, the effect of scintillation is less prominent on the probability of miss. The solid lines are calculations and the points are simulations. . . . 24

2.8 Probability of miss for $L = 32$. The solid lines are calculations and the points are simulations. For $\sigma = 0.6$ and 0.8, the lines are dashed to indicate that the calculation could not be done by numerical integration using Barakat's formula for the lognormal characteristic function. 25

3.1 Block diagram for optical communications system through the turbulent atmosphere. 30

3.2 Probability mass function for Poisson distribution given by (3-18), approximate probability mass function for conditional Poisson distribution given by (3-26) and normal approximation for conditional Poisson distribution given by (3-32), where $K_0 = 50$, $K_b = 10$ and $\sigma_\chi = 0.08$. 37

3.3 Probability of miss for quantum-limited detection, where $K_0 = 4$ and $L' = 32$. 42

3.4 Probability of miss for $L' = 32$, $\sigma_\chi \in \{0.0, 0.04, 0.08, 0.12, 0.16, 0.20\}$, $R_b = 2.4$ Gb/s, $R_L = 50\ \Omega$, $T = 295$ K, $K_0 = 5800$ and $K_b = 10$. The lines with circles, squares and triangles are simulations and lines without are calculated using (3-38). 44

3.5 System performance for $L' = 32$, $\sigma_\chi \in \{0.0, 0.04, 0.08, 0.12, 0.16, 0.20\}$, $R_b = 2.4$ Gb/s, $R_L = 50\ \Omega$, $T = 295$ K, $K_0 = 3500$ and $K_b = 10$. The lines with circles, squares and triangles are simulations and lines without are calculated using (3-38). 45

3.6 System performance for $L' = 32$, $\sigma_\chi \in \{0.0, 0.04, 0.08, 0.12, 0.16, 0.20\}$, $R_b = 2.4$ Gb/s, $R_L = 50\ \Omega$, $T = 295$ K, $K_0 = 5800$ and $K_b = 10$. The lines with circles, squares and triangles are simulations and lines without are calculated using (3-38). 46

3.7 System performance at the optimum threshold setting v_T^o assuming the log-amplitude signal fluctuation $\sigma_\chi = 0.20$, data rate $R_b = 2.4$ Gb/s, load resistance $R_L = 50\ \Omega$, receiver temperature $T = 295$ K and mean background noise count $K_b = 10$. 47

3.8 Optimum signal length L^o for different detection probabilities assuming the log-amplitude signal fluctuation $\sigma_\chi = 0.20$, data rate $R_b = 2.4$ Gb/s, load resistance $R_L = 50\ \Omega$, receiver temperature $T = 295$ K and mean background noise count $K_b = 10$. 48

4.1 Block diagram for optical communications system through the turbulent atmosphere. 53

4.2 Quantum limited probability of miss calculated using the Webb approximation (Eq. (4-34)) and the Gaussian approximation (Eq. (4-35)) for (4-12). The simulation results, in which the MC distribution was used in (4-12), are also plotted. The parameters used were mean signal count $K_0 = 10$ and 100 and signal length $L' = 8$. 65

4.3 Probability of miss in atmospheric turbulence. The lines with circles, squares and triangles were found by simulation using the MC distribution for the total electron count given by (4-13). The bare lines were calculated using numerical integration using the Webb distribution. The parameters used were $L' = 8$, $\sigma_\chi \in \{0.08, 0.16, 0.24, 0.32, 0.40\}$, $K_b = 2$ and $K_0 = 100$. 66

4.4 Probabilities of miss and false alarm for signal lengths $L' \in \{8, 16, 32, 64\}$ and log-amplitude signal standard deviation $\sigma_\chi = 0.40$. The parameters used were $K_b = 2$ and $K_0 = 100$. 67

5.1 Probability of miss using using p-i-n photodiode in moderate atmospheric turbulence ($C_n^2 = 10^{-15}$). The optical transmit power

is constant at $P_t = 1$ mW and the range of path lengths is 1 to 6 km. 80

5.2 Probability of miss using using p-i-n photodiode in strong atmospheric turbulence ($C_n^2 = 10^{-13}$). The optical transmit power is constant at $P_t = 1$ mW and the range of path lengths is 1 to 5 km. . . . 81

5.3 Probability of miss using using APD in moderate atmospheric turbulence ($C_n^2 = 10^{-15}$). The optical transmit power is constant at $P_t = 1$ mW and the range of path lengths is 1 to 8 km. . . . 82

5.4 Probability of miss using using APD in strong atmospheric turbulence ($C_n^2 = 10^{-13}$). The optical transmit power is constant at $P_t = 1$ mW and the range of path lengths is 0.5 to 3 km. . . 83

5.5 Probability of miss using using p-i-n for a constant path length $L_p = 2.5$ km and varying turbulence strength. The optical transmit power is constant at $P_t = 1$ mW. 84

5.6 Probability of miss using using APD for a constant path length $L_p = 2$ km and varying turbulence strength. The optical transmit power is constant at $P_t = 1$ mW. 85

5.7 Probability of miss using using p-i-n for a constant path length $L_p = 2.5$ km, constant turbulence strength $C_n^2 = 10^{-13}$ and varying signal length. The optical transmit power is constant at $P_t = 1$ mW. In this case, $\sigma_R^2 = 21.53, \beta = 1.04, \alpha = 1.51$ and $\sigma_I^2 = 2.26$. 86

5.8 Probability of miss using using APD for a constant path length $L_p = 2.5$ km, constant turbulence strength $C_n^2 = 10^{-13}$ and varying signal length. The optical transmit power is constant at $P_t = 1$ mW. In this case, $\sigma_R^2 = 21.53, \beta = 1.04, \alpha = 1.51$ and $\sigma_I^2 = 2.26$. 87

Chapter 1

Introduction

Communications through the atmosphere using an optical signal is emerging as a viable solution for many applications. Compared to radio frequency (RF) communications, optical communications through the atmosphere offer the potential of more security with higher directivity and lower cost in unlicensed frequency bands. Furthermore, optical wireless communications (OWC) links are quicker and cheaper to establish than fiber links in many situations such as urban environments. Some of the other applications include ground-to-satellite links which the Jet Propulsion Laboratory has been doing for years, air-to-air links which are being investigated for communications between unmanned aerial vehicle swarms [**1**] and high data rate ground-to-ground links such as the one demonstrated in [**2**] for a path length greater than 4.4 km. Although OWC has important potential advantages, it also has difficult obstacles, not present in RF, to overcome.

In addition to inclement weather conditions such as rain and snow, which inhibit reliable optical wireless communications, clear air atmospheric turbulence also detrimentally effects an optical wireless link. Clear air atmospheric turbulence results from micro-fluctuations in the air temperature and pressure, which lead to variations in the optical index of refraction. An electromagnetic wave propagating horizontally through this atmospheric turbulence will acquire a distorted wavefront because each part of the wavefront takes a different optical path. When this distorted wavefront is collected by the optical receiver, the received intensity will have temporal variations, which are called scintillation, the same phenomenon as starlight twinkle. In order to study the effect of scintillation upon the performance of a optical communications system operating through the atmosphere, a probabilistic model is required to describe strength of the received intensity fluctuations. Throughout the literature

dealing with atmospheric turbulence, many different models have been proposed. In this work, three models are chosen: the lognormal distribution, valid for weak turbulence, the gamma-gamma distribution, valid for a range of turbulence strengths and the exponential distribution, valid for the saturation regime of signal scintillation.

In a communication system, before the information in the signal can be demodulated and decoded, the signal must be detected. When detecting a signal, two errors can occur: 1) a miss, in which the signal was present but the detector determined that it was not and 2) a false alarm, in which the signal was not present but the detector determined that it was. In any signal detection scheme increasing the signal length will decrease the probabilities of miss and false alarm, at the cost of a more expensive signal detector. In addition to the signal length, the detection threshold setting is crucial in the signal detector design. If the threshold is too high the probability of miss is too high, and if it is too low the probability of false alarm is too high. Therefore, to determine the appropriate settings for signal length and detection threshold the probability of miss must be known. The majority of this work is devoted to determining how to derive or numerically calculate the probability of miss for an optical signal propagating through atmospheric turbulence. Single-pulse optical detection statistics in a weak turbulent atmosphere have been reported in [**3**, **4**] for lognormal statistics. Single-pulse statistics are sufficient for determining the demodulator performance in terms of the bit-error-rate (BER). For signal detection and synchronization, however, a multiple-pulse signal is required and, therefore, the multiple-pulse detection statistics must be known in order to design the signal detector.

The remainder of this work is split into four chapters. In each chapter, the goal is the same, i.e., for an optical communications system transmitting through atmospheric turbulence, calculate the probabilities of miss and false alarm and find the signal length and detection threshold to maintain the link above a predetermined

performance. What differentiates each chapter is the system and channel models employed and the mathematical methods utilized to calculate the detection statistics. In Chapter 2, the lognormal turbulence model is used and the photodiode output current is assumed constant. In Chapters 3 and 4, the lognormal turbulence model is also employed, however, the photoelectron count follows Poisson and Webb statistics, respectively, corresponding to the implementation of p-i-n and avalanche photodiodes in the receiver. Chapter 5 contains the detection statistics for a system operating in strong atmospheric turbulence modeled by the gamma-gamma distribution and reports results for both p-i-n and avalanche photodiodes. Finally, Chapter 6 summarizes and concludes the study.

Chapter 2

Detection Statistics for Optical Signal Through Weak Turbulence With Chernoff Bound

2.1. Introduction

Optical communications through the atmosphere is important to commercial and defense applications. Two of these applications are last-mile links [**5**] and mobile battlefield networks [**6**]. The advantages of optical communications through the atmosphere over radio communications include increased security and unlicensed, large bandwidth. Packet switching is widely employed in optical communications through the atmosphere access networks [**7**]. One of the challenges to optical communications through the atmosphere is overcoming the effect of turbulence on the signal as it propagates through the atmosphere. Atmospheric turbulence is caused by small fluctuations in temperature and pressure, which affects the propagating optical signal as random changes in the index of refraction [**8**, **9**]. At the receiver focal plane, this causes small fluctuations (scintillation) of the received optical intensity and polarization, which can degrade the performance of the communication system.

In packet-switched networks, the information is sent out in packets in which the first portion of each packet is a unique sequence of bits called the preamble, which is known to the receiver. The receiver determines that a packet is present when it detects the presence of the preamble. Once the receiver detects that a packet is present, it performs parameter estimation, synchronization and demodulation. The detection of this preamble in an atmospheric turbulence channel is a discrete signal

detection problem expressed by the hypothesis test

$$H_0 \quad : \quad r_k = n_k, \quad k = 1, 2, \ldots, L \tag{2-2}$$

versus

$$H_1 \quad : \quad r_k = A_k d_k + n_k, \quad k = 1, 2, \ldots, L, \tag{2-3}$$

where $\underline{r} = [r_1, r_2, \ldots, r_L]$ is the observation vector, $\{n_k\}$ are samples of an AWGN process representing the thermal noise of the receiver, $\underline{d} = [d_1, d_2, \ldots, d_L]$ is the sequence to be detected and $\{A_k\}$ are samples from the stochastic process determined by the turbulent atmospheric channel which controls the strength of the signal. When the signal is present, the observation is the signal degraded by the channel plus the AWGN, whereas only the AWGN is observed when the signal is absent. During the signal detection operation, one of following two events may occur to degrade the performance of the system: 1) miss detection or 2) false alarm. Miss detection is false rejection of H_1 and false alarm is the false rejection of H_0. The probability of a miss detection and the probability of a false alarm are important measures in the system design as they determine the signal length L in symbols to meet the system specifications for optical communications and LIDAR systems.

The rest of this chapter is organized as the following. In Section 2.2, the system model is described. In Section 2.3, a Chernoff bound is derived for the distribution of the sum of L lognormal random variables. In Section 2.4, an approximation for the lognormal sum is investigated. In Section 2.5, a series approximation to the characteristic function of a lognormal random variable is applied to the problem. In Section 2.6, the detection problem is studied with AWGN included. Conclusions are provided in Section 2.7.

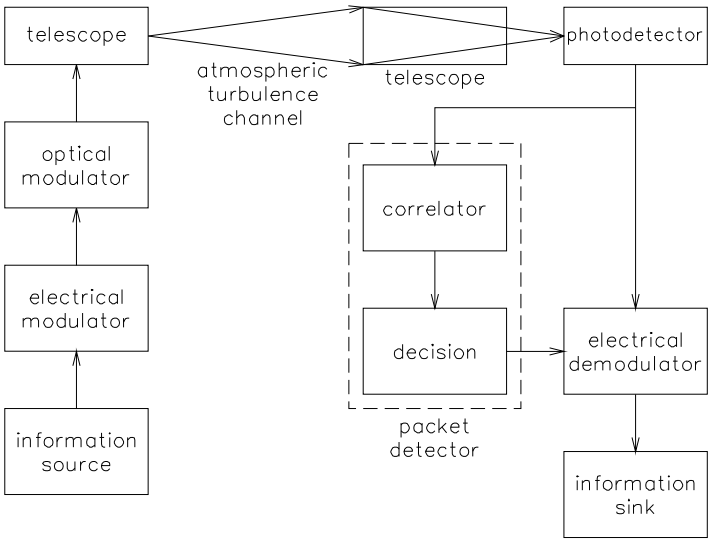

Figure 2.1: Block diagram for optical communications system through the turbulent atmosphere.

2.2. System Model

Suppose that a binary sequence $\{d_i\}_{i=1}^{L}$ of length L will be transmitted over a free-space optical channel. To accomplish this, a system is required in which a transmitter prepares the sequence for transmission over the channel and a receiver detects the signal when it arrives. Figure 2.1 illustrates the model for such a system. The transmitter is composed of an electrical modulator, an optical modulator and a transmitting telescope. In the electrical modulator an information sequence is impressed upon an electrical signal. This electrical signal is then used to modulate the intensity of an optical source. On-off keying (OOK) and subcarrier phase-shift keying (PSK) are two methods employed for optical intensity modulation in optical communications through the atmosphere [**8**]. After the signal propagates through the atmospheric channel, it passes through the receiver optics and enters the photodetector, which converts the optical signal intensity into an electrical signal. The electrical signal is then sent to the detector, in which it is determined whether the signal has arrived. When a signal is detected, the detector triggers the demodulator.

2.2.1. Received Signal. OOK is a binary modulation scheme in which the optical source is switched on to transmit bit "1" and turned off to transmit bit "0". The transmitted optical signal is the random process

$$s(u,t) = I_s \sum_{i=1}^{L} d_i g(t - iT_s), \tag{2-4}$$

where I_s is the average intensity of the field, $\{d_i\}_{i=1}^{L}$ (with $d_i \in \{0, +1\}$) is a unique sequence, $g(t)$ is the shaping pulse and T_s is the symbol time [**8**]. At the photodetector, the received optical intensity is

$$I(u,t) = A(u,t)P \sum_{i=1}^{L} d_i g(t - iT_s), \tag{2-5}$$

where $A(u,t)$ is a lognormal random process representing scintillation and P is the maximum received intensity. In the receiver, the photodetector converts the received optical intensity into an electrical signal given by

$$r(u,t) = A(u,t)K \sum_{i=1}^{L} d_i g(t - iT_s) + n(u,t), \tag{2-6}$$

where K is a constant determined by the received intensity and the photoelectric conversion efficiency of the detector and $n(u,t)$ is an AWGN process. Without loss of generality, the constant K can be dropped. After $r(u,t)$ is sampled at time $t = iT_s$, each bit is given its corresponding random variable:

$$r_i(u) = \begin{cases} n_i(u), & \text{(bit "0")} \\ A_i(u) + n_i(u), & \text{(bit "1").} \end{cases} \tag{2-7}$$

Thus, when the full signal for detection is in the correlator, the bit "0" random variables drop out because they are multiplied by 0 and the correlator output is

$$c(u) = \sum_{i=1}^{W} A_i(u) + n_i(u), \tag{2-8}$$

where $W < L$ is the weight of the signal sequence.

In an optical communications system employing the subcarrier binary PSK (BPSK) modulation scheme, the information sequence modulates the phase of a sinusoidal electrical signal, which then modulates the output of the optical source. The transmitted optical signal is the random process

$$s(u,t) = \frac{I_s}{2}\left[1 + \sum_{i=1}^{L} d_i g(t - iT_s)\cos(\omega_c t)\right], \tag{2-9}$$

where ω_c is the intermediate angular frequency and $\{d_i\}_{i=1}^{L}$ (where $d_i \in \{-1, +1\}$) is a unique sequence. After transmission through atmosphere and conversion in the photodetector the received electrical signal is

$$r(u,t) = A(u,t)\left[1 + \sum_{i=1}^{L} d_i g(t - iT_s)\cos(\omega_c t)\right] + n(u,t). \tag{2-10}$$

The DC term in (2-10) can be filtered out. After down-conversion and sampling, each bit is given by its corresponding random variable:

$$r_i(u) = \begin{cases} -A_i(u) + n_i(u), & \text{(bit "0")} \\ A_i(u) + n_i(u), & \text{(bit "1").} \end{cases} \tag{2-11}$$

After $\{r_i(u)\}_{i=1}^{L}$ is correlated with the sequence $\{d_i\}_{i=1}^{L}$, the output of the correlator is given by

$$c(u) = \sum_{i=1}^{L} A_i(u) + n_i(u). \tag{2-12}$$

The design of the sequence is important in the total system design. For information on design of $(0, 1)$ sequences, which are the codewords of optical orthogonal codes, see [**10**] and for $(-1, +1)$ sequences, see [**11**].

2.2.2. Atmospheric Turbulence. In (2-3), the stochastic process A is the representation of scintillation of the signal, which is modeled as a lognormal random

process given by

$$A(u,t) = e^{x(u,t)}, \tag{2-13}$$

where $x(u,t)$ is a stationary Gaussian random process with mean μ and variance σ^2. The probability density function (PDF) of A is

$$f(x) = \frac{1}{\sqrt{2\pi}\sigma x} \exp\left[-\frac{(\ln x + \mu)^2}{2\sigma^2}\right], \tag{2-14}$$

where the variance σ^2 is a measure of the strength of the scintillation. In this chapter, μ is set to 0. The value of σ is often referred to as the scintillation index. Many efforts have been made to measure the strength of the intensity scintillation [**12**, **13**]. In [**13**], scintillation measurements were performed on a typical day and σ never increased beyond about 0.75. It has been measured that the scintillation strength saturates after about 700 m of horizontal propagation near the ground [**14**]. In this study, the probability of a miss detection will be derived for the range of scintillation index appropriate for near-earth horizontal laser propagation.

2.2.3. Signal Shot Noise. The current in a p-i-n photodiode induced by an incident deterministic optical field intensity is a shot noise process in which the number of photo-generated electrons is Poisson distributed [**8**]. Thus, randomness in the received signal develops not only as a result of atmospheric turbulence, but also from signal shot noise inherent in the optical detection process. This signal shot noise is directly proportional to the signal power level [**8**, pp. 102-107].

When the signal power is low (i.e., the number of incident signal photons during a symbol interval is small), the discrete Poisson distribution should be used to model the number of photoelectrons. During deep signal fades, however, when the atmospheric turbulence is worst, the effect of thermal noise on detection performance is more significant than the effect of signal shot noise. Therefore, the signal shot noise is

negligible in these instances, which are those that ultimately limit the performance of the system.

On the other hand, when the signal power is high, a Gaussian distribution approximation can be substituted for the Poisson distribution to model the number photoelectrons in a p-i-n photodiode [**8**, p. 107]. Hence, in the case of zero turbulence, the Gaussian noise process models the effects of both thermal noise and signal shot noise. This situation models the best possible detection performance at a certain SNR.

2.2.4. Signal Detection. The signal detector declares the arrival of a signal if

$$c(u) \geq \alpha, \tag{2-15}$$

where α is a predetermined threshold. This means studying the sum of L lognormal and L Gaussian random variables, where L is the weight of the sequence in OOK systems or the signal length in subcarrier BPSK systems. In this study, it is assumed that the correlation time of the atmospheric turbulence is less than the symbol time T_s; therefore, the lognormal random variables are independent. The determination of α is critical in system design [**15**]. If the detection sequence is present but $c(u) < \alpha$, the signal was missed. If the detection sequence was not sent but $c(u) \geq \alpha$, a false alarm has occured.

Finding the probability of miss means finding the cumulative distribution function (CDF) of $c(u)$. If the SNR is taken to be ∞, $c(u)$ is the sum of L i.i.d. lognormal random variables. This corresponds to high SNR systems and allows the study of the effect of the atmospheric turbulence alone. In the next few sections, different methods to find the CDF of the sum of multiple i.i.d. lognormal random variables will be explored.

2.3. Chernoff Bound on Lognormal Sum Distribution

In this section, a Chernoff bound is derived to find a bound on the distribution of a sum of L lognormal random variables. Suppose that $\left\{e^{X_i}\right\}_{i=1}^{L}$ is a set of lognormal random variables, each with mean $m \neq 0$. The Chernoff bound for the sum of these random variables is [**16**]

$$\left[\mathbf{E}\left\{e^{\lambda_0(e^X-(m+\epsilon))}\right\}\right]^L \geq \begin{cases} \Pr\left\{\frac{1}{L}\sum_{i=1}^{L} e^{X_i} \geq m+\epsilon\right\}, & \epsilon > 0 \\ \\ \Pr\left\{\frac{1}{L}\sum_{i=1}^{L} e^{X_i} \leq m+\epsilon\right\}, & \epsilon < 0 \end{cases} \tag{2-16}$$

where λ_0 is defined by

$$\frac{\mathbf{E}\left\{e^X e^{\lambda_0 e^X}\right\}}{\mathbf{E}\left\{e^{\lambda_0 e^X}\right\}} = m + \epsilon, \tag{2-17}$$

and $\mathbf{E}$ denotes the expectation operator.

The fact that

$$\mathbf{E}\left\{e^{te^X}\right\} = \infty, \forall t > 0 \tag{2-18}$$

makes it difficult to find λ_0 in (2-17). Therefore, an approximation for e^X will be made using the Taylor series

$$e^x = \sum_{n=0}^{\infty} \frac{x^n}{n!}. \tag{2-19}$$

Using the second order approximation, the denominator in (2-17) is

$$\mathbf{E}\left\{e^{\lambda_0(1+x)}\right\} = e^{\lambda_0} e^{\frac{\sigma^2\lambda_0^2}{2}}, \tag{2-20}$$

where it is assumed that the Gaussian mean $\mu = 0$. The numerator in (2-17) is

$$\mathbf{E}\left\{(1+x)e^{\lambda_0(1+x)}\right\} = e^{\lambda_0}\left(e^{\frac{\sigma^2\lambda_0^2}{2}} + \lambda_0\sigma^2 e^{\frac{\sigma^2\lambda_0^2}{2}}\right). \tag{2-21}$$

Thus,

$$m + \epsilon = 1 + \lambda_0\sigma^2. \tag{2-22}$$

Solving for λ_0 and noting that the mean of a lognormal random variable $m = e^{\mu+\sigma^2/2}$ gives

$$\lambda_0 = \frac{1}{\sigma^2}\left(e^{\sigma^2/2} - 1 + \epsilon\right). \tag{2-23}$$

Substituting the second order Taylor approximation, the expectation in (2-16) is

$$\mathbf{E}\left\{e^{\lambda_0(1+x-(m+\epsilon))}\right\} = \exp\left\{\frac{-1}{2\sigma^2}\left(e^{\sigma^2/2} - 1 + \epsilon\right)^2\right\}. \tag{2-24}$$

Taking the bottom portion of (2-16) ($\epsilon < 0$), the CDF for the sum is bounded as follows

$$\Pr\left\{\sum_{i=1}^{L} e^{X_i} \le L\left(e^{\sigma^2/2} + \epsilon\right)\right\} \le \left[\exp\left\{\frac{-1}{2\sigma^2}\left(e^{\sigma^2/2} - 1 + \epsilon\right)^2\right\}\right]^L. \tag{2-25}$$

Figure 2.2 shows the bound on the CDF computed with the Chernoff bound of (2-25) for four different values of σ compared with simulations. First, note that the Chernoff bounds do not intersect while the simulations do. These results are encouraging enough (especially for $\sigma = 0.2$) to proceed to investigate what happens to the bound if the next term in the Taylor approximation is included.

The following three integrals are used in computing the Chernoff bound using the third order Taylor approximation of e^x:

$$I_1 = \mathbf{E}\left\{e^{\lambda_0(x+x^2/2)}\right\} = \frac{1}{\sqrt{1-\sigma^2\lambda_0}}\exp\left\{\frac{\sigma^2\lambda_0^2}{2\left(1-\sigma^2\lambda_0\right)}\right\}, \tag{2-26}$$

$$I_2 = \mathbf{E}\left\{xe^{\lambda_0(x+x^2/2)}\right\} = \frac{\sigma^2\lambda_0}{\left(1-\sigma^2\lambda_0\right)^2}\exp\left\{\frac{\sigma^2\lambda_0^2}{2\left(1-\sigma^2\lambda_0\right)}\right\} \tag{2-27}$$

and

$$\begin{aligned} I_3 &= \mathbf{E}\left\{x^2e^{\lambda_0(x+x^2/2)}\right\} \\ &= \frac{\sigma^2}{\left(1-\sigma^2\lambda_0\right)^{3/2}}\left(1 + \frac{\sigma^2\lambda_0^2}{1-\sigma^2\lambda_0}\right)\exp\left\{\frac{\sigma^2\lambda_0^2}{2\left(1-\sigma^2\lambda_0\right)}\right\}. \end{aligned} \tag{2-28}$$

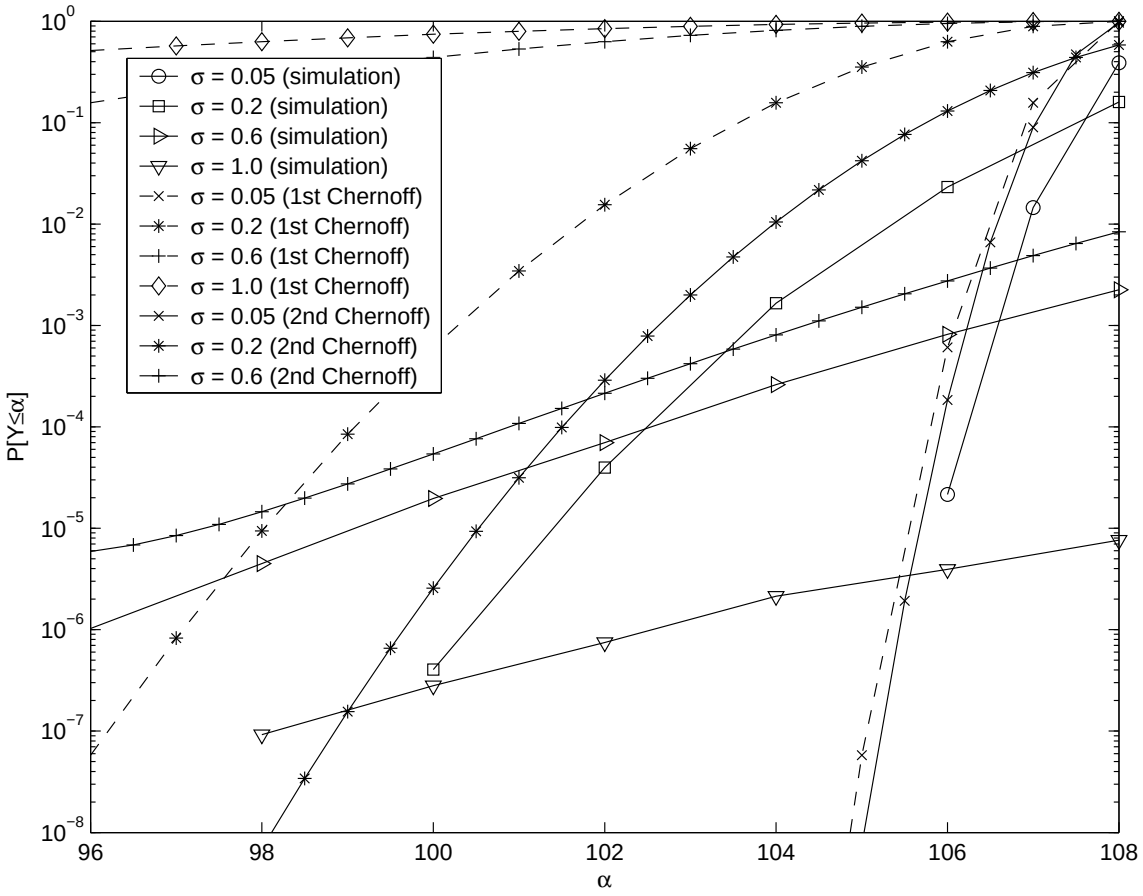

Figure 2.2: Chernoff bound on the lognormal sum CDF computed using the 2nd and 3rd order Taylor approximation of e^x ($L = 108$). The dashed lines are the bounds computed with the 2nd order approximation and the solid lines are the bounds computed with the 3rd order approximation.

Now, the equation for λ_0 is

$$\begin{aligned} m + \epsilon &= \frac{I_1 + I_2 + \frac{1}{2} I_3}{I_1} \\ &= 1 + \frac{\sigma^2 \lambda_0}{\left(1 - \sigma^2 \lambda_0\right)^{3/2}} + \frac{\sigma^2}{2\left(1 - \sigma^2 \lambda_0\right)} \left(1 + \frac{\sigma^2 \lambda_0^2}{1 - \sigma^2 \lambda_0}\right). \end{aligned} \tag{2-29}$$

Equation (2-29) is plotted in Fig. 2.3. The graph shows that many of the values of the normalized threshold $\alpha_N = \alpha / L$ that are important in finding the bound are absent from the range of $\alpha_N(\lambda_0)$.

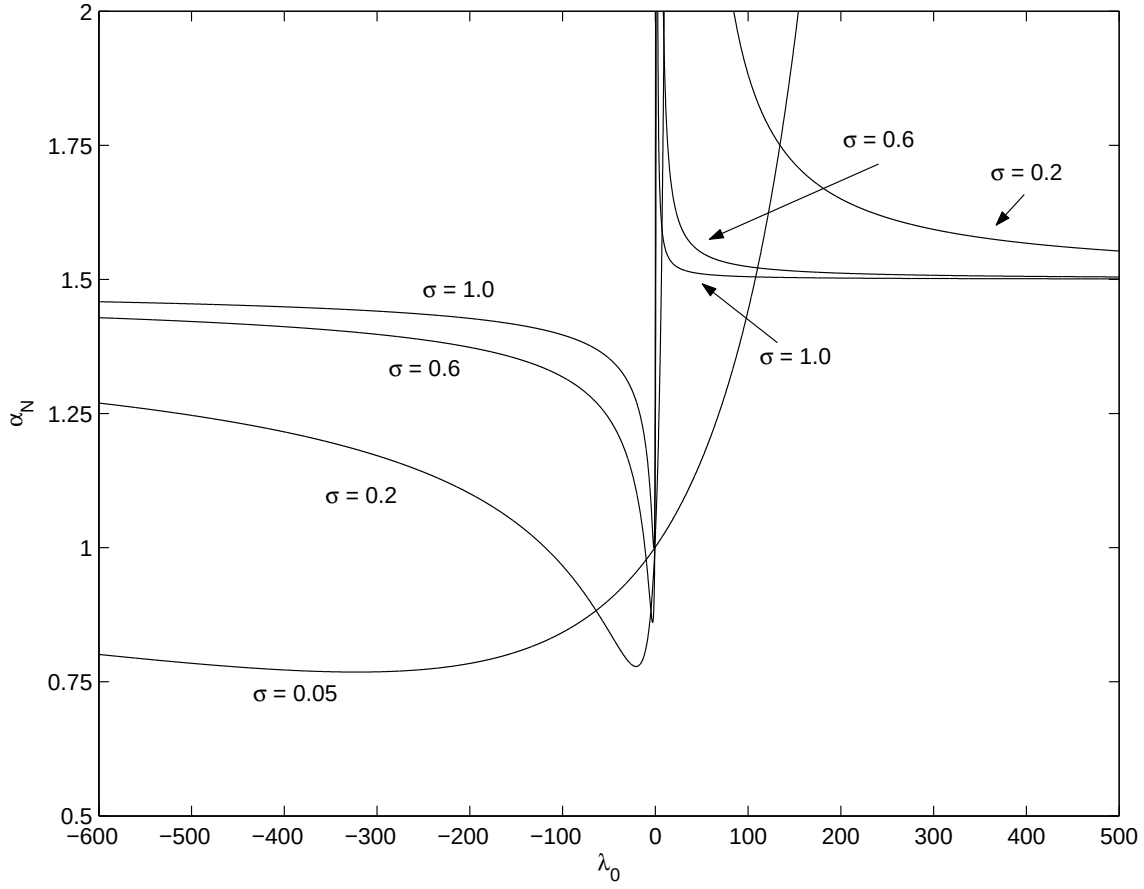

Figure 2.3: Graph of Eq. (2-29) for four different values of the scintillation index. λ_0 is the parameter which minimizes the Chernoff bound at normalized threshold α_N.

To find the bound for a certain threshold, first λ_0 is found numerically in (2-29). Then, λ_0 is used in

$$\begin{aligned} \Pr\left\{\sum_{i=1}^{L} e^{X_i} \leq \alpha\right\} &\leq \left[I_1 \exp\left\{1 - \frac{\alpha}{L}\right\}\right]^L \\ &= \left[\frac{1}{\sqrt{1-\sigma^2\lambda_0}} \exp\left\{\frac{\sigma^2\lambda_0^2}{2\left(1-\sigma^2\lambda_0\right)} + 1 - \frac{\alpha}{L}\right\}\right]^L. \end{aligned} \tag{2-30}$$

For those values of the threshold which λ_0 can be found the Chernoff bound computed using the third order approximation is tighter than the bound computed using the second order approximation. No Chernoff bound is present in Fig. 2.2 for

$\sigma = 1.0$ when the 3rd order approximation is used because no values of λ_0 exist when $\alpha_N < 1$ as shown in Fig. 2.3. The computation of the integrals in (2-26)-(2-28) was simple, but if the fourth term in the Taylor series for e^x was added these integrals become difficult to compute.

In this section, the Chernoff bound is derived for the sum of lognormal random variables in detection of optical signal through the atmosphere. The computation of the Chernoff bound is discussed. Using the third order Taylor approximation for e^x, one can have a good upper bound of the lognormal sum CDF for low to moderate scintillation.

2.4. Approximation of the Lognormal Sum Distribution

In order to approximate the distribution of the lognormal sum, one may guess that the central limit theorem may be invoked in order to approximate the sum as a Gaussian random variable. Unfortunately, the central limit theorem does not apply to the lognormal random variable because after many lognormals are summed together, the tail of the lognormal remains. This is known as the permanence of the lognormal distribution [**17**]. As a result of this and the fact that the lognormal distribution is important as a model for the attenuation due to shadowing in wireless mobile communications, many methods have been proposed to approximate the distribution of the sum of multiple lognormal random variables [**18**–**21**].

Of the proposed methods for approximating the lognormal sum distribution proposed in the literature, Fenton's moments matching method [**18**] is simple to implement and closely matches the CDF for values of the scintillation index and the range of the CDF which are relevant to the present detection problem. Fenton's approach begins by assuming that the distribution of the sum of lognormals is itself lognormal

as in

$$Y = \sum_{i=1}^{L} e^{X_i} \approx e^{Z}, \tag{2-31}$$

where Z is Gaussian. Now the first two moments of Y are calculated and used to find the first two moments of Z. This method is outlined below.

The raw moments the lognormal distribution are given by

$$\mathbf{E}\left\{\left(e^{X}\right)^{n}\right\} = e^{\mu n} e^{\frac{1}{2}\sigma^2 n^2}, \tag{2-32}$$

Hence, the mean of e^X is

$$\mathbf{E}\left\{e^{X}\right\} = e^{\mu} e^{\frac{1}{2}\sigma^2} \tag{2-33}$$

and the variance of e^X is

$$\mathbf{E}\left\{\left(e^{X} - \mathbf{E}\left\{e^{X}\right\}\right)^{2}\right\} = e^{2\mu} \cdot e^{\sigma^2}\left(e^{\sigma^2} - 1\right). \tag{2-34}$$

Since the lognormals in the sum are i.i.d. the mean and variance of the sum distribution are

$$m = \mathbf{E}\left\{\sum_{i=1}^{L} e^{X_i}\right\} = L e^{\mu} e^{\frac{1}{2}\sigma^2} \tag{2-35}$$

and

$$\lambda^2 = \mathbf{Var}\left\{\sum_{i=1}^{L} e^{X_i}\right\} = L e^{2\mu} \cdot e^{\sigma^2}\left(e^{\sigma^2} - 1\right), \tag{2-36}$$

respectively. To find the mean and variance of Z, Eq. (2-33) and Eq. (2-34) are solved for μ and σ^2. Then m and λ^2 are substituted for the mean and variance of e^X, respectively. One has

$$\mu_Z = \ln\left(L e^{\mu} e^{\frac{1}{2}\sigma^2}\right) - \frac{\sigma_Z^2}{2} \tag{2-37}$$

and

$$\sigma_Z^2 = \ln\left(\frac{e^{\sigma^2} - 1}{L} - 1\right). \tag{2-38}$$

The CDF of Y is given by

$$\begin{aligned}\Pr\left\{e^Z \leq \alpha\right\} &= \Pr\left\{Z \leq \ln\alpha\right\} \\ &= \frac{1}{2}\left[1 + \operatorname{erf}\left(\frac{\ln\alpha - \mu_Z}{\sqrt{2}\sigma_Z}\right)\right],\end{aligned} \tag{2-39}$$

where

$$\operatorname{erf}(x) = \frac{2}{\sqrt{\pi}}\int_0^x e^{-t^2}dt. \tag{2-40}$$

Figure 2.4 shows the CDF of Y plotted for $\mu = 0$ and four different values of the scintillation index σ. For $\sigma = 0.05$ and 0.2, the approximation matches up with simulation. But the curves for $\sigma = 0.6$ and 1.0 show that as σ increases, the accuracy of the approximation decreases.

In order to handle the AWGN process in detection and find the PDF of $c(u)$, the PDF of the lognormal sum $f_A(x)$ is convolved with the PDF of the Gaussian sum $f_n(x)$ as in

$$f_c(\alpha) = \int_{-\infty}^{\infty} f_A(x) f_n(\alpha - x)dx, \tag{2-41}$$

where μ_Z and σ_Z are plugged into (2-14) to find $f_A(x)$. The PDF of the Gaussian sum is given by

$$f_n(x) = \frac{1}{\sqrt{2\pi L}\sigma_g} e^{-x^2/\left(2L\sigma_g^2\right)}. \tag{2-42}$$

Integrating (2-41) will result in CDF of $c(u)$:

$$\Pr\left\{c(u) \leq \alpha\right\} = \int_{-\infty}^{\alpha} f_c(x)dx. \tag{2-43}$$

Using this approach, Fig. 2.5 shows the probability of miss for three different values of the scintillation index when the SNR = 10 dB and $L = 108$. This approach to calculating the probability of miss isn't accurate because the lognormal sum PDF calculated using the moments found with Fenton's moment matching method is not a good approximate of the actual lognormal sum PDF.

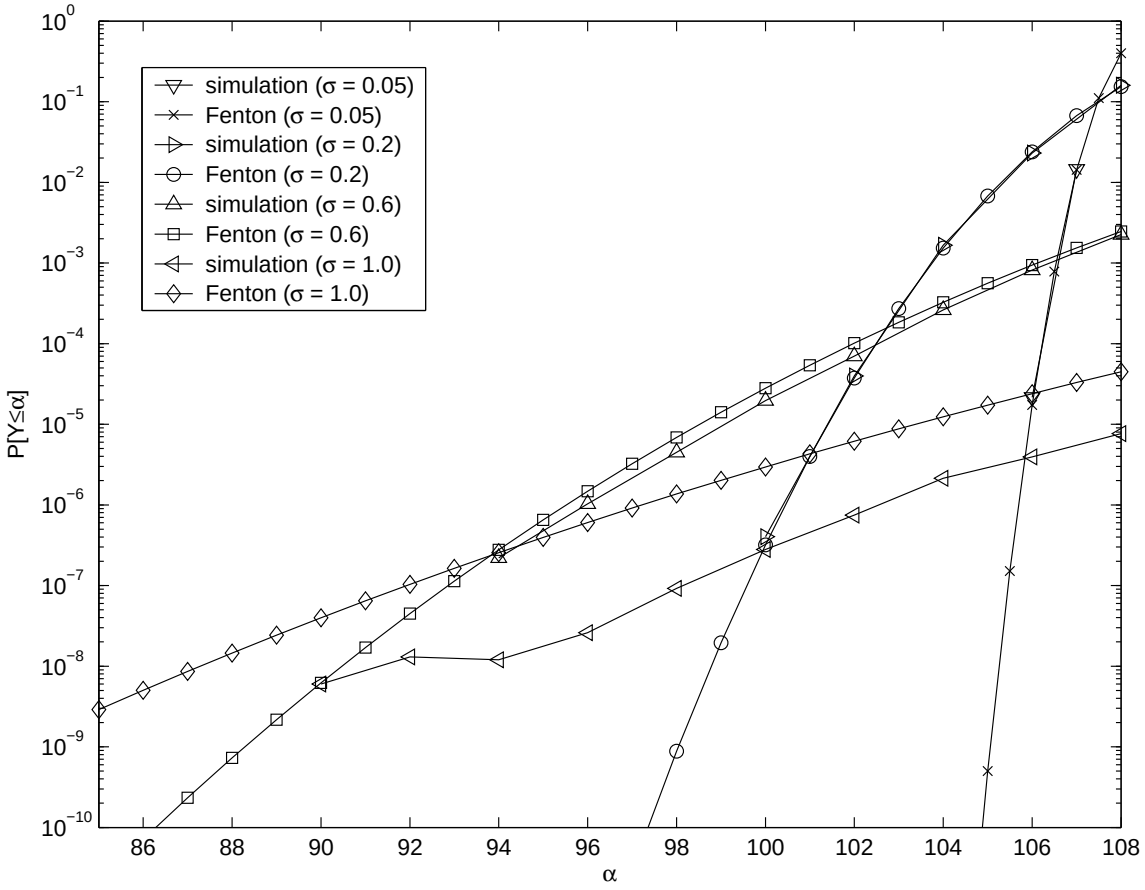

Figure 2.4: Fenton's approximation of the lognormal sum CDF ($\mu = 0; L = 108$)

In this section, it is found that the Fenton's approximation is useful when dealing with the atmospheric turbulence alone. However, the Fenton's approximation can not help when the AWGN process is included in the calculation of the probability of miss.

2.5. Calculation of Lognormal Sum Distribution using Lognormal characteristic function

One method that can be used to find the CDF of a sum of random variables involves using the characteristic functions of the random variables in the sum. The

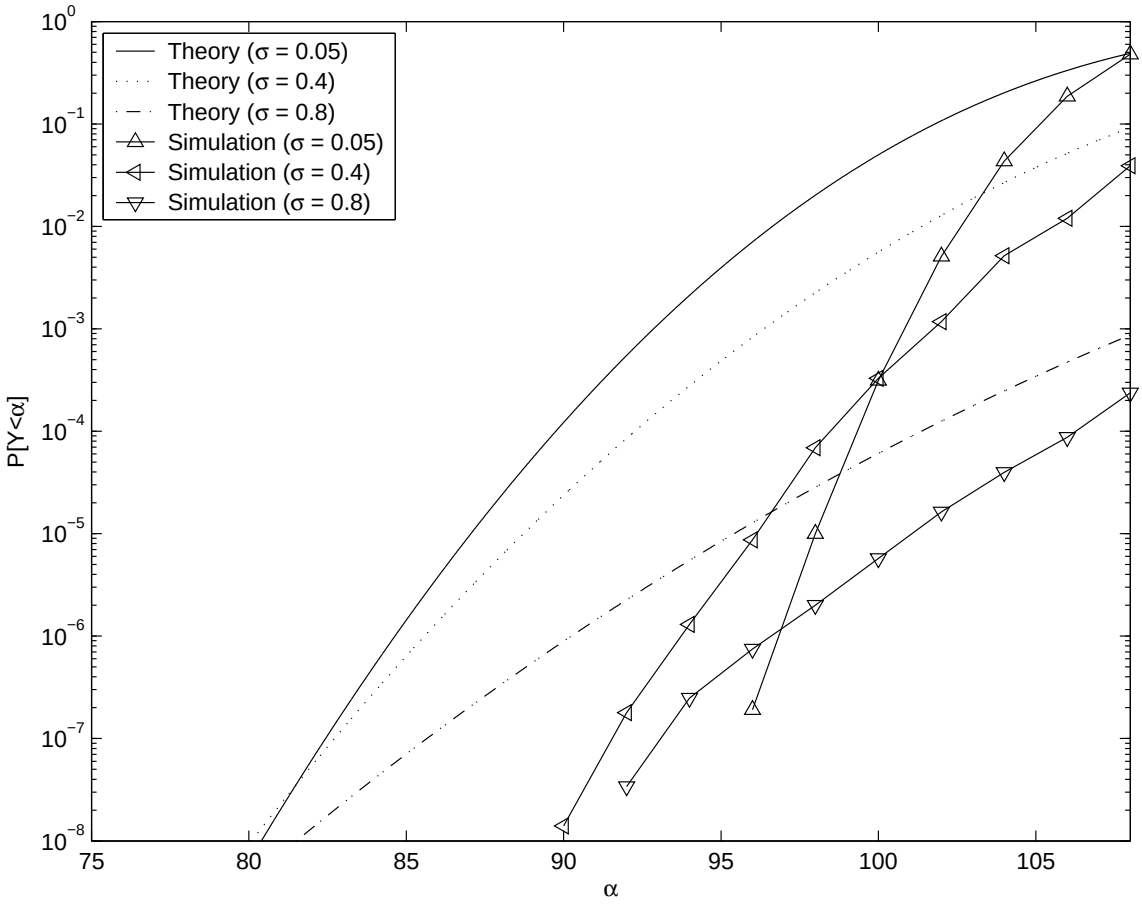

Figure 2.5: Probability of miss calculated using (2-43) for three different values of the scintillation index, SNR = 10 dB and $L = 108$.

characteristic function of a random variable X is defined as

$$\phi_x(\tau) = \int_{-\infty}^{\infty} f_x(x) e^{j\tau x} dx, \tag{2-44}$$

where $f_x(x)$ is the PDF of X. The characteristic function of the sum of multiple random variables is the product of the characteristic functions of the random variables in the sum; therefore,

$$\phi_y(\tau) = \prod_{k=1}^{L} \phi_{x_k}(\tau), \tag{2-45}$$

where $\phi_y(\tau)$ is the characteristic function of the lognormal sum and ϕ_{x_k} is the characteristic function of the kth lognormal random variable. The PDF of Y is the inverse Fourier transform of $\phi_y(\tau)$ given by

$$f_y(y) = \frac{1}{2\pi} \int_{-\infty}^{\infty} \phi_y(\tau) e^{-jy\tau} d\tau. \tag{2-46}$$

The CDF of Y can be found by integrating the PDF as in

$$F_y(y) = \int_{-\infty}^{y} f_y(u) du. \tag{2-47}$$

Thus, with knowledge of the characteristic function of a lognormal random variable, the CDF of a lognormal sum can be calculated.

In [**22**], the following series is given for the characteristic function of a lognormal random variable:

$$\phi_x(\tau) = e^{j\tau - \tau^2\sigma^2/2} \sum_{n=0}^{\infty} \frac{(j\sigma)^n}{n!} a_n(j\tau) h_n(\sigma\tau), \tag{2-48}$$

where a_n are Taylor series coefficients given by

$$a_n(j\tau) = \frac{d^n}{dz^n} \exp\left\{j\tau\left(e^z - z - 1\right)\right\}_{z=0} \tag{2-49}$$

and h_n are Hermite polynomials given by the recursive formula

$$\begin{aligned} h_0(z) &= 1, \\ h_1(z) &= z, \\ h_{n+1}(z) &= z h_n(z) - n h_{n-1}(z). \end{aligned} \tag{2-50}$$

The first twelve coefficients a_n and first six hermite polynomials h_n are given in [**22**] and can be obtained with the aid of a symbol-manipulating program such as Maple. This function converges quickly for $\sigma < 1$, which is the range of σ applicable to

atmospheric turbulence in optical communications. Although less terms may have sufficed, twelve terms were used for the sum in this study.

Computing the PDF will be difficult because of the oscillatory nature of $\phi(\tau)$. In practice, the integration limit T in

$$f_y(y) = \frac{1}{2\pi} \int_{-T}^{T} \phi_y(\tau) e^{jy\tau} d\tau. \tag{2-51}$$

will have to be set at a carefully selected finite value. If T is too small, too much of the integration will be shut out and if it is too large, the computation of the characteristic function in (2-48) near the limits may diverge due to numerical inaccuracies. The CDF of Y is found by integrating (2-51). A discussion on the best numerical integration technique for this integral is given in [**21**]. Figure 2.6 shows the CDF for four different values of σ. Comparison of the calculated CDF with simulations shows that this method produces accurate results.

2.6. Probability of Miss

Optical communications systems through the atmosphere are power-limited. When finding the probability of miss, the effect of the AWGN process inherent in the receiver electronics must be included. In this section, the probability of miss will be calculated for practical values of SNR in optical communications through the atmosphere.

Noting that (2-45) is valid even if the characteristic functions in the product are different, the AWGN can be included in the calculation of the probability of miss by including the Gaussian characteristic function. The characteristic function of $c(u)$ is, thus, given by

$$\phi_c(\tau) = \prod_{k=1}^{L} \phi_{x_k}(\tau) \phi_{g_k}(\tau), \tag{2-52}$$

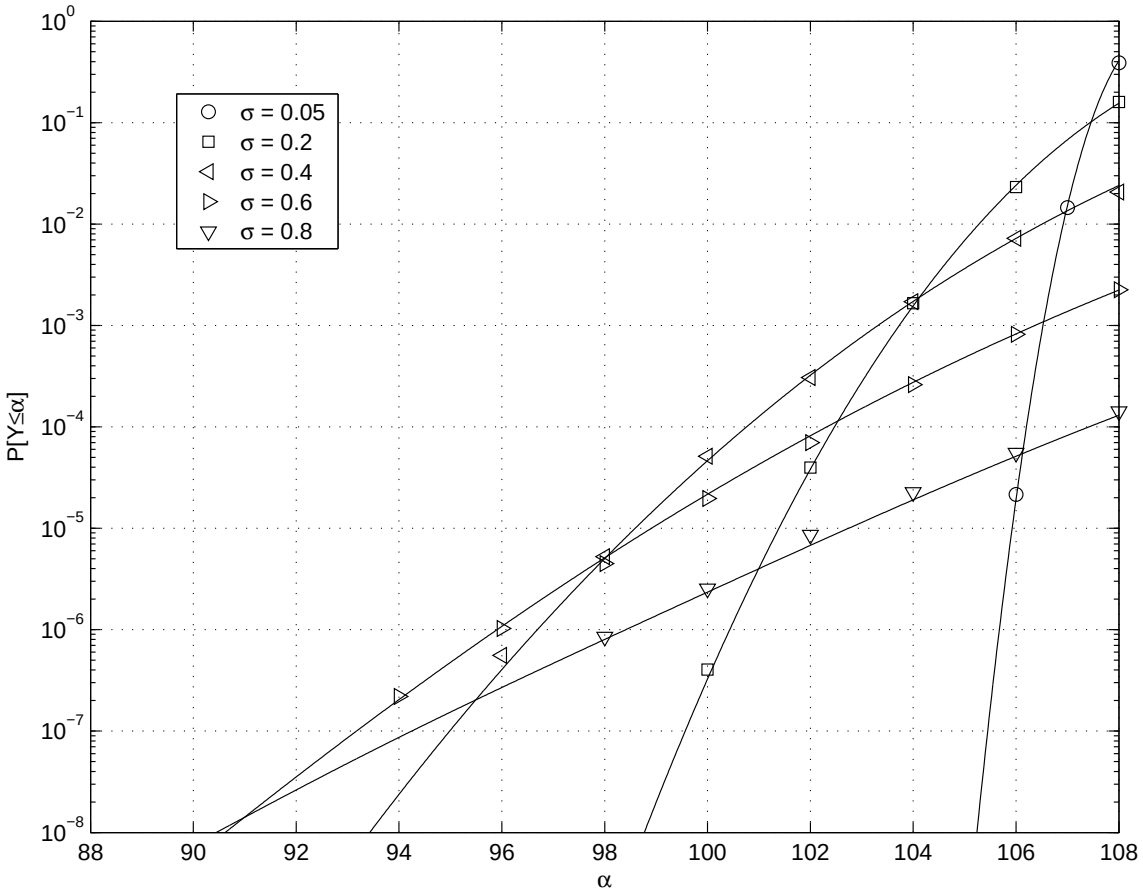

Figure 2.6: CDF of sum of 108 i.i.d. lognormal rv's for $\sigma \in \{0.05, 0.2, 0.4, 0.6, 0.8\}$. The solid lines are calculations and the points are simulations.

where $\phi_g(\tau)$ is the characteristic function of a zero-mean Gaussian random variable given by

$$\phi_g(\tau) = \exp\left\{-\frac{1}{2}\sigma_g^2\tau^2\right\} \tag{2-53}$$

and σ_g^2 is the power of the AWGN.

The CDF of $c(u)$ for a signal of length $L = 108$ and five values of the scintillation index σ is shown in Fig. 2.7(a) for SNR = 30 dB and in Fig. 2.7(b) for SNR = 10 dB. The solid curves are the calculated probability of miss and the simulation points are represented by the indicated shapes for each scintillation index. The theoretical curves match well with simulation for low to moderate strengths of atmospheric turbulence.

When $\sigma = 0.8$, the theoretical probability of miss begins to deviate from simulation at $\Pr\{Y \leq \alpha\} \approx 10^{-6}$, which is a result of the fact that not enough terms were used in the calculation of the characteristic function of the lognormal [**22**]. Comparing Fig. 2.7(a) to Fig. 2.7(b), one can see the diminishing effect of the scintillation strength on the probability of miss as the SNR decreases. In Fig. 2.7(a), the probability of miss curves for different values of σ diverge from each other, whereas in Fig. 2.7(b) the curves are grouped together for different values of σ.

A good choice for the detection threshold setting α is the point at which the probability of false alarm is equal to the probability of miss. For this system, the probability of false alarm is the probability that the sum of L zero-mean Gaussian random variables is greater than α which is

$$P_{FA}(\alpha) = \frac{1}{2}\left[1 - \text{erf}\left(\frac{\alpha}{\sqrt{2L\sigma_g^2}}\right)\right]. \tag{2-54}$$

For an optical wireless system operating through the turbulent atmosphere, the worse case scenario for probability of miss is when σ is maximum. For $L = 108$, the probability of miss and the probability of false alarm do not intersect at any practical value for the probability of miss. Hence, a shorter signal length is considered.

For a signal of length $L = 32$, the false alarm rate and miss rate are plotted in Fig. 2.8(a) and Fig. 2.8(b) for SNR = 10 dB and SNR = 5 dB, respectively. Figure 2.8(a) shows that a system operating at SNR = 10 dB could use a signal of length 32 with a detection threshold set at $\alpha = 12$ in order to obtain a probability of false alarm or miss detection that is below 10^{-10}. When the SNR = 5 dB, Fig. 2.8(b) shows that the high scintillation probability of miss and the probability of false alarm intersect at about $\alpha = 13$ and a probability less than 10^{-8}. If a lower probability is desired when SNR = 5 dB, then the signal length L must be extended.

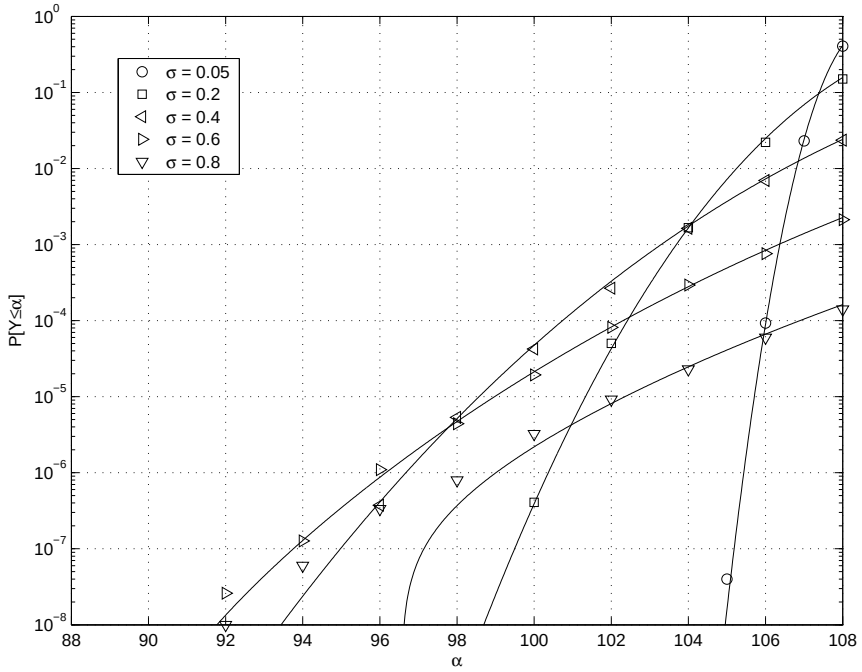

(a) SNR = 30 dB

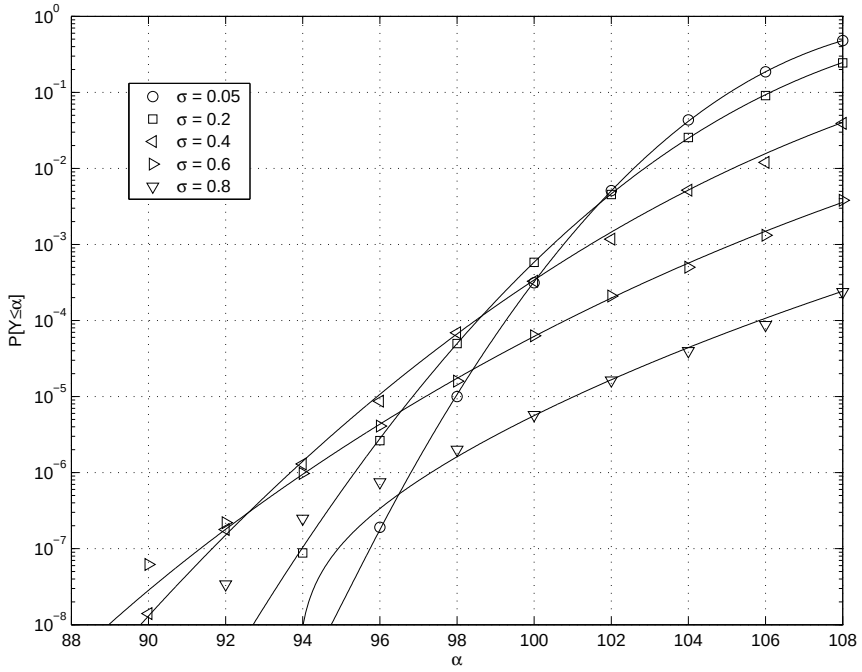

(b) SNR = 10 dB

Figure 2.7: Probability of miss for $L = 108$. As the SNR decreases, the effect of scintillation is less prominent on the probability of miss. The solid lines are calculations and the points are simulations.

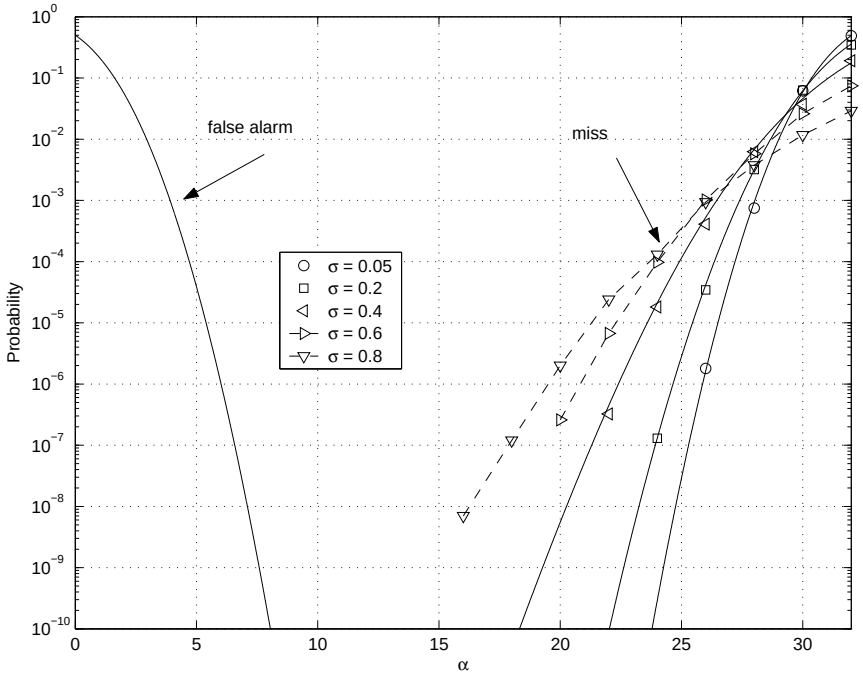

(a) SNR = 10 dB

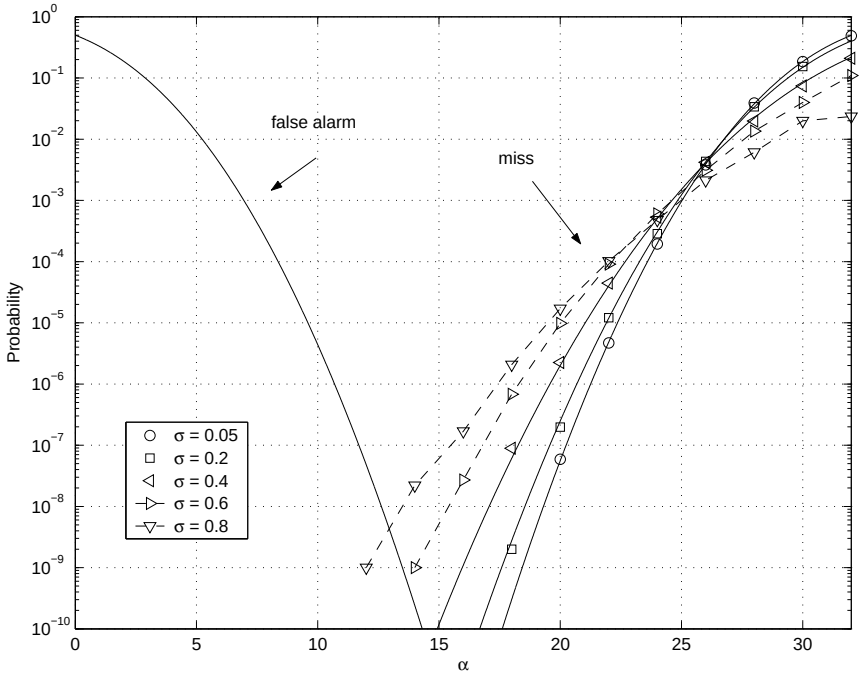

(b) SNR = 5 dB

Figure 2.8: Probability of miss for $L = 32$. The solid lines are calculations and the points are simulations. For $\sigma = 0.6$ and 0.8, the lines are dashed to indicate that the calculation could not be done by numerical integration using Barakat's formula for the lognormal characteristic function.

2.7. Conclusions

In this chapter, the probability of miss for optical communications system operating through the atmosphere in the presence of scintillation and AWGN is found. The Chernoff bound is derived for the CDF of the sum of lognormal random variables. The bound can be applied to find the probability of miss when the atmospheric scintillation is in the low to moderate range, and the signal to electronics noise power ratio is high. Fenton's approximation is considered in finding the CDF of the sum of lognormal random variables. This approximation is valid for dealing with the scintillation alone. When the receiver electronics noise is included, Fenton's approximation fails. The probability of miss is found using the characteristics function of the the received signal. The approach in this chapter can help the system designer to find the appropriate system parameters including signal length, detection threshold, and SNR to meet system specifications for detection. It also can be used to evaluate system performance. Further investigation into signal detection in optical communications through the atmosphere might include finding the probability of miss for a constant false alarm rate (CFAR) detector.

Chapter 3

Detection Statistics for Optical Signal Through Weak Turbulence Using p-i-n Photodiode

3.1. Introduction

Optical communications through the atmosphere experienced strong growth in the last decade. In [**2**], 16 separate 2.5 Gbps wavelength data channels were transmitted over a horizontal free space distance of 4.4 km. In [**23**], an 8×10 Gbps terrestrial optical free-space transmission over 3.4 km was demonstrated using an optical repeater in the middle. These systems can also be used for airborne [**24**] and ground-to-space [**25**] communication links. Optical wireless communication products supporting data rates over 1 Gbps are available from several communication equipment manufacturers. However, optical communications systems through the atmosphere are subject to many phenomena including random jitter of the beam [**26**], atmospheric precipitation and atmospheric turbulence, which can significantly degrade the system performance. Atmospheric turbulence is caused by inhomogeneities in the temperature and pressure of the atmosphere, which creates fluctuations in the received signal intensity. These fluctuations are also called scintillations and are the same phenomenon observed when stars twinkle.

Many different stochastic models exist for the effect of atmospheric turbulence on optical signals. Each gives a probability density function (PDF) for the distribution of the optical intensity of the signal. One of the first proposed, valid for weak atmospheric turbulence, is the lognormal model, which can be theoretically derived [**27**] and experimentally verified [**12**, **13**, **28**, **29**]. Two heuristic models that have been proposed are the K-distribution [**30**] and the gamma-gamma distribution [**31**]. The

K-distribution is applicable to strong atmospheric turbulence, which was experimentally verified in [**32**]. The gamma-gamma model can be used to fit the effects of the weak and strong turbulence. Simulation methods have also been used to determine the statistics of the optical intensity fluctuations [**33**]. In this chapter, the lognormal model is used. Therefore, the results herein are applicable to weak atmospheric scintillation.

Packet switching is widely employed in modern optical communications systems. In packet-switched optical communication systems, each packet begins with a predetermined sequence, the preamble, which must be detected by the receiver for synchronization, parameter estimation and demodulation. The detection of this packet is essentially a discrete signal detection problem described by the following hypothesis test:

$$H_0 \quad : \quad r_k = n_k, \quad k = 1, 2, \ldots, L \tag{3-2}$$

versus

$$H_1 \quad : \quad r_k = A_k d_k + n_k \quad k = 1, 2, \ldots, L, \tag{3-3}$$

where $\underline{r} = [r_1, r_2, \ldots, r_L]$ is the observation vector, $\{n_k\}$ are samples of an additive white Gaussian noise (AWGN) process representing the thermal noise of the receiver, L is the signal length, $\underline{d} = [d_1, d_2, \ldots, d_L]$ is the sequence to be detected and $\{A_k\}$ are samples from the stochastic process determined by the turbulent atmospheric channel which affects the signal strength.

Understanding the performance of signal detection is critical to the design of optical communications systems through the turbulent atmosphere. In packet-switched systems, it is typical to have packet loss rate not higher than 10^{-7} in the packet detection stage [**34**]. A system designer can determine the length of the preamble only after having analytical and numerical tools to evaluate signal detection performance

in the presence of atmospheric turbulence. In [**35**], the probability of miss in the detection of a signal in an optical communications system through the turbulent atmosphere using intensity modulation was studied. The received signal intensity in the presence of atmospheric turbulence was treated as a lognormal random process, and the received background radiation and electronic noise in the receiver were treated as AWGN. A series solution for the characteristic function of the lognormal random variable was used to find the probability of miss and compared with numerical results. In [**36**], the probability of miss was derived using methods of Fenton and Schwartz and Yeh to approximate the distribution of the sum of lognormal random variables. Statistics of photoelectron count vary with photodetectors, and make the analysis of signal detection performance very difficult. In these prior studies, statistics of photoelectron count were not considered.

The system under consideration in this work is an optical communications system using intensity modulation and direct detection (IM/DD) in the presence of atmospheric turbulence. The photodetector may either use a p-i-n photodiode or an avalanche photodiode (APD). The current induced by an optical signal impinging on a p-i-n photodiode is a shot noise process in which the photoelectron count is a Poisson process. In some instances the shot noise can be approximated by a Gaussian noise process. Many bit-error-rate (BER) studies have been presented in which it is assumed that the signal shot noise is Gaussian including [**29**]. Some previous work in signal detection has assumed that this signal shot noise is additive, white and Gaussian [**36**]. In [**4**], the detection of a single optical pulse in lognormal atmospheric turbulence is studied using p-i-n statistics and including background radation. In this chapter, the study is extended to the detection of multiple symbols in lognormal turbulence including the effects of background radiation and thermal electronic noise.

The remainder of this chapter will proceed with a description of the system model in Section 3.2, a discussion of the photoelectron count statistics in Section 3.3, a

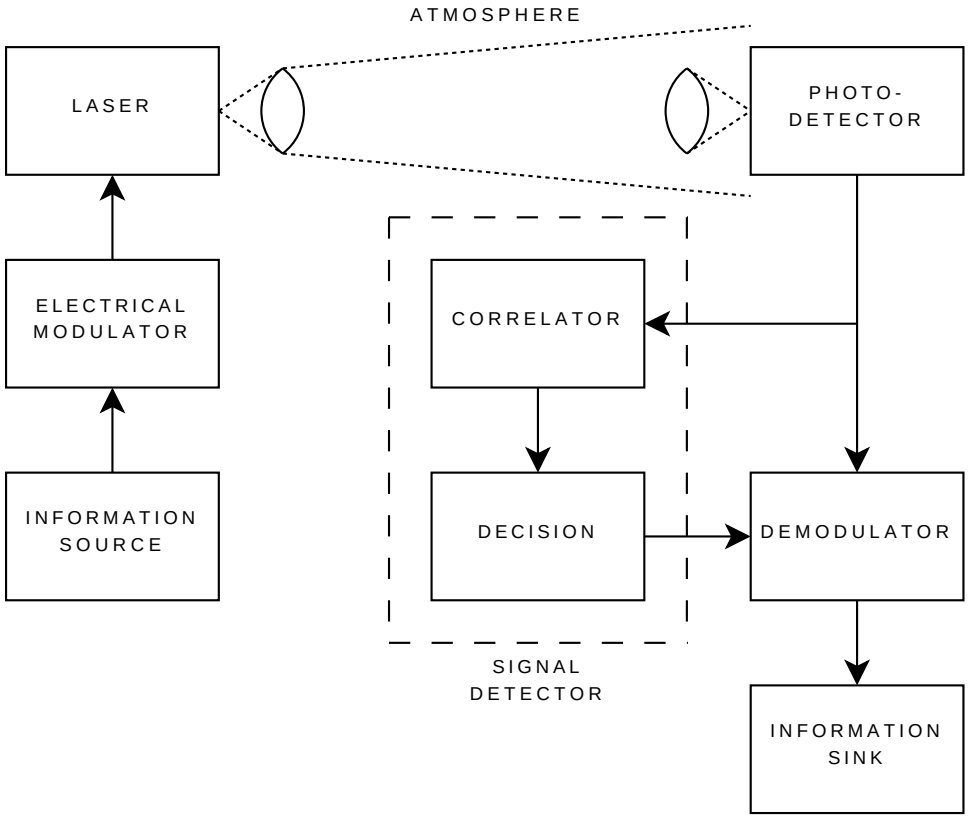

Figure 3.1: Block diagram for optical communications system through the turbulent atmosphere.

discussion of the probabilities of miss and false alarm in Section 3.4, an explanation of how the signal length and detection threshold settings can be determined in Section 3.5 and finally a brief summary and conclusions in Section 3.6.

3.2. System Model

Fig. 3.1 illustrates the block diagram for the optical wireless communication system. In this system a digital information source modulates an electrical signal. This electrical signal is then used to modulate the output field intensity of an optical source, a laser. The laser output propagates through the atmospheric channel and is distorted by turbulence. The optical receiver is a direct detection receiver meaning that it responds to changes in the intensity of the transmitted signal. After passing

through the receiver's optics, the signal impinges on the surface of the photodetector, where, as a result of photon-atom interactions, the light intensity is converted into electrical current.

The output current of the photodetector is

$$i(t) = i_p(t) + i_n(t), \tag{3-4}$$

where $i_p(t)$ is the photo-generated current and $i_n(t)$ is the thermal noise current. Note that $i_p(t)$ is the result of the received signal and background radiation. This current is passed to the signal detector. If the signal detector determines that a packet has arrived, then it triggers the demodulator to recover the remainder of the information.

3.2.1. Signal Detector. The signal detector is a linear correlator [**15**]. The detector is composed of an integrator which integrates the current in T_s second intervals. The output of the ith integration is

$$v_i = ek\left(iT_s, (i+1)T_s\right) + v_{n,i}, \tag{3-5}$$

where e is the electron charge, T_s is the symbol time, $k(t_1, t_2)$ is the number of electrons generated in the time interval (t_1, t_2) as a result of photodetection and $v_{n,i}$ is the integrated thermal noise current. For clarity, k_i is used to denote $k\left(iT_s, (i+1)T_s\right)$ throughout the remainder of this chapter. The current integrations are passed into a register which holds L integrations, where L is the length of the signal to be detected. The contents of the register are multiplied by the binary sequence to be detected and summed to obtain

$$v = \sum_{i=0}^{L-1} d_i \left(ek_i + v_{n,i}\right), \tag{3-6}$$

where $\{d_i\}_{i=0}^{L-1}$ is the binary sequence. Finally, v is compared to a threshold v_T to determine if the signal was received.

If the signal was sent, but $v < v_T$, then a miss detection occurs. Hence, the probability of miss is

$$P_M(v_T) = P\left[v_s < v_T\right], \tag{3-7}$$

where v_s represents the correlator output when the signal was sent. If the signal was not sent and $v > v_T$, then a false alarm occurs. If v_n represents the correlator output when no signal was transmitted and the detector correlates with only noise, the probability of false alarm is

$$P_{FA}(v_T) = P\left[v_n > v_T\right]. \tag{3-8}$$

3.2.2. Received Signal. In an optical wireless communication system using on-off keying (OOK) intensity moduation and direct detection, the received field intensity is

$$I_r(u,t) = I_s(u,t)\sum_{i=1}^{L} d_i g(t - iT_s) + I_b(u,t), \tag{3-9}$$

where I_s is the recieved signal intensity, $g(t)$ is the shaping pulse and I_b is the background radiation intensity. Due to atmospheric turbulence, I_s is a lognormal random process representing optical scintillation.

The scintillation process is a result of fluctuations in the atmospheric index of refraction caused by turbulence. The index of refraction at a position in space $\vec{r}$ can be modeled as

$$n(\vec{r}) = n_0 + n_1(\vec{r}), \tag{3-10}$$

where $n_1(\vec{r})$ represents random changes about the mean n_0. In [**27**], it is shown that using this model and the Rytov transformation when solving Maxwell's equations for the electromagnetic plane wave, the amplitude of the optical field is

$$A = A_0 e^{\chi}, \tag{3-11}$$

where A_0 is the free-space solution and χ, termed the log-amplitude fluctuation, is a normal random variable with mean $\bar{\chi}$ and variance σ_χ^2. This means that A is a lognormal variable. Since the field intensity $I = A^2$, I is also a lognormal random variable and has density

$$f_I(I) = \frac{1}{\sqrt{8\pi}\sigma_\chi I} \exp\left[-\frac{(\ln(I/I_0) - \bar{\chi})^2}{8\sigma_\chi^2}\right], \tag{3-12}$$

where $I_0 = A_0^2$. For energy conservation, which requires that atmospheric turbulence neither amplifies nor attenuates the signal,

$$E(I) = I_0 e^{2\bar{\chi}+2\sigma_\chi^2} = I_0 \tag{3-13}$$

so that $\bar{\chi} = -\sigma_\chi^2$. Many experimental studies have been conducted in which data have shown that intensity fluctuations due to weak atmospheric turbulence follow a lognormal distribution [**12**, **13**, **28**].

3.3. Photoelectron Count Statistics

The theory of photoelectron count statistics in semiconductor photodetectors is well-developed [**8**]. In this section, the photoelectron count will be found with and without the effects of atmospheric turbulence.

3.3.1. Photoelectron Count in the Absence of Turbulence. In order to find the electric current induced by the optical signal, the mean number of primary electrons that will be emitted over the observation volume $V = A_d \times T_s$ must be determined, where A_d is the area of photodetecting surface. Primary electrons are those which are released from the photodetector surface as a result of the absorption of photons. The mean number of primary electrons over V is

$$m_v = \frac{\eta}{h\nu} \int_V I_r(u,t) dV \tag{3-14}$$

where η is the quantum efficiency of the photosensitive material, h is Planck's constant and ν is the optical frequency. During an "on" symbol and an "off" symbol the mean count is

$$m_v = \begin{cases} K_s + K_b, & d_i = 1 \\ K_b, & d_i = 0, \end{cases} \tag{3-15}$$

respectively, where K_s is the average signal electron count and K_b is the average background noise electron count. In the absence of atmospheric turbulence, the value of I_s is constant throughout V and

$$K_s = \frac{\eta}{h\nu} A_d T_s I_s. \tag{3-16}$$

In a photodetector which receives a constant optical field intensity, the number of primary electrons k_1 is a Poisson distribution given by

$$P[k_1 = k] = \text{Pois}(k, m_v) = \frac{m_v^k}{k!} e^{-m_v} \tag{3-17}$$

so that in an "on" symbol

$$P[k_1 = k] = \frac{(K_s + K_b)^k}{k!} e^{-(K_s + K_b)}. \tag{3-18}$$

3.3.2. Photoelectron Count in the Presence of Turbulence. When the received optical field intensity is stochastic, k_1 is no longer Poisson distributed. Since the atmospheric turbulence channel is a slow fading channel, the signal intensity I_s can be assumed constant for one symbol interval and, as a result, the mean signal count K_s is constant for one symbol interval. For convenience, K_0 is defined as the mean signal electron count without atmospheric turbulence so that $K_s = K_0 e^{2\chi}$.

To find the distribution of k_1, the Poisson probability is averaged over the density $f_m(m)$ of m_v to get

$$E(P[k_1 = k]) = \int_0^\infty \text{Pois}(k, m) f_m(m) dm. \tag{3-19}$$

This type of probability is called a conditional Poisson probability. In [**4**], (3-19) is computed numerically in order to find the probability of detection of a single symbol in lognormal atmospheric turbulence. In the remainder of this section, a normal approximation is found for (3-19) which allows for simpler calculation of the probabilities of detection and miss, in particular for multiple symbol detection.

First, (3-19) is written

$$\begin{aligned} E(P[k_1 = k]) &= \int_{-\infty}^{\infty} \frac{\left(K_0 e^{2x} + K_b\right)^k}{k!} e^{-\left(K_0 e^{2x} + K_b\right)} f_\chi(x) dx \\ &= \int_{-\infty}^{\infty} \frac{\left(K_0 e^{2x} + K_b\right)^k}{k!} e^{-K_b} \exp\left[-K_0 \sum_{n=0}^{\infty} \frac{2^n}{n!} x^n\right] f_\chi(x) dx, \end{aligned} \tag{3-20}$$

where $f_\chi(x)$ is the density of χ. The log-amplitude signal fluctuation χ is distributed as $N(-\sigma_\chi^2, \sigma_\chi^2)$, where $\sigma_\chi \in [0, 0.2]$. Since χ is small, only the first three terms in the Taylor series are kept leaving

$$\begin{aligned} E(P[k_1 = k]) &\approx \int_{-\infty}^{\infty} \frac{\left(K_0 e^{2x} + K_b\right)^k}{k!} e^{-K_b} e^{-K_0(1+2x+2x^2)} f_\chi(x) dx \\ &= \int_{-\infty}^{\infty} \frac{\left(K_0 e^{2x} + K_b\right)^k}{k!} e^{-K_b} e^{-K_0(1+2x+2x^2)} \frac{1}{\sqrt{2\pi}\sigma_\chi} e^{-(x+\sigma_\chi^2)^2/2\sigma_\chi^2} dx. \end{aligned} \tag{3-21}$$

Using the binomial theorem to expand the term raised to the kth power in (3-21) results in

$$\begin{aligned} E(P[k_1 = k]) \approx \frac{e^{-(K_0+K_b)}}{k!} \int_{-\infty}^{\infty} \sum_{m=0}^{k} \binom{k}{m} \left(K_0 e^{2x}\right)^{k-m} K_b^m \\ \cdot e^{-K_0\left(2x+2x^2\right)} \frac{1}{\sqrt{2\pi}\sigma_\chi} e^{-(x+\sigma_\chi^2)^2/2\sigma_\chi^2} dx, \end{aligned} \tag{3-22}$$

where

$$\binom{k}{m} = \frac{k!}{m!\,(k-m)!}. \tag{3-23}$$

The exponential terms in (3-22) are grouped together to obtain

$$E(P[k_1 = k]) \approx \frac{e^{-(K_0+K_b)}}{k!} \sum_{m=0}^{k} \binom{k}{m} K_0^{k-m} K_b^m \frac{1}{\sqrt{2\pi}\sigma_\chi} \int_{-\infty}^{\infty} e^A dx, \tag{3-24}$$

where

$$A = 2\left(k-m\right)x - 2K_0 x - 2K_0 x^2 - \frac{\left(x+\sigma_\chi^2\right)^2}{2\sigma_\chi^2}. \tag{3-25}$$

After completing the square in A and integrating, the following approximation is obtained:

$$\begin{aligned} P[k_1 = k] \approx & \frac{e^{-\sigma_\chi^2/2}}{\sqrt{4\sigma_\chi^2 K_0 + 1}} \frac{e^{-(K_0+K_b)}}{k!} \sum_{m=0}^{k} \binom{k}{m} K_0^{k-m} K_b^m \\ & \cdot \exp\left\{ \frac{\sigma_\chi^2 \left[2\left(k-m-K_0\right)-1\right]^2}{2\left(4\sigma_\chi^2 K_0 + 1\right)} \right\}. \end{aligned} \tag{3-26}$$

Although (3-26) is not a probability mass function because it diverges as $k \longrightarrow \infty$, it does sum to approximately 1 for $k \in [0, 2K_0]$. The probability mass function for the Poisson distribution given by (3-18) and the conditional Poisson given by (3-26) are plotted in Fig. 3.2 for $K_0 = 50$, $K_b = 10$ and $\sigma_\chi = 0.08$. The conditional Poisson distribution is shown to have a larger variance and be more skewed to the right than the Poisson distribution. This approximation does lend insight into the conditional Poisson distribution, but it is too complicated for quick calculation of the probability of miss.

After rearranging terms, (3-26) can be written

$$\begin{aligned} P[k_1 = k] \approx & \frac{e^{-\sigma_\chi^2/2}}{\sqrt{4\sigma_\chi^2 K_0 + 1}} \sum_{m=0}^{k} \frac{K_0^{k-m}}{(k-m)!} e^{-K_0} \frac{K_b^m}{m!} e^{-K_b} \\ & \cdot \exp\left\{ \frac{\sigma_\chi^2 \left[2\left(k-m-K_0\right)-1\right]^2}{2\left(4\sigma_\chi^2 K_0 + 1\right)} \right\}. \end{aligned} \tag{3-27}$$

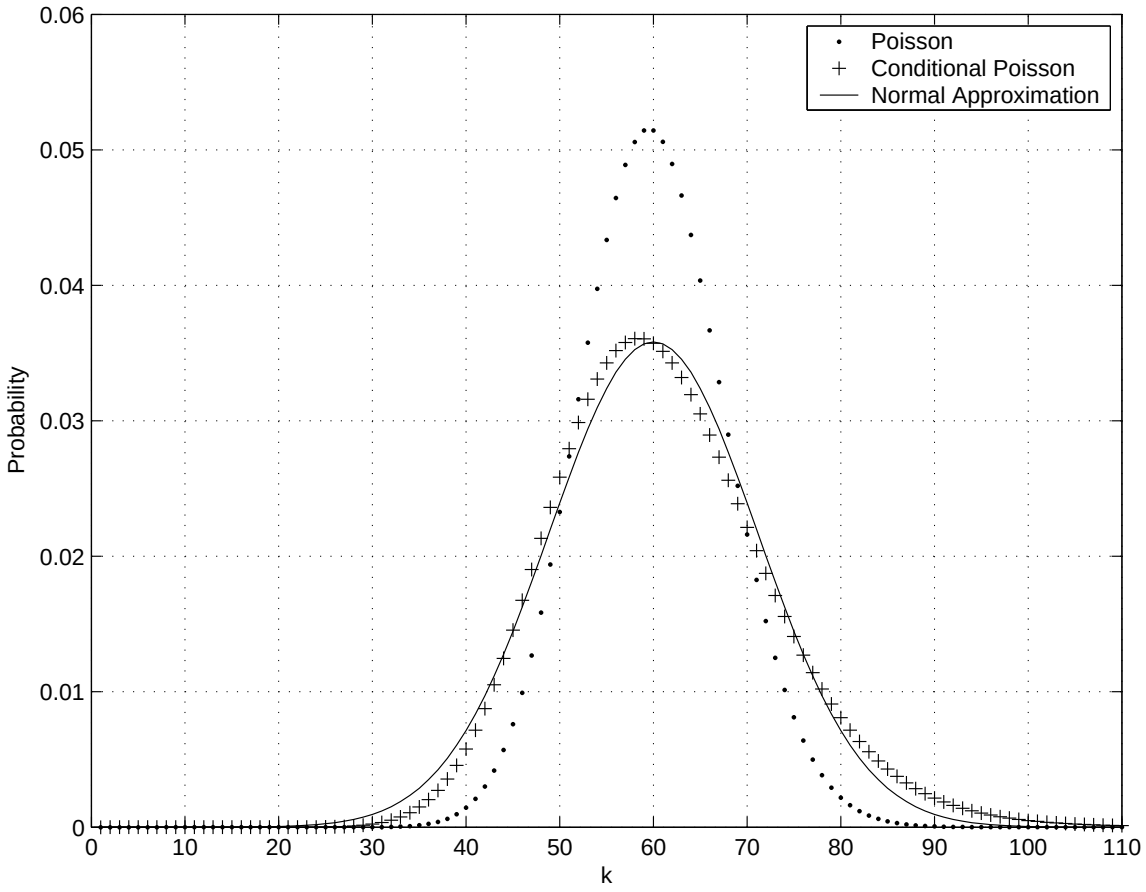

Figure 3.2: Probability mass function for Poisson distribution given by (3-18), approximate probability mass function for conditional Poisson distribution given by (3-26) and normal approximation for conditional Poisson distribution given by (3-32), where $K_0 = 50$, $K_b = 10$ and $\sigma_\chi = 0.08$.

The Poisson distribution with mean λ is approximated by the Gaussian distribution with mean λ and variance λ for large λ [**37**, p. 190], that is

$$\frac{\lambda^n}{n!}e^{-\lambda} \approx \frac{1}{\sqrt{2\pi\lambda}}e^{-\frac{(n-\lambda)^2}{2\lambda}} \tag{3-28}$$

when λ is large. It may seem logical to substitute this Gaussian approximation at the beginning of this derivation in (3-20), but that results in an integral that is more complicated than the one that has been solved. Instead, the two Poisson terms in

(3-27) are replaced with the Gaussian approximation to obtain

$$\begin{aligned} P[k_1 = k] \approx \sum_{m=0}^{k} & \frac{1}{\sqrt{2\pi K_0}} e^{-\frac{(k-m-K_0)^2}{2K_0}} \frac{1}{\sqrt{2\pi K_b}} e^{-\frac{(m-K_b)^2}{2K_b}} \\ & \cdot \frac{e^{-\sigma_\chi^2/2}}{\sqrt{4\sigma_\chi^2 K_0 + 1}} \exp\left\{ \frac{\sigma_\chi^2 \left[2\left(k-m-K_0\right)-1\right]^2}{2\left(4\sigma_\chi^2 K_0 + 1\right)} \right\}. \end{aligned} \tag{3-29}$$

Since K_0 is large, the -1 in the squared term of the last exponential is negligible. After eliminating the -1, there exists a common $(k-m-K_0)^2$ term in the first and last exponentials so that (3-29) can be rewritten

$$\begin{aligned} P[k_1 = k] &\approx \sum_{m=0}^{k} \frac{e^{-\sigma_\chi^2/2}}{\sqrt{2\pi K_0\left(4\sigma_\chi^2 K_0 + 1\right)}} \\ &\quad \cdot \exp\left[(k-m-K_0)^2 \left(\frac{2\sigma_\chi^2}{4\sigma_\chi^2 K_0 + 1} - \frac{1}{2K_0} \right) \right] \frac{1}{\sqrt{2\pi K_b}} e^{-\frac{(m-K_b)^2}{2K_b}} \\ &= \sum_{m=0}^{k} \frac{e^{-\sigma_\chi^2/2}}{\sqrt{2\pi K_0\left(4\sigma_\chi^2 K_0 + 1\right)}} \exp\left[-\frac{(k-m-K_0)^2}{2K_0(4\sigma_\chi^2 K_0 + 1)} \right] \frac{1}{\sqrt{2\pi K_b}} e^{-\frac{(m-K_b)^2}{2K_b}}. \end{aligned} \tag{3-30}$$

The $e^{-\sigma_\chi^2/2}$ term is near unity for relevant values of σ_χ and, as such, does not significantly effect the calculation of the probability of miss. After removing it,

$$\begin{aligned} P[k_1 = k] \approx \sum_{m=0}^{k} & \frac{1}{\sqrt{2\pi K_0\left(4\sigma_\chi^2 K_0 + 1\right)}} \exp\left[-\frac{(k-m-K_0)^2}{2K_0(4\sigma_\chi^2 K_0 + 1)} \right] \\ & \cdot \frac{1}{\sqrt{2\pi K_b}} \exp\left[-\frac{(m-K_b)^2}{2K_b} \right]. \end{aligned} \tag{3-31}$$

Eq. (3-31) is the discrete convolution of two Gaussian density functions, which is itself Gaussian with mean and variance equal to the sum of the means and the variances of the input Gaussians, respectively. Therefore, the distribution of k_1 can be approximated as

$$k_1 \sim N(\mu_k, \sigma_k^2) = N(K_0 + K_b, K_0(4\sigma_\chi^2 K_0 + 1) + K_b). \tag{3-32}$$

This normal approximation is plotted in Fig. 3.2 for $K_0 = 50$, $K_b = 10$ and $\sigma_\chi = 0.08$.

3.4. Probabilities of Miss and False Alarm

In this section the probability of miss and the probability of false alarm are formulated. Since the modulation scheme is OOK, the "off" symbols drop out in (3-6) and

$$v = \sum_{i=0}^{L'-1} ek_i + v_{n,i}, \tag{3-33}$$

where L' is the Hamming weight of the binary sequence to be detected. The k_i's are independent. Also, the thermal electronic noise is independent from the photoelectron count. Therefore, to find the probability of miss and the probability of false alarm, one must determine the cumulative distribution function (CDF) and complementary cumulative distribution function (CCDF) of the sum of L' independent random variables, respectively.

3.4.1. Quantum Limited Detection. When the background radiation and thermal electronic noise are negligible, the detection performance is limited only by the signal shot noise. This is called quantum limited detection. The probability of false alarm is zero because in this case no current exists in the receiver in the absence of a signal.

In the presence of atmospheric turbulence, the probability of miss is

$$P_M(k_T) = P\left[\sum_{i=0}^{L'-1} k_i < k_T\right], \tag{3-34}$$

where each k_i has conditional Poisson distribution given by (3-20). Since the thermal noise is negligible, a signal count threshold $k_T = \lfloor v_T/e \rfloor$ is defined. Quantum-limited detection is equivalent to counting the total number of photons received in the "on" symbols and comparing that to k_T to determine if the signal is present.

In the absence of atmospheric turbulence, each k_i is Poisson with mean count K_s. Noting that the distribution of the sum of L independent and identically distributed Poisson random variables with common mean m is Poisson with mean Lm, the probability of miss is calculated as

$$\begin{aligned} P_M(k_T) &= \sum_{n=0}^{k_T-1} \frac{(L'K_s)^n}{n!} e^{-L'K_s} \\ &= 1 - \frac{K_s}{(k_T-1)!} \int_0^{L'} e^{K_s x} (K_s x)^{(k_T-1)} dx, \end{aligned} \tag{3-35}$$

where the last equality can be found in [**38**, p. 345]. This equation represents the lower bound on detection performances achievable in (3-34).

3.4.2. Detection in Thermal Electronic Noise. In any power-limited system, the thermal electronic noise is non-negligible and must be considered. In this case, the probability of miss is

$$P_M(v_T) = P\left[\sum_{i=0}^{L'-1} ek_i + v_{n,i} < v_T\right], \tag{3-36}$$

where each k_i has conditional Poisson distribution given by (3-20). Each thermal noise integration $v_{n,i}$ is Gaussian with zero mean and variance

$$\sigma_n^2 = \frac{2k_B T}{R_L} T_s, \tag{3-37}$$

where k_B is Boltzmann's constant, T is the receiver's temperature, R_L is the load resistance and T_s is the symbol time. Using the normal approximation for the distribution of k_1 given by (3-32), the sum in (3-36) is a sum of normal random variables so that the sum has mean $eL'\mu_k$ and variance $L'(\sigma_n^2 + e^2\sigma_k^2)$. Therefore, probability of miss is approximated by

$$P_M(v_T) = \frac{1}{2}\left[1 + \operatorname{erf}\left(\frac{v_T - eL'\mu_k}{\sqrt{2L'(\sigma_n^2 + e^2\sigma_k^2)}}\right)\right], \tag{3-38}$$

where erf$(\cdot)$ is the error function defined as

$$\text{erf}(x) = \frac{2}{\sqrt{\pi}} \int_0^x e^{-t^2} dt. \tag{3-39}$$

In the next section, (3-38) is compared with simulations.

In the event of a false alarm, no signal is present so that only background noise counts and thermal noise integrations are present in the correlator. Therefore, the probability of false alarm is

$$\begin{aligned} P_{FA}(v_T) &= P\left[\sum_{i=0}^{L'-1} ek_i + v_{n,i} > v_T\right] \\ &= \frac{1}{2}\left[1 - \text{erf}\left(\frac{v_T - eL'K_b}{\sqrt{2L'\left(\sigma_n^2 + e^2K_b\right)}}\right)\right]. \end{aligned} \tag{3-40}$$

In the next section, (3-38) and (3-40) are used to determine the required signal length L' and detection threshold v_T to achieve a desired performance.

3.5. Determination of Signal Length and Detection Threshold

Appropriate settings for the signal length L' and detection threshold v_T are critical in the design of a packet-switched system. The goals are 1) to minimize L' while maintaining required detection performance and 2) to determine v_T such that the probabilities of miss and false alarm are below the required performance. First, a simple quantum-limited example will be presented and then an example with thermal electronic noise.

3.5.1. Quantum Limited Detection. In the quantum-limited detection regime, the thermal noise is negligible and the performance is only limited by the signal shot noise. In this case, it is assumed that there is no current in the receiver in the absence of the signal and, therefore, a false alarm is impossible. In Fig. 3.3, the probability of

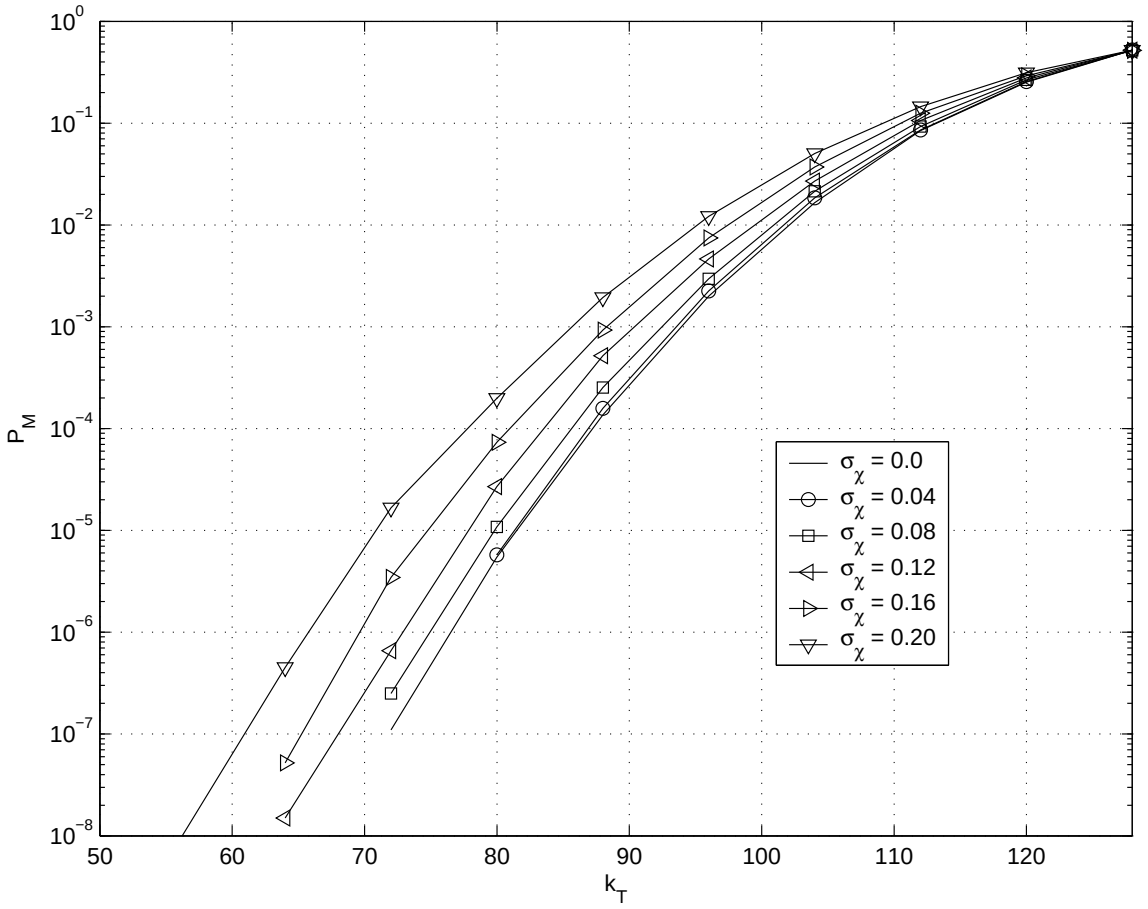

Figure 3.3: Probability of miss for quantum-limited detection, where $K_0 = 4$ and $L' = 32$.

miss is plotted for $K_0 = 4$ and $L' = 32$. The plot illustrates that, at these parameters, a threshold set at $k_T = 60$ would achieve a probability of miss of at least 10^{-7} for atmospheric turbulence when $\sigma_\chi \leq 0.20$. This is an extremely low signal count which may be applicable to very low power systems such as space systems.

3.5.2. Detection in Thermal Electronic Noise. Now a system is simulated in which the thermal noise is not negligible. The detection performance has been simulated with the following parameters: signal length $L' = 32$, data rate $R_b = 2.4$ Gb/s, load resistance $R_L = 50\ \Omega$ and receiver temperature $T = 295$ K.

In order to compute the background noise signal count, first the power of the background radiation is calculated as [**8**]

$$P_b = W(\lambda)(\Delta\lambda)\Omega_{fv}A_l, \tag{3-41}$$

where $W(\lambda)$ (W/cm^2-μm-sr) is the spectral radiance of the background at wavelength λ, $\Delta\lambda$ is the bandwidth of the background radiation which is collected, $\Omega_{fv} = 4\pi\sin^2(\theta/4)$ is the solid angle of the receiver field of view, θ is the receiver field of view angle and A_l is the area of the receiving aperture. In the daytime, the diffuse (indirect sunlight) spectral radiance $W(\lambda) \approx 10^{-3}$ (W/cm^2-μm-sr) at $\lambda = 850$ nm [**8**]. Using $\Delta\lambda = 30$ nm, receiver field of view angle $\theta = 3$ mrad and aperture diameter $D = 18$ cm, the collected background energy in one symbol time $P_bT_s \approx 2.25 \cdot 10^{-17}$ J, which is about $P_bT_s/(h\nu) = 100$ background photons. For a photodiode with quantum efficiency $\eta = 0.1$, the average number of background photoelectrons $K_b = \eta P_bT_s = 10$, which is what is used for the numerical calculations in this study.

Fig. 3.4 shows the probability of miss for $K_0 = 5800$. The approximate probability of miss calculated using (3-38) agrees well with simulations. Figs. 3.5 and 3.6 show the detection performances when the mean signal photoelectron count without scintillation $K_0 = 3500$ and 5800, respectively. When $K_0 = 3500$, a threshold setting near $v_T = 0.8 \cdot 10^{-14}$, which is equivalent to $\lfloor v_T/e \rfloor = 49938$ electrons, is required to achieve the best performance of about 10^{-7} when $\sigma_\chi = 0.20$. If better performance is required at this signal level, then the signal length must be increased. When $K_0 = 5800$ a threshold setting of $10^{-14} \leq v_T \leq 1.5 \cdot 10^{-14}$ or $62422 \leq \lfloor v_T/e \rfloor \leq 93633$ would make it possible to obtain a detection performance better than 10^{-8}.

In the preceding paragraph, the analysis was limited to one signal length and two different mean counts. It is possible to obtain a broader perspective when the analysis is restricted to the worst possible scintillation strength, which in this study is $\sigma_\chi = 0.20$. The probability of miss can be no worse than when the scintillation

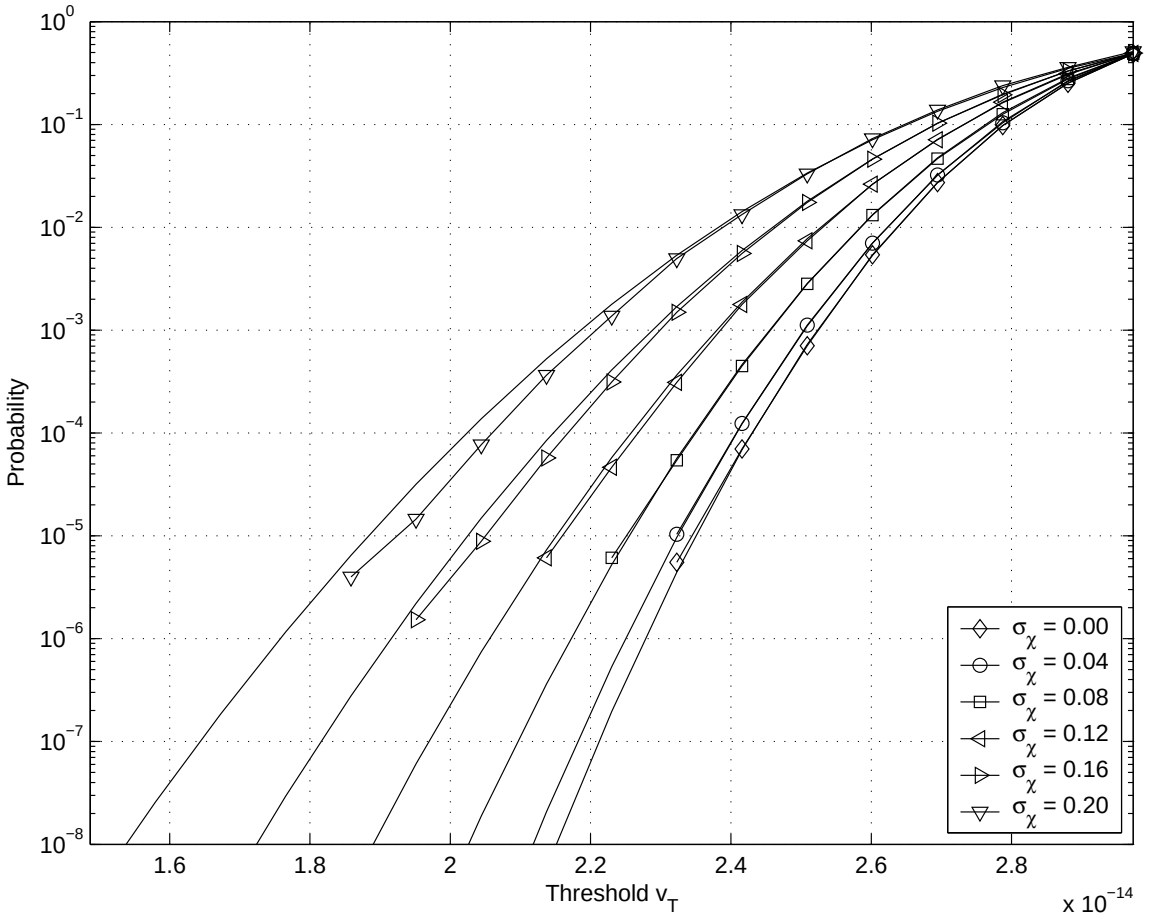

Figure 3.4: Probability of miss for $L' = 32$, $\sigma_\chi \in \{0.0, 0.04, 0.08, 0.12, 0.16, 0.20\}$, $R_b = 2.4$ Gb/s, $R_L = 50\ \Omega$, $T = 295$ K, $K_0 = 5800$ and $K_b = 10$. The lines with circles, squares and triangles are simulations and lines without are calculated using (3-38).

strength is the highest. Therefore, letting $\sigma_\chi = 0.20$ when calculating (3-38) results in an upper bound on the probability of miss over all cases of atmospheric turbulence. Fixing σ_χ and setting $P_M(v_T) = P_{FA}(v_T)$, the optimum threshold is found as

$$v_T^o = eL' \left[K_0 \left(1 + \sqrt{1 + \frac{e^2 K_0 \left(4\sigma_\chi^2 K_0 + 1\right)}{\sigma_n^2 + e^2 K_b}} \right)^{-1} + K_b \right]. \tag{3-42}$$

By plotting the detection performance at this optimum threshold versus the mean signal count without scintillation, a signal length can be determined which achieves

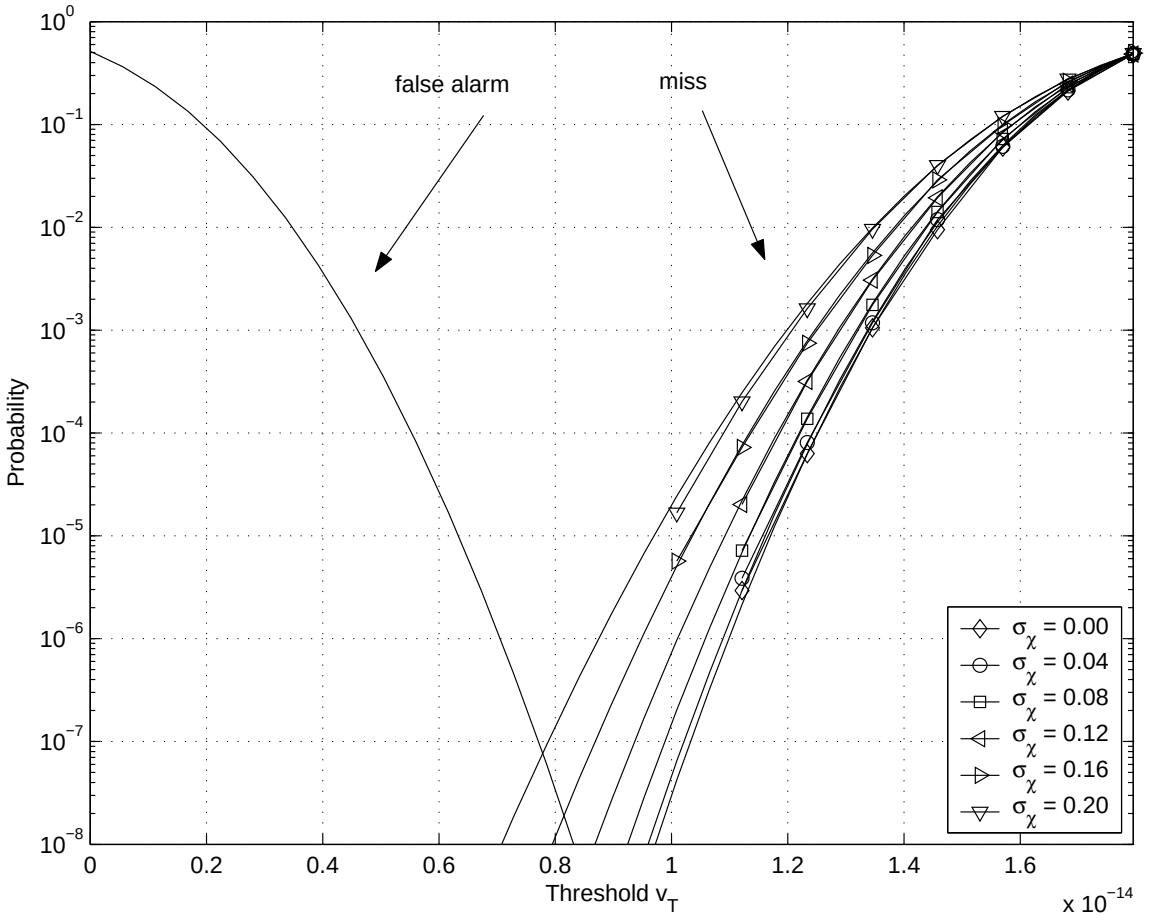

Figure 3.5: System performance for $L' = 32$, $\sigma_\chi \in \{0.0, 0.04, 0.08, 0.12, 0.16, 0.20\}$, $R_b = 2.4$ Gb/s, $R_L = 50\ \Omega$, $T = 295$ K, $K_0 = 3500$ and $K_b = 10$. The lines with circles, squares and triangles are simulations and lines without are calculated using (3-38).

the required detection performance. Such a plot is presented in Fig. 3.7. For example, if $K_0 = 6000$ and a performance of 10^{-8} is required, then Fig. 3.7 illustrates that a signal length of $L' = 24$ is sufficient. The signal length may also be determined by plugging the optimum threshold v_T^o of (3-42) into (3-40) to get

$$L^o = \frac{2\left(\sigma_n^2 + e^2 K_b\right)}{e^2 K_0^2}\left(1 + \sqrt{1 + \frac{e^2 K_0\left(4\sigma_\chi^2 K_0 + 1\right)}{\sigma_n^2 + e^2 K_b}}\right)^2 \left[\text{erfinv}\left(1 - 2P_{FA}(v_T^o)\right)\right]^2, \tag{3-43}$$

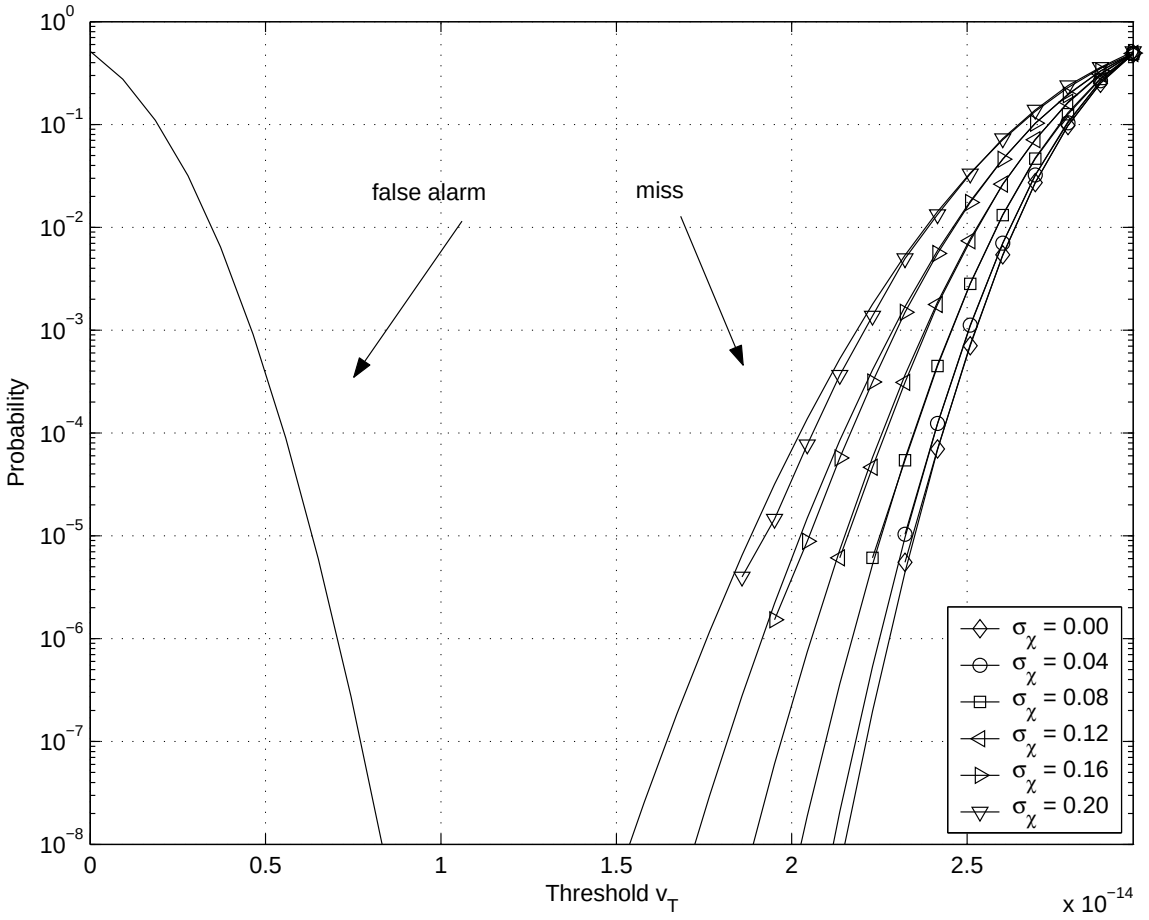

Figure 3.6: System performance for $L' = 32$, $\sigma_\chi \in \{0.0, 0.04, 0.08, 0.12, 0.16, 0.20\}$, $R_b = 2.4$ Gb/s, $R_L = 50\ \Omega$, $T = 295$ K, $K_0 = 5800$ and $K_b = 10$. The lines with circles, squares and triangles are simulations and lines without are calculated using (3-38).

where erfinv$(\cdot)$ is the inverse error function. Again if a performance of 10^{-8} is required, then (3-43) can be plotted as in Fig. 3.8 to show the optimum signal length as a function of K_0.

The average signal to noise power ratio in a optical communications system employing OOK can be estimated as [**8**]

$$\text{SNR} \approx \frac{(eK_0)^2}{(\sqrt{e^2\left(K_0 + K_b\right) + \sigma_n^2} + \sqrt{e^2 K_b + \sigma_n^2})^2}. \tag{3-44}$$

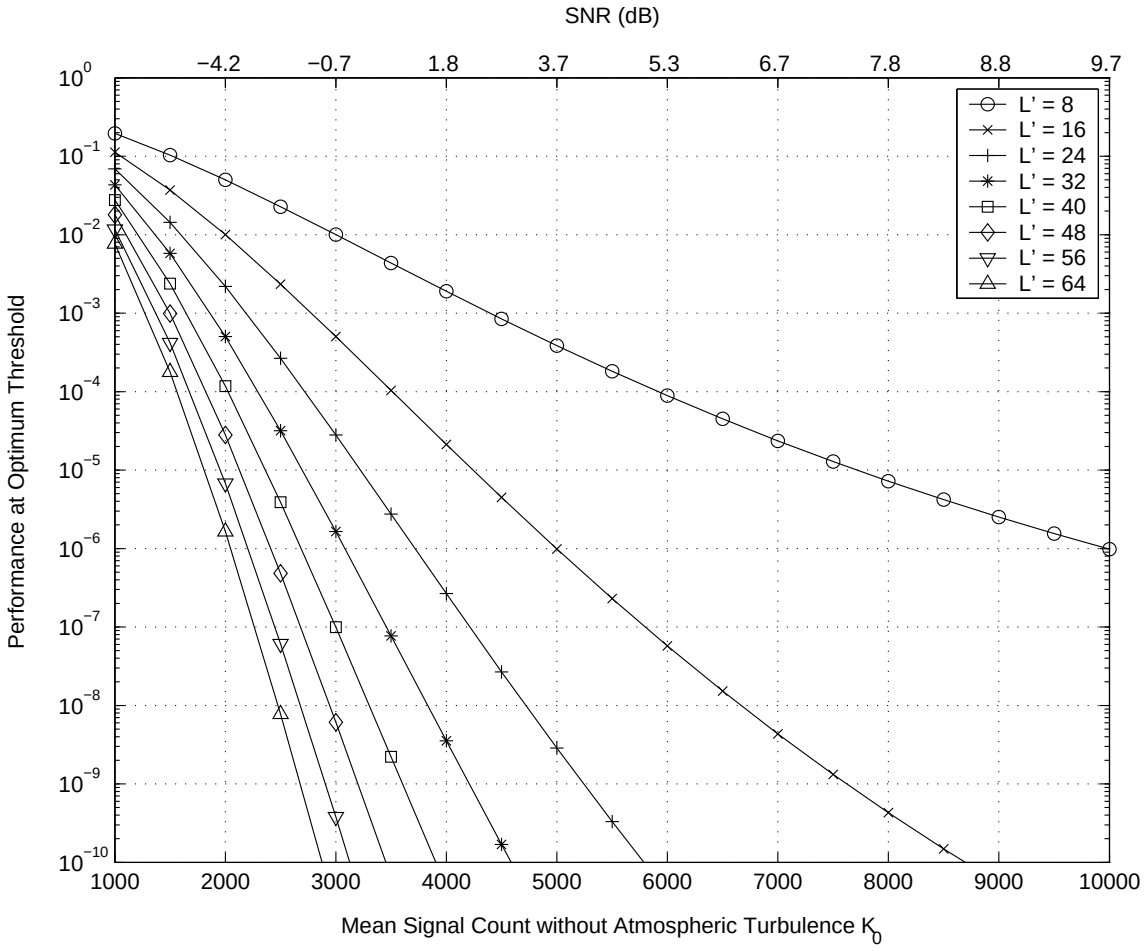

Figure 3.7: System performance at the optimum threshold setting v_T^o assuming the log-amplitude signal fluctuation $\sigma_\chi = 0.20$, data rate $R_b = 2.4$ Gb/s, load resistance $R_L = 50\ \Omega$, receiver temperature $T = 295$ K and mean background noise count $K_b = 10$.

For reference, the SNR is reported on the top x-axis of Fig. 3.7.

3.6. Conclusions

In this chapter, optical signal detection for an IM/DD system operating in the turbulent atmosphere has been studied. Atmospheric turbulence has been modeled as a lognormal process, which is applicable for weak turbulence. The photoelectron count statistics have been used in the calculations and simulations, so that the signal shot

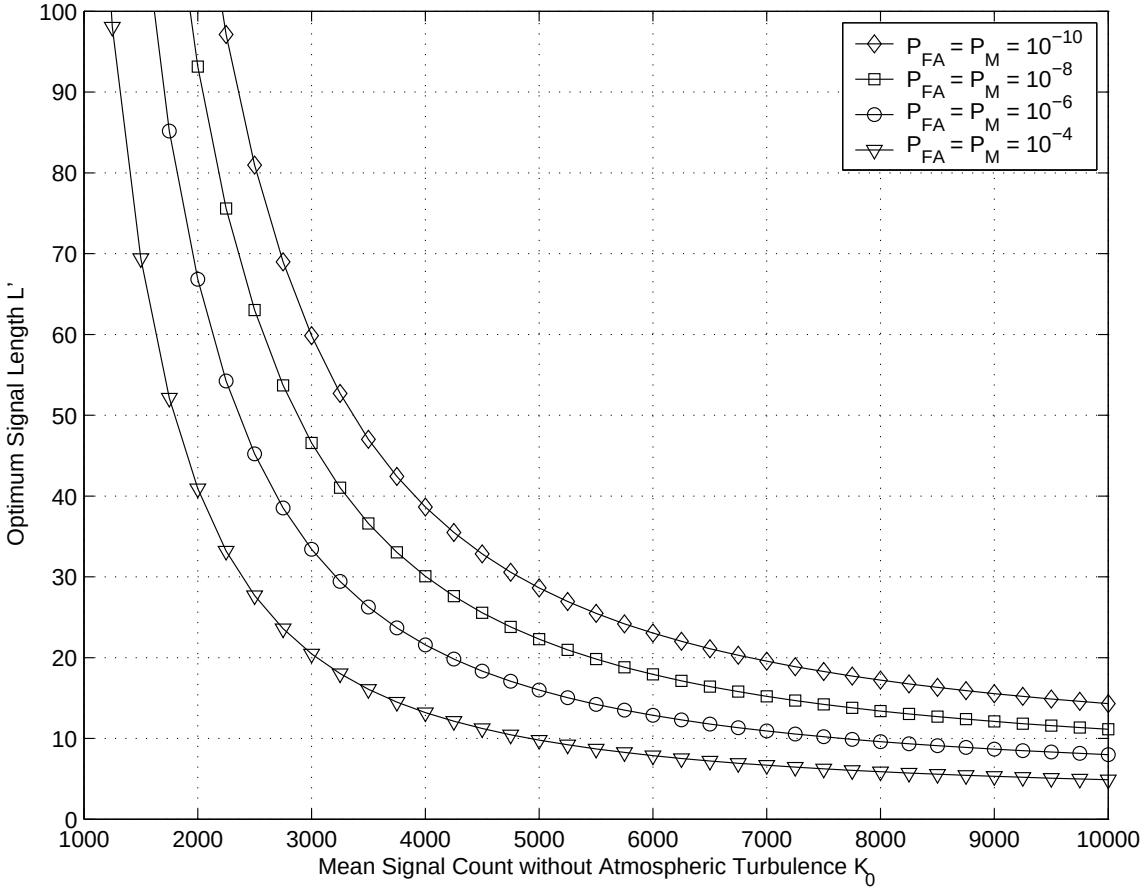

Figure 3.8: Optimum signal length L^o for different detection probabilities assuming the log-amplitude signal fluctuation $\sigma_\chi = 0.20$, data rate $R_b = 2.4$ Gb/s, load resistance $R_L = 50\ \Omega$, receiver temperature $T = 295$ K and mean background noise count $K_b = 10$.

noise inherent in the photodetection process is included in the results. Scintillation of the received signal caused by atmospheric turbulence results in a photoelectron count that is a conditional Poisson process in which the mean count is lognormal. Using these statistics, a normal approximation has been found for this conditional Poisson distribution. The normal approximation provides a means to a quick and simple calculation of the probability of miss in thermal electronic noise which matches well with simulations. After measuring or calculating the mean signal and background radiation photoelectron counts, the system designer can use the equations for probabilities

of miss and false alarm to find settings for the signal length and detection threshold so that system specifications for detection performance are met.

The model developed in this chapter relied on the lognormal model for the distribution of the intensity fading caused by atmospheric turbulence, which is valid in the weak scintillation regime. In the case of strong turbulence, the distribution is no longer lognormal and a different model such as the K or gamma-gamma distribution must be used. Further work is needed to investigate the signal detection performance using photoelectron count statistics and assuming strong atmospheric turbulence.

Chapter 4

Detection Statistics for Optical Signal Through Weak Turbulence Using Avalanche Photodiode

4.1. Introduction

Optical communications through the atmosphere is an appealing technology for various applications such as last-mile broadband service [**5**], airborne communications [**24**] and mobile battlefield communications [**39**]. One difficulty associated with free-space optical communications is atmospheric turbulence which causes random fluctuations or scintillation of the received optical intensity. Scintillation can deteriorate the performance of the communications system. As a result, much work has gone into determining how to mitigate the effects of atmospheric turbulence in these systems.

One technique that is often employed in optical communications systems is packet-switching, in which information is transmitted in packets. The first operation that must be performed in a packet-switched receiver is the detection of the packet preamble, which is a predetermined binary sequence at the beginning of the packet. After packet detection, synchronization, estimation and demodulation of the signal are carried out. The decision of the packet detector whether or not the signal is present is described by the following discrete hypothesis test:

$$\begin{aligned} H_0 &: v_k = ek_{2,k}(I_b, g) + n_k, \;\; k = 1, 2, \ldots, L \\ &\quad \text{versus} \\ H_1 &: v_k = ek_{2,k}(I_s(\chi), I_b, g)d_k + n_k, \;\; k = 1, 2, \ldots, L, \end{aligned} \tag{4-2}$$

where $\underline{v} = [v_1, v_2, \ldots, v_L]$ is the observation vector which represents the photoelectron count plus thermal noise, $\{n_k\}$ are samples of an additive white Gaussian noise (AWGN) process representing the thermal noise of the receiver, L is the signal length, e is the electron charge, $\underline{d} = [d_1, d_2, \ldots, d_L]$ is the sequence to be detected and $\{k_2\}$ are samples from a discrete stochastic process representing the photoelectron count. Under H_0, the signal has not arrived and k_2 is dependent upon the background radiation intensity I_b and the random photomultiplication gain g. Under H_1, the signal is present and k_2 is additionally dependent upon the optical signal intensity I_s, which is subject to atmospheric turbulence represented by χ. In order to properly design the signal detector the probabilities of miss, the false rejection of H_1, and false alarm, the false rejection of H_0, must be calculated or simulated so that an appropriate signal length and detection threshold can be determined.

As a result of atmospheric turbulence, the optical signal intensity I_s is a random process. Many different models have been proposed for the distribution of the intensity of an optical wave propagating through atmospheric turbulence. The lognormal model has been experimentally verified to apply to the weak atmospheric turbulence case [**13**, **29**]. For strong turbulence, the K-distribution has been shown to fit [**32**] and the gamma-gamma distribution, of which the K-distribution is a special case, has been introduced as a model that can be used for weak to strong turbulence [**31**]. In this study, the lognormal model is used. However, the method used herein to calculate the probability of miss is applicable to any model for which the probability density function (PDF) of the turbulence-induced intensity fluctuations is available.

In this chapter, the system under consideration is a intensity modulated, direct detection (IM/DD) optical wireless communications system employing on-off keying (OOK) modulation. When building the optical communications system the designer can choose from two types of photodetectors: p-i-n photodiodes or avalanche photodiodes (APDs). These two devices operate in fundamentally different ways and,

as a result, the communication channel model depends upon which one is used. Besides optical communications through the atmosphere, this study is also applicable to detection statistics for laser radar [**3**, **4**, **40**]. The single-symbol detection statistics for a p-i-n photodiode in lognormal atmospheric turbulence are given in [**4**] and extended to the multiple-symbol case in [**41**, **42**]. In [**3**], the detection statistics in atmospheric turbulence are given for a system using a photomultiplier tube. For APDs, the single-symbol detection statistics in the absence of atmospheric turbulence are reported in [**4**, **40**]. (In [**40**], atmospheric turbulence is acknowledged, but not included in the calculations.) In this study, the multiple-symbol detection statistics in atmospheric turbulence are reported for optical communications systems employing APDs.

Owing to the complexity of the exact distribution of the photoelectron count in an APD [**43**, **44**], many different methods have been proposed for calculating or estimating the performance of APD-based systems including a modified Chernoff bound, saddlepoint approximation, large deviations theory and Gaussian approximation (see [**45**] and references therein). The Webb distribution [**46**] is an approximation for the exact distribution which simplifies calculations. In this chapter, the probabilities of miss and false alarm will be found by numerical integration using the characteristic function of the Webb distribution, which was formulated in [**45**].

This chapter proceeds with a description of the system model in Section 4.2, derivations of the probabilities of miss and false alarm in Section 4.3, a discussion about the signal length and detection threshold settings in Section 4.4 and a brief conclusion in Section 4.5.

4.2. System Model

The system model for a optical communications through atmospheric turbulence is given in Fig. 4.1. In this system an information source is fed into an electrical

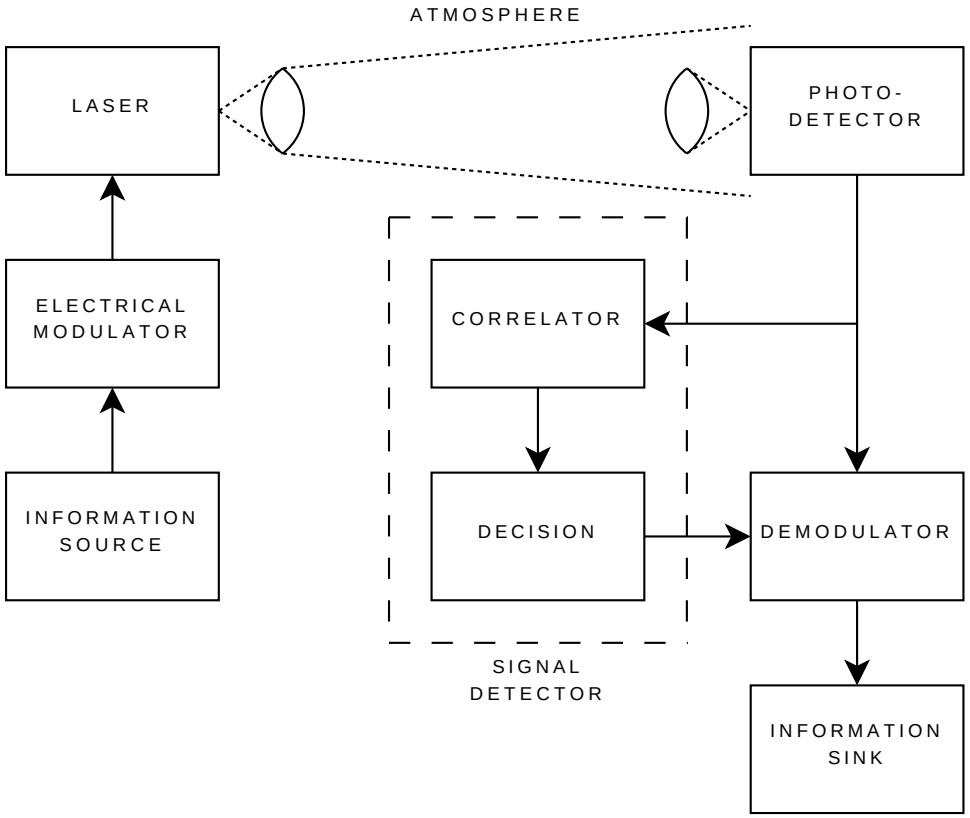

Figure 4.1: Block diagram for optical communications system through the turbulent atmosphere.

modulator. The electrical signal directly modulates a laser, whose light is transmitted through an optical front end. After propagation through the atmosphere, the light is focused by the receiver's optics onto a photodetector, which is an APD. Within the APD, the received light is converted into electrical current through the process of photodetection and the current is increased through the process of photomultiplication. The light-induced current is then fed into a signal detector to determine if the signal has arrived. If the detector determines that the signal has arrived, it triggers the demodulator to recover the information from the remainder of the signal.

4.2.1. Received Signal. In an IM/DD optical wireless communication system using OOK, the received field intensity is

$$I_r(u,t) = I_s(u,t)\sum_{i=1}^{L} d_i g(t - iT_s) + I_b(u,t), \tag{4-3}$$

where $I_s(u,t)$ is the received signal intensity, $g(t)$ is the shaping pulse, T_s is the symbol time and $I_b(u,t)$ is the background radiation intensity. Due to atmospheric turbulence, $I_s(u,t)$ is a stationary stochastic process representing optical scintillation.

The scintillation process is a result of fluctuations in the atmospheric index of refraction caused by turbulence. In [**27**], it is shown that the received optical field intensity in weak turbulence is represented as

$$I_s(u,t) = I_0 e^{2\chi(u,t)}, \tag{4-4}$$

where I_0 is the free-space solution to Maxwell's equations for the field intensity and $\chi(u,t)$ is the log-amplitude fluctuation, which is a stationary normal random process with mean $\overline{\chi}$, autocorrelation function $R_\chi(\tau)$ and average power $R_\chi(0) = \sigma_\chi^2$. Fixing $t = t_0$, a sample of the lognormal process $I_s(u,t_0)$ has a PDF given by

$$f_I(I) = \frac{1}{\sqrt{8\pi}\sigma_\chi I}\exp\left[-\frac{(\ln(I/I_0) - \overline{\chi})^2}{8\sigma_\chi^2}\right]. \tag{4-5}$$

For energy conservation, which requires that atmospheric turbulence neither amplifies nor attenuates the signal,

$$E[I] = I_0 e^{2\overline{\chi}+2\sigma_\chi^2} = I_0 \tag{4-6}$$

where $E[\cdot]$ denotes the expectation, so that $\overline{\chi} = -\sigma_\chi^2$. Experimental studies have been conducted in which data have shown that intensity fluctuations due to weak atmospheric turbulence follow a lognormal distribution [**12**].

The normalized variance of the optical intensity, which is called the scintillation index, is commonly used to measure the strength of the atmospheric turbulence. For

the lognormal distribution, the scintillation index is given by

$$\frac{E[I^2]}{(E[I])^2} - 1 = e^{4\sigma_\chi^2} - 1. \tag{4-7}$$

Since the lognormal distribution is valid when the scintillation index is less than 1 [**9**], this chapter will use $\sigma_\chi \in [0, 0.4]$.

4.2.2. Photoelectron Count Statistics. The theory of photoelectron count statistics in semiconductor photodetectors is well-developed [**8**]. In order to find the electric current induced by the optical signal, the mean number of primary electrons that will be emitted over the observation volume $V = A_d \times T_s$ must be determined, where A_d is the area of photodetecting surface. Primary electrons are those which are released from the photodetector surface as a result of the absorption of photons. The mean number of primary electrons over V is

$$\overline{k_1} = \frac{\eta}{h\nu} \int_V I_r(u,t) dV, \tag{4-8}$$

where η is the quantum efficiency of the photosensitive material, h is Planck's constant and ν is the optical frequency. During an "on" symbol and an "off" symbol the mean count is

$$\overline{k_1} = \begin{cases} K_s + K_b, & d_i = 1 \\ K_b, & d_i = 0, \end{cases} \tag{4-9}$$

respectively, where K_s is the average signal electron count and K_b is the average background noise electron count. Since the atmospheric turbulence channel is a slow fading channel, it can be assumed that the value of I_s is constant throughout V and

$$K_s = \frac{\eta}{h\nu} A_d T_s I_s, \tag{4-10}$$

which means K_s is also a lognormal random variable. For convenience, K_0 is defined as the mean signal electron count without atmospheric turbulence so that $K_s = K_0 e^{2\chi}$.

In a photodetector which receives a constant optical field intensity, the number of primary electrons k_1 is a Poisson distribution given by

$$P[k_1 = k] = \text{Pois}(k, \overline{k_1}) = \frac{\overline{k_1}^k}{k!} e^{-\overline{k_1}}. \tag{4-11}$$

After photomultiplication in the APD, the total output electron count is k_2 with probability

$$P[k_2] = \sum_{k_1=0}^{\infty} P[k_2|k_1]P[k_1], \tag{4-12}$$

where $P[k_2|k_1]$ is the conditional probability of k_2 given k_1 primary electrons. McIntyre has derived [**43**] and Conradi has experimentally verified [**44**] that

$$P[k_2|k_1] = \frac{k_1\Gamma\left(\dfrac{k_2}{1-\gamma}+1\right)}{k_2(k_2-k_1)!\Gamma\left(\dfrac{\gamma k_2}{1-\gamma}+1+k_1\right)} \left[\frac{1+\gamma(\overline{g}-1)}{\overline{g}}\right]^{k_1+\gamma k_2/(1-\gamma)} \left[\frac{(1-\gamma)(\overline{g}-1)}{\overline{g}}\right]^{k_2-k_1}, \tag{4-13}$$

where $\Gamma(\cdot)$ is the gamma function, γ is the ionization coefficient of the semiconductor and $\overline{g}$ is the mean gain. When k_1 is Poisson distributed, the Webb distribution [**46**] is used as an approximation for (4-12). The density of the Webb distribution is

$$P_W(k_2) = \frac{1}{\sqrt{2\pi\overline{k_1}\overline{g}^2 F}\left(1+\dfrac{k_2-\overline{g}\overline{k_1}}{\overline{k_1}\overline{g}F/(F-1)}\right)^{3/2}} \exp\left[-\frac{\left(k_2-\overline{g}\overline{k_1}\right)^2}{2\overline{k_1}\overline{g}^2 F\left(1+\dfrac{k_2-\overline{g}\overline{k_1}}{\overline{k_1}\overline{g}F/(F-1)}\right)}\right], \tag{4-14}$$

where

$$F = \frac{\overline{g^2}}{\overline{g}^2} = \gamma\overline{g} + \left(2-\frac{1}{\overline{g}}\right)(1-\gamma) \tag{4-15}$$

is the excess noise factor of the APD. If $\overline{k_1}F \gg 1$, then (4-14) approaches the Gaussian density [**47**] given by

$$P_G(k_2) = \frac{1}{\sqrt{2\pi\overline{g}^2\overline{k_1}F}} \exp\left[-\frac{\left(k_2-\overline{g}\overline{k_1}\right)^2}{2\overline{g}^2\overline{k_1}F}\right]. \tag{4-16}$$

When possible, (4-14) and (4-16) will be used to derive expressions for the probability of miss in the next section.

4.2.3. Signal Detector. The output current of the photodetector is

$$i(t) = i_p(t) + i_n(t), \tag{4-17}$$

where $i_p(t)$ is the photo-generated current and $i_n(t)$ is the thermal noise current. Note that $i_p(t)$ is the result of the received signal and background radiation. This current is passed to the signal detector.

The optimum signal detector is found by computing the likelihood ratio [**15**] of the hypothesis test of (4-2) given by

$$L(\underline{v}) = \frac{E_\chi \left[E_g \left[f_n \left(\underline{v} - \underline{k}_2(I_s(\chi), I_b, g) \right) \right] \right]}{E_g \left[f_n(\underline{v} - \underline{k}_2(I_b, g)) \right]}, \tag{4-18}$$

where $E_x[\cdot]$ denotes expectation with respect to x and $f_n(\cdot)$ is the PDF of the AWGN. Since the photoelectron counts are assumed independent from symbol to symbol, (4-18) is equivalent to

$$L(\underline{v}) = \prod_{i=1}^{L} \frac{E_\chi \left[E_g \left[f_n \left(v_i - k_{2,i}(I_s(\chi), I_b, g) \right) \right] \right]}{E_g \left[f_n(v_i - k_{2,i}(I_b, g)) \right]}. \tag{4-19}$$

A closed form expression for (4-19) could not be found and, therefore, neither could the optimum detector. Instead, the suboptimum but simple correlation detector [**15**] will be employed.

The signal detector is composed of an integrator which integrates the current in T_s second intervals, a correlator and a threshold comparator. The output of the ith integration is

$$v_i = ek\left(iT_s, (i+1)T_s\right) + v_{n,i}, \tag{4-20}$$

where e is the electron charge, T_s is the symbol time, $k(t_1, t_2)$ is the number of electrons generated in the time interval (t_1, t_2) as a result of photodetection and $v_{n,i}$ is

the integrated thermal noise current. For clarity, k_i is used to denote $k\left(iT_s,(i+1)T_s\right)$ throughout the remainder of this chapter. The current integrations are passed into a register which holds L integrations, where L is the length of the signal to be detected. The contents of the register are multiplied by the binary sequence to be detected and summed to obtain

$$v=\sum_{i=1}^{L} d_i\left(ek_i+v_{n,i}\right), \tag{4-21}$$

where $\{d_i\}_{i=0}^{L-1}$ is the binary sequence. Finally, v is compared to a threshold v_T to determine if the signal was received.

If the signal was sent, but $v<v_T$, then a miss detection occurs. Hence, the probability of miss is

$$P_M(v_T)=P\left[v_s<v_T\right], \tag{4-22}$$

where v_s represents the correlator output when the signal was sent. If the signal was not sent and $v>v_T$, then a false alarm occurs. If v_n represented the correlator output when no signal was transmitted and the detector correlates with only noise, the probability of false alarm is

$$P_{FA}(v_T)=P\left[v_n>v_T\right]. \tag{4-23}$$

4.3. Probabilities of Miss and False Alarm

In this section the probability of miss and the probability of false alarm are formulated. Since the modulation scheme is OOK, the "off" symbols drop out in (4-21) and

$$v=\sum_{i=1}^{L'} ek_i+v_{n,i}, \tag{4-24}$$

where L' is the Hamming weight of the binary sequence to be detected. The k_i's are independent. Also, the thermal electronic noise is independent from the photoelectron count. Therefore, to find the probability of miss and the probability of false

alarm, one must determine the cumulative distribution function (CDF) and complementary cumulative distribution function (CCDF) of the sum of L' independent random variables, respectively.

The analysis and results of this study are not only applicable to IM/DD systems using OOK, but also to systems using subcarrier binary phase shift keying (BPSK). As pointed out in [**41**], the difference is that the upper limit in the sum of (4-24) is the binary sequence length for subcarrier BPSK as opposed to the Hamming weight for OOK. Also, for ac-coupled systems such as subcarrier BPSK, the background radiation is filtered out ($K_b = 0$) as long as the lower cutoff frequency of the receiver pass band is high enough.

4.3.1. Quantum Limited Detection. In the absence of thermal electronic noise (or if it is negligible), the probability of miss is

$$P_M(k_T) = P\left[\sum_{i=1}^{L'} k_{2,i} < k_T\right]. \tag{4-25}$$

First, (4-25) will be calculated for the zero turbulence case using the Webb and Gaussian densities for k_2 given in (4-14) and (4-16), respectively.

In [**48**], it is shown that the Webb density is an inverse Gaussian density. The result of [**48**] is briefly summarized here as it is required to find (4-25). The PDF of an inverse Gaussian random variable X is

$$f_X(x;\mu,\beta) = \begin{cases} \sqrt{\dfrac{\beta}{2\pi}} x^{-3/2} \exp\left[\dfrac{-\beta\left(x-\mu\right)^2}{2\mu^2 x}\right], & x > 0 \\ 0, & o.w. \end{cases} \tag{4-26}$$

To indicate that X is distributed as an inverse Gaussian random variable with parameters μ and β, one writes $X \sim IG(\mu, \beta)$. The CDF of X is

$$F_X(x;\mu,\beta) = \frac{1}{2}\left[1+\text{erf}\left(\sqrt{\frac{\beta}{2x}}\left(-1+\frac{x}{\mu}\right)\right)\right]+\frac{e^{2\beta/\mu}}{2}\left[1+\text{erf}\left(-\sqrt{\frac{\beta}{2x}}\left(1+\frac{x}{\mu}\right)\right)\right], \tag{4-27}$$

where

$$\text{erf}(x) = \frac{2}{\sqrt{\pi}}\int_0^x e^{-t^2}dt \tag{4-28}$$

is the error function.

By substituting

$$X = 1+\left(\frac{k_2 - K_0\overline{g}}{\sigma\lambda}\right) \tag{4-29}$$

in (4-14), where $\sigma^2 = K_0\overline{g}^2F$ and $\lambda = \sqrt{K_0F}/(F-1)$, the density of X is

$$f_X(x;1,\lambda^2) = \begin{cases} \dfrac{\lambda}{\sqrt{2\pi}}x^{-3/2}\exp\left[\dfrac{-\lambda^2(x-1)^2}{2x}\right], & x>0 \\ 0, & o.w. \end{cases} \tag{4-30}$$

Since (4-25) involves a sum of Webb random variables (or inverse Gaussian random variables), the following property of inverse Gaussian random variables is required [**49**]: If $X_i \sim IG(\mu w_i, \beta w_i^2)$, $i = 1, 2, \ldots, n$ and the X_i are independent, then

$$S = \sum_{i=1}^{n} X_i \sim IG(\mu\overline{w}, \beta\overline{w}^2), \tag{4-31}$$

where

$$\overline{w} = \sum_{i=1}^{n} w_i. \tag{4-32}$$

Thus, the sum of L' i.i.d. random variables represented by (4-29) and (4-30) is given by

$$T = \sum_{i=1}^{L'} X_i \sim IG\left(L', (\lambda L')^2\right). \tag{4-33}$$

Therefore, the quantum limited probability of miss calculated using the Webb approximation is

$$\begin{aligned} P_M(k_T) &= P\left[\sum_{i=1}^{L'}\left(K_0\overline{g}+\sigma\lambda(X_i-1)\right)<k_T\right] \\ &= P\left[\sum_{i=1}^{L'}X_i<\frac{k_T}{\sigma\lambda}-L'\left(\frac{K_0\overline{g}}{\sigma\lambda}-1\right)\right] \\ &= F_X\left(\frac{k_T}{\sigma\lambda}-L'\left(\frac{K_0\overline{g}}{\sigma\lambda}-1\right);L',(\lambda L')^2\right). \end{aligned} \tag{4-34}$$

The quantum limited probability of miss calculated using the Gaussian approximation is

$$P_M(k_T)=\frac{1}{2}\left[1+\operatorname{erf}\left(\frac{k_T-L'\overline{g}K_0}{\sqrt{2L'\overline{g}^2K_0F}}\right)\right]. \tag{4-35}$$

The probability of miss calculated using (4-34) and (4-35) are presented in the next section along with simulation results.

4.3.2. Detection in Thermal Electronic Noise. In most communications systems such as a terrestrial optical system transmitting through the atmosphere, the electrical equipment operates at room temperature and the transmitter's power is limited so that the thermal electrical noise is nonnegligible. Thus, the probability of miss is

$$P_M(v_T)=P\left[\sum_{i=1}^{L'}ek_{2,i}^{s+n}+v_{n,i}<v_T\right], \tag{4-36}$$

where each thermal noise integration v_n is a zero-mean random variable with variance

$$\sigma_n^2=\frac{2k_BT}{R_L}T_s, \tag{4-37}$$

k_B is Boltzmann's constant, T is the receiver's temperature, R_L is load resistance and T_s is the symbol time. The superscript $s+n$ refers to the fact that the photoelectron count k_2 is the result of the signal and background noise.

In the absence of atmospheric turbulence, if the distribution of k_2 is assumed to follow the Gaussian approximation of (4-16), then the sum in (4-36) is a sum of Gaussian random variables and the probability of miss is easily calculated as

$$P_M(v_T) = \frac{1}{2}\left[1 + \text{erf}\left(\frac{v_T - eL'\bar{g}K_0}{\sqrt{2L'\left(\sigma_n^2 + e^2L'\bar{g}^2K_0F\right)}}\right)\right]. \tag{4-38}$$

In the presence of atmospheric turbulence, the scintillation of the signal is accounted for by averaging the characteristic function of the secondary photoelectron count k_2 over the PDF of the signal intensity or, equivalently, the PDF of the log-amplitude signal fluctuation χ. Therefore, to find the average Webb characteristic function of k_2 over χ, the following integral is computed:

$$\Phi_k(\omega) = \int_{-\infty}^{\infty} \Phi_W(\omega) f_\chi(x) dx, \tag{4-39}$$

where

$$\Phi_W(\omega) = \exp\left\{\frac{(K_0e^{2\chi} + K_b)F}{(F-1)^2}\left[1 - \sqrt{1 - 2(F-1)\bar{g}j\omega}\right] - \frac{(K_0e^{2\chi} + K_b)\bar{g}}{F-1}j\omega\right\} \tag{4-40}$$

is the characteristic function of the Webb distribution [**45**]. Since the photoelectron counts and the thermal noise are independent, the characteristic function of v is

$$\Phi_v^{s+n}(\omega) = \left[\Phi_k(\omega)\Phi_n(\omega)\right]^{L'}. \tag{4-41}$$

where $\Phi_n(\cdot)$ is the characteristic function of the AWGN. The CDF of v, which is the probability of miss, can be calculated numerically by inserting (4-41) into

$$P_M(v_T) = \frac{1}{2} + \frac{1}{\pi}\int_0^{\infty} \frac{\sin(\omega v_T)\text{Re}\left\{\Phi_v^{s+n}(\omega)\right\}}{\omega} - \frac{\cos(\omega v_T)\text{Im}\left\{\Phi_v^{s+n}(\omega)\right\}}{\omega} d\omega, \tag{4-42}$$

where $\text{Re}\{\cdot\}$ and $\text{Im}\{\cdot\}$ refer to the real and imaginary parts of the argument, respectively [**50**].

In the event of a false alarm, no signal is present so that only background photoelectrons and thermal noise integrations are present in the correlator. Therefore, the probability of false alarm is

$$\begin{aligned} P_{FA}(v_T) &= P\left[\sum_{i=1}^{L'} ek_{2,i}^n + v_{n,i} > v_T\right] \\ &= \frac{1}{2} - \frac{1}{\pi}\int_0^\infty \frac{\sin(\omega v_T)\mathrm{Re}\left\{\Phi_v^n(\omega)\right\}}{\omega} - \frac{\cos(\omega v_T)\mathrm{Im}\left\{\Phi_v^n(\omega)\right\}}{\omega} d\omega, \end{aligned} \tag{4-43}$$

where

$$\Phi_v^n(\omega) = \left[\Phi_W(\omega, K_0 = 0)\Phi_n(\omega)\right]^{L'} \tag{4-44}$$

is the characteristic function of the sum when no signal is present. When the background radiation is negligible ($K_b = 0$), the probability of false alarm is simplified to

$$\begin{aligned} P_{FA}(v_T) &= P\left[\sum_{i=1}^{L'} v_{n,i} > v_T\right] \\ &= \frac{1}{2}\left[1 - \mathrm{erf}\left(\frac{v_T}{\sqrt{2L'\sigma_n^2}}\right)\right]. \end{aligned} \tag{4-45}$$

4.4. Determination of Signal Length and Detection Threshold

Appropriate settings for the signal length L' and detection threshold v_T are critical in the design of a packet-switched system. The goals are 1) to minimize L' while maintaining required detection performance and 2) to determine v_T such that the probabilities of miss and false alarm are below the required performance. First, a simple quantum-limited example will be presented and then an example with thermal electronic noise. Table 4.1 lists the parameters that were used for the APD characteristics and the thermal noise in the calculations that were made for the figures.

Table 4.1: APD and Thermal Noise Parameters

mean photomultiplication gain	$\overline{g}$	100
ionization coefficient	γ	0.028
bit rate	R_b	2.4 Gb/s
receiver temperature	T	295 K
load resistance	R_L	50 Ω

Fig. 4.2 shows the probability of miss versus normalized threshold $k_N = k_T/(L'\overline{g}K_0)$ for a zero-turbulence, quantum-limited system in which the signal length $L' = 8$ and the mean signal count $K_0 = 10$ and 100. The probability of miss has been calculated using (4-34) and (4-35), which use the Webb approximation and Gaussian approximation, respectively. Also, displayed is the probability of miss found as a result of simulations using the MC distribution. The Webb approximation is better than the Gaussian approximation in both cases. However, the Gaussian approximation improves as the photoelectron count increases.

Fig. 4.3 illustrates the probability of miss in atmospheric turbulence, modeled using the lognormal distribution, when the background noise count $K_b = 2$ and thermal electronic noise is present. The probability of miss was found by simulation using the MC distribution and by numerical integration using (4-42), in which the Webb distribution was used. It is apparent from the plot how well the probability of miss is approximated using the Webb distribution for the photoelectron count.

In order to determine the proper setting for the signal length L' and detection threshold k_T, one might assume the worst case fading ($\sigma_\chi = 0.4$) and plot the probabilities of false alarm and miss versus the normalized threshold k_N for different signal lengths. Such a plot is given in Fig. 4.4 for four different signal lengths. For a given signal length the best threshold setting would be at the point where $P_M = P_{FA}$. If the intersection point is below the required detection performance, then that signal length is sufficient. If, for example, the system designer required $P_{FA} < 10^{-7}$, by looking at Fig. 4.4, he or she can see that if $L' = 8$, the $P_M = P_{FA}$ at about 10^{-4}

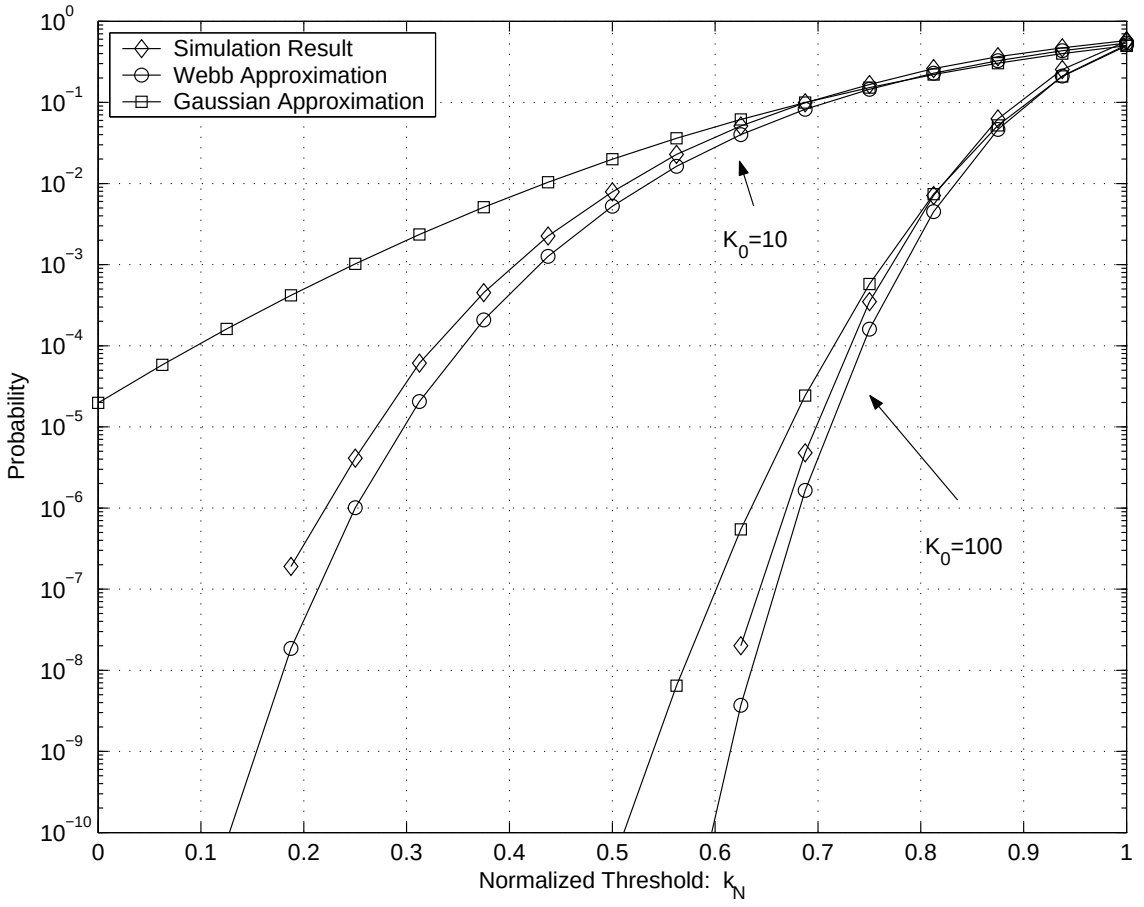

Figure 4.2: Quantum limited probability of miss calculated using the Webb approximation (Eq. (4-34)) and the Gaussian approximation (Eq. (4-35)) for (4-12). The simulation results, in which the MC distribution was used in (4-12), are also plotted. The parameters used were mean signal count $K_0 = 10$ and 100 and signal length $L' = 8$.

and, therefore, $L' = 8$ is not sufficient. When $L' = 16$, however, $P_M = P_{FA}$ below 10^{-7}. Thus, $L' = 16$ and $k_N \approx 0.23$ are appropriate choices for this example.

4.5. Conclusions

In this chapter, the performance of a correlation detector in an optical communications system operating through the turbulent atmosphere and employing an APD has been studied. The effect of the atmospheric turbulence on the transmitted optical

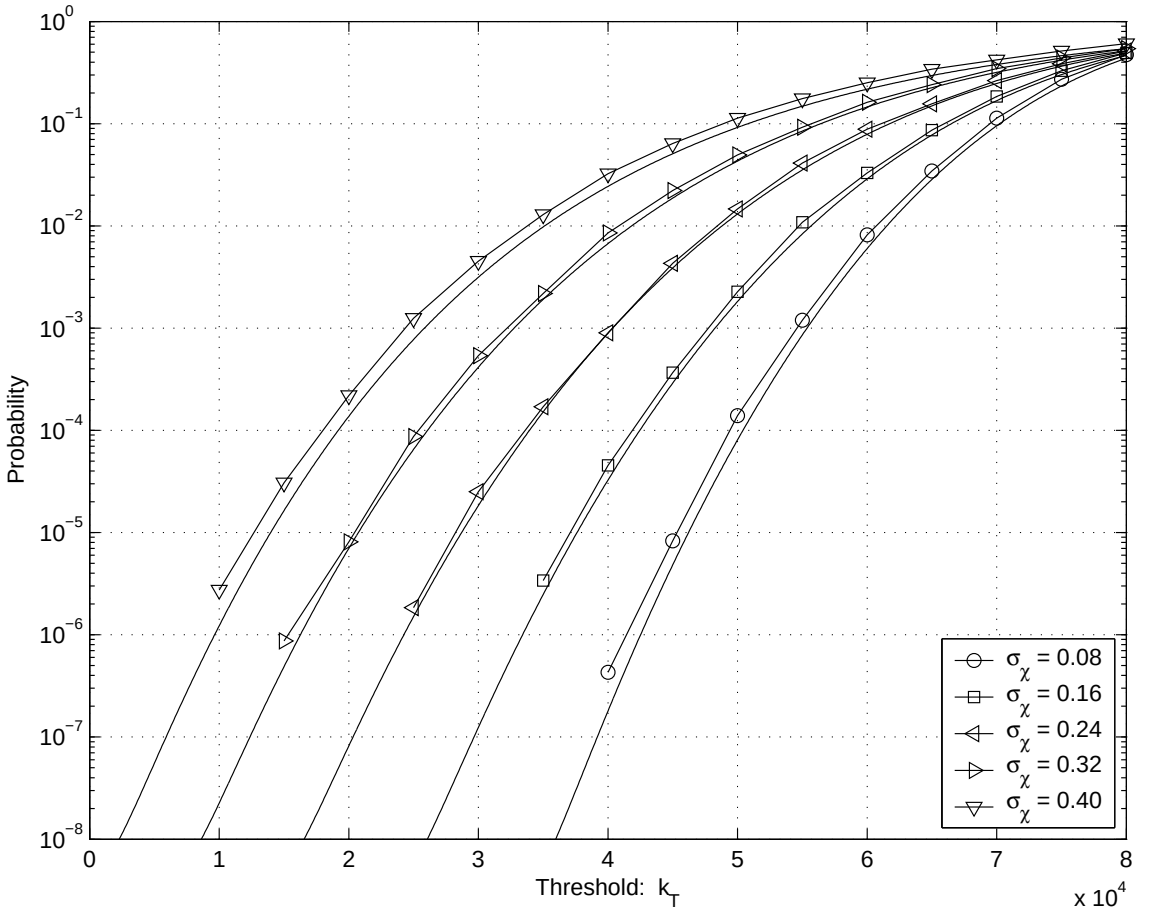

Figure 4.3: Probability of miss in atmospheric turbulence. The lines with circles, squares and triangles were found by simulation using the MC distribution for the total electron count given by (4-13). The bare lines were calculated using numerical integration using the Webb distribution. The parameters used were $L' = 8$, $\sigma_\chi \in \{0.08, 0.16, 0.24, 0.32, 0.40\}$, $K_b = 2$ and $K_0 = 100$.

signal has been modeled as a lognormal random process and, therefore, the results are applicable to weak turbulence. Using the Webb and Gaussian approximations for the APD photoelectron count the probability of miss has been derived for the zero-turbulence, quantum-limited case. In the case of detection in atmospheric turbulence and thermal electronic noise, the probability of miss is simulated using the MC distribution for the APD photoelectron count and compared to the probability of miss calculated using numerical integration, in which the Webb characteristic function is

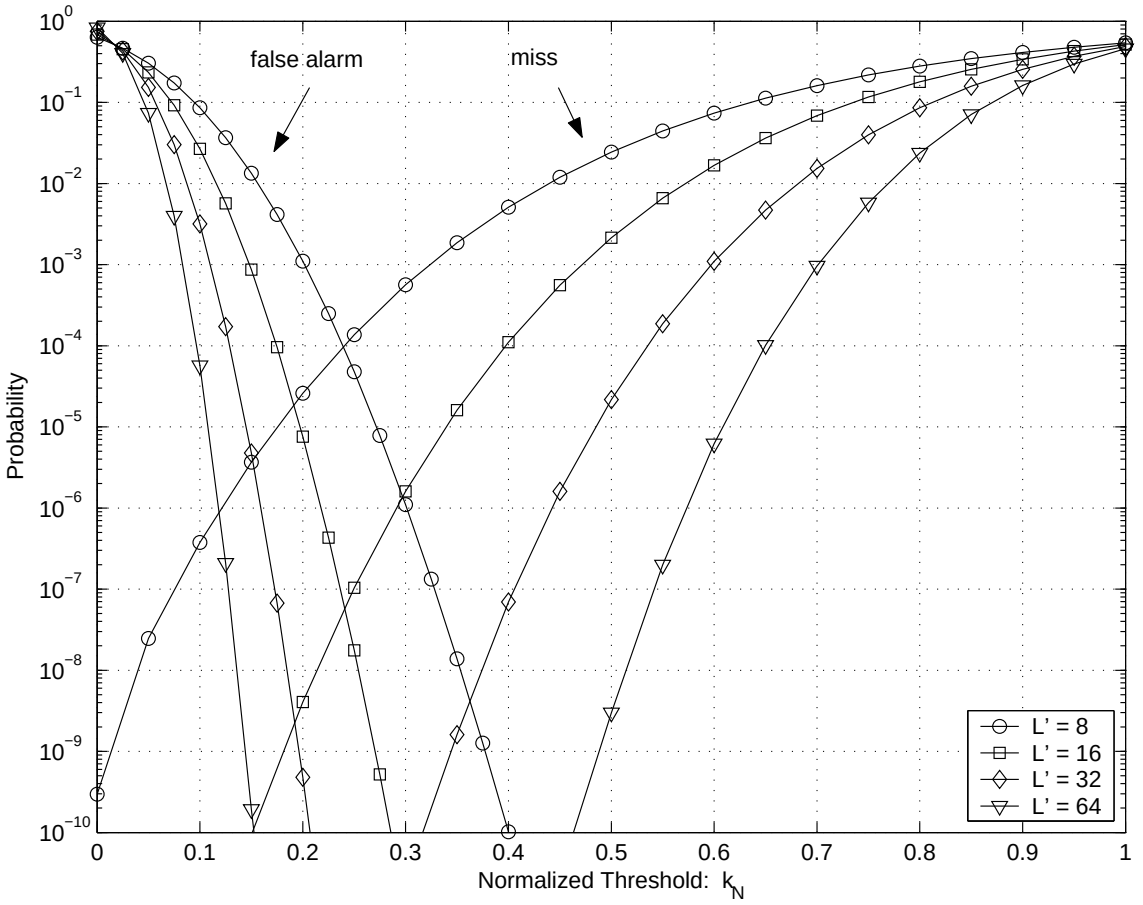

Figure 4.4: Probabilities of miss and false alarm for signal lengths $L' \in \{8, 16, 32, 64\}$ and log-amplitude signal standard deviation $\sigma_\chi = 0.40$. The parameters used were $K_b = 2$ and $K_0 = 100$.

used. The faster numerical integration is shown to provide accurate approximation to the more time-consuming simulation method. Using the methods described in this chapter, the system designer can find appropriate values for the signal detector's signal length and detection threshold in an APD based IM/DD optical wireless communications system.

Chapter 5

Detection Statistics for Optical Signal Through Strong Turbulence

5.1. Introduction

Atmospheric turbulence, which results from small temperature variations, causes signal intensity fluctuations called scintillation at the receiver and can significantly impair communications performance. Many models have been proposed for the effect of atmospheric turbulence on a propagating optical wave, which lead to a probability density function (PDF) for the scintillation or fade statistics at the receiver [**51**]. The first and most widely utilized model is the lognormal PDF which is applicable to weak turbulence conditions. For weak to strong turbulence, the gamma-gamma model introduced in [**52**] and based on theory in [**31**] has gained acceptance as a reputable model due to its good agreement with simulation and experiment and the ease with which it can be fit to measured turbulence data. Many studies of performance of OWC in the presence of atmospheric turbulence represented by the gamma-gamma model have been carried out including [**53**–**55**]. These studies are focused on demodulation and decoding performance in the presence of gamma-gamma atmospheric turbulence.

Before estimation, demodulation or decoding can be performed, however, the signal must be detected. In this chapter, the problem that is studied is the determination of the signal length and detection threshold necessary to maintain a satisfactory OWC link in the presence of gamma-gamma turbulence. In order to determine this the probability of miss in atmospheric turbulence must be calculated and compared to the probability of false alarm. Optical detection statistics in a weak turbulent atmosphere have been reported in [**3**, **4**, **42**] for lognormal statistics. This chapter focuses on strong turbulence and compares the results with moderate turbulence using

the gamma-gamma model. It is assumed that the scintillation fade of each symbol is independent and identically distributed (IID). Therefore, these results are valid for OWC links in which the coherence time of the scintillation fades is less than the symbol interval.

The remainder of this chapter proceeds as follows: Section 5.2 explains the system model for the received signal, atmospheric turbulence and signal detector, Section 5.3 shows how to calculate the probabilities of miss and false alarm, Section 5.4 presents two exercises illustrating how to find the required signal length and detection threshold and Section 5.5 ends the chapter with concluding remarks.

5.2. System Model

Relevant to this study is an intensity modulated, direct detection (IM/DD) optical communications system that employs on-off keying (OOK) [**8**]. The received optical signal and noise is given by

$$s(u,t) = A(u,t)I_s \sum_{i=1}^{L} g(t)d_i + I_b(u,t), \tag{5-2}$$

where u is an event in the sample space, t is time, $A(u,t)$ is the scintillation process resulting from atmospheric turbulence, I_s is the collected signal power in the absence of turbulence, L is the signal length, $g(t)$ is the pulse shape, $\{d_i : d_i \in \{0,1\}\,; i = 1,\ldots,L\}$ is the sequence to be detected and $I_b(u,t)$ is the background radiation.

After photodetection, the current at the output of the photodetector is $i(u,t) = i_s(u,t) + i_b(u,t) + i_n(u,t)$, where $i_s(u,t)$ is due to the received signal light, $i_b(u,t)$ is due to background radiation and $i_n(u,t)$ is due to thermal noise. Using an integrate and dump receiver, the integrated current in one symbol interval T_s is

$$v = eK_s + eK_b + n, \tag{5-3}$$

where e is the electronic charge, K_s is the signal photoelectron count, K_b is the background photoelectron count and n is a zero-mean Gaussian random variable, representing the integrated thermal noise. The variance of n is [**8**]

$$\sigma_n^2 = \frac{2k_B T}{R_L} T_s, \tag{5-4}$$

where k_B is Boltzmann's constant, T is the receiver temperature and R_L is the load resistance.

5.2.1. Atmospheric Turbulence Channel. In clear air conditions micro-fluctuations in temperature create variations in the index of refraction, which is optical turbulence. As an optical beam propagates though turbulence, the wavefront is distorted. This distortion leads to variations in the received power, called scintillation. The strength of the scintillation is quantified by the Rytov variance given by

$$\sigma_R^2 = 1.23 C_n^2 k^{7/6} L_p^{11/6}, \tag{5-5}$$

where C_n^2 is the refractive index structure parameter, $k = 2\pi/\lambda$ is the optical wave number, λ is the laser wavelength and L_p is the propagation distance. Various models have been proposed for C_n^2, but it can be measured [**51**]. For horizontal links near the ground, C_n^2 varies from 10^{-17} for weak turbulence to 10^{-13} for strong turbulence [**56**].

5.2.1.1. *Gamma-Gamma Model.* In the gamma-gamma turbulence model [**52**], the propagating optical wave is subject to large scale turbulent eddies which are modulated by small scale eddies and the received optical intensity is a product $I = xy$, wherein x and y are independent gamma random variables with parameters α and β, respectively. Thus, the probability density function (PDF) for a gamma-gamma random variable A can be found to be

$$f_A(x) = \frac{2}{\Gamma(\alpha)\Gamma(\beta)} \left(\frac{\alpha\beta}{A_0}\right)^{\frac{\alpha+\beta}{2}} x^{\frac{\alpha+\beta}{2}-1} K_{\alpha-\beta}\left(2\sqrt{\frac{\alpha\beta x}{A_0}}\right), \tag{5-6}$$

where $\Gamma(\cdot)$ is the gamma function, $K_\nu(\cdot)$ is the νth order modified Bessel function of the second kind and A_0 is the mean of A. If either α or β equals 1, then (5-6) reduces to the PDF of the K distribution. The normalized variance of the intensity, called the scintillation index, for this PDF is given by

$$\sigma_A^2 = \frac{1}{\alpha} + \frac{1}{\beta} + \frac{1}{\alpha\beta}. \tag{5-7}$$

The parameters α and β are calculated using measured values of C_n^2 and the inner scale diameter l_0, which is the scale of the smallest turbulent eddies. Depending on the turbulence properties, different formulas are available for α and β, but for a plane wave and non-zero inner scale the following two formulas are used [**52**]:

$$\begin{aligned}\frac{1}{\alpha} = \exp\Bigg\{ & 0.16\sigma_R^2 \left(\frac{2.61\eta_l}{2.61 + \eta_l + 0.45\sigma_R^2 \eta_l^{7/6}} \right)^{7/6} \\ & \cdot \left[1 + 1.753 \left(\frac{2.61}{2.61 + \eta_l + 0.45\sigma_R^2 \eta_l^{7/6}} \right)^{1/2} \right. \\ & \left. - 0.252 \left(\frac{2.61}{2.61 + \eta_l + 0.45\sigma_R^2 \eta_l^{7/6}} \right)^{7/12} \right] \Bigg\} - 1\end{aligned} \tag{5-8}$$

$$\frac{1}{\beta} = \exp\left[\frac{0.51\sigma_R^2}{\left(1 + 0.69\sigma_R^{12/5}\right)^{7/6}} \right] - 1, \tag{5-9}$$

where $\eta_l = 10.89(R_F/l_0)^2$ and R_F is the radius of the Fresnel zone. For the examples given in Section 5.4, (5-8) and (5-9) are used.

5.2.1.2. *Negative Exponential Model.* As the path length increases, the scintillation does not increase without bound, instead it saturates at a certain distance [**14**]. In the saturation regime, in which $\sigma_R^2 = 25$, the intensity fluctuations can be modeled as an negative exponential process for which the PDF of a sample is

$$f_A(x) = \frac{1}{A_0} e^{-x/A_0}, \tag{5-10}$$

where A_0 is the mean. The scintillation index for this PDF is $\sigma_A^2 = 1$.

5.2.2. Signal Detection. In this signal detection problem, the goal is to determine if the transmitted optical signal $I_s(u,t)$, which is a stochastic process as a result of atmospheric turbulence, is present in the receiver. In the receiver, the optical signal is converted to an electrical signal by the (p-i-n or APD) photodetector. It is assumed that the turbulence channel is slowly varying so that the number of photo-generated electrons $k_s(u)$ in one symbol interval is Poisson distributed or Webb distributed for p-i-n or APD, respectively. In order to detect the signal, the detector must overcome both the background optical radiation $I_b(u,t)$ and the thermal electronic noise $n(u,t)$.

The detection problem is modeled as the following discrete hypothesis test:

$$\begin{aligned} &H_0 : v_i = eK_{b,i}(I_b, g) + n_i, \;\; i = 1, 2, \ldots, L \\ &\quad \text{versus} \\ &H_1 : v_i = eK_{s,i}(I_s, g)d_i + eK_{b,i}(I_b, g) + n_i, \;\; i = 1, 2, \ldots, L, \end{aligned} \tag{5-11}$$

where v is the current integration during one symbol interval and g is the photomultiplication gain ($g = 1$ for p-i-n). The decision device considered in this chapter is the correlation detector which can be represented as

$$v = \sum_{i=1}^{L} v_i d_i \underset{H_0}{\overset{H_1}{\gtrless}} v_T, \tag{5-12}$$

where v_T is the detection threshold. Assuming that the laser transmits zero energy for a "0" symbol, the "0" symbols do not contribute to the sum in (5-12) and

$$v = \sum_{\{j : d_j = 1\}} v_j. \tag{5-13}$$

The cardinality of the set $\{j : d_j = 1\}$ is the Hamming weight of the sequence $\{d_i : i = 1, \ldots, L\}$ and will be labeled L' in this chapter.

Under (5-11), two types of errors can occur: a miss, when H_1 is true and the detector chooses H_0, and a false alarm, when H_0 is true and the detector chooses H_1. The probability of miss is

$$P_M(v_T) = P\left[v < v_T | H_1 \text{ is true}\right] \tag{5-14}$$

and the probability of false alarm is

$$P_F(v_T) = P\left[v > v_T | H_0 \text{ is true}\right]. \tag{5-15}$$

The goal of this signal detection problem is to determine the signal length L' and detection threshold v_T necessary to stay below a certain probability of miss, while staying below a set probability of false alarm. In order to find these settings the probabilities of miss and false alarm must be calculated.

5.3. Probabilities of Miss and False Alarm

Computing the probabilities of miss and false alarm for the test in (5-12) is equivalent to calculating the cumulative distribution function (CDF) and complementary cumulative distribution function (CCDF) of the sum in (5-12), respectively. Under the assumption of independence between symbol integrations, which is valid for channels in which the symbol time is less than the atmospheric coherence time ($T_s < \tau_0$), the CDF and CCDF will be calculated using the method of characteristic functions (CFs), i.e., the CFs for each symbol integration will be computed, they will be multiplied together and finally, the CDF and CCDF will be computed using an inversion formula.

5.3.1. Conditional Poisson and Webb Counts. For a p-i-n photodiode, the photoelectron count is Poisson distributed, i.e., the probability mass function for the

count in one symbol interval conditioned on the intensity process $\lambda(u,t)$ is

$$p(k|\lambda) = (k!)^{-1} \left(\int_{T_s} \lambda(u,t)dt \right)^k \exp\left(- \int_{T_s} \lambda(u,t)dt \right). \tag{5-16}$$

The quantity $\int_T \lambda dt$ is called the rate of the Poisson process. In this case, the intensity

$$\lambda(u,t) = \frac{\eta}{h\nu} s(u,t) = \xi s(u,t), \tag{5-17}$$

where η is the photodiode quantum efficiency, h is Planck's constant and ν is the laser frequency. Thus, during an "ON" symbol, the intensity $\lambda(u,t) = \xi \left(A(u,t)P_s + I_b(u,t) \right)$. Due to the mathematical intractability of integrating this stochastic process, it is assumed that the signal fade due to scintillation is constant for one symbol interval so that it can be treated as a random variable. Therefore, the intensity $\lambda = \xi \left(AP_s + I_b \right)$ and the rate is $\xi(AP_s + I_b)T_s = Ak_s + k_b$, where k_s is the mean signal count without fading and k_b is the mean background noise count. The Poisson count is now found by computing the expectation over the density of A as

$$E\left[p(k|\lambda)\right] = \int_0^\infty \frac{(xk_s + k_b)^k}{k!} e^{-(xk_s + k_b)} f_A(x)dx, \tag{5-18}$$

where $f_A(\cdot)$ is the fading PDF. Similarly, the Poisson CF averaged over the fading distribution is

$$\begin{aligned} \phi_p(\omega) &= E\left[\exp\left[(Ak_s + k_b)\left(e^{j\omega} - 1 \right) \right] \right] \\ &= \exp\left[k_b(e^{j\omega} - 1) \right] E\left[\exp\left[Ak_s(e^{j\omega} - 1) \right] \right]. \end{aligned} \tag{5-19}$$

As in [**8**], comparing (5-19) to the characteristic function of the fade distribution $\phi_A(\omega) = E\left[e^{j\omega A} \right]$, (5-19) can be written

$$\phi_p(\omega) = \exp\left[k_b(e^{j\omega} - 1) \right] \phi_A(\omega)|_{j\omega \to k_s(e^{j\omega} - 1)}. \tag{5-20}$$

The gamma-gamma characteristic function, which can be found using [**57**, Eq. (6.643.3)] (similar to the calculation in [**54**]), is

$$\begin{aligned}\phi_g(\omega) =& \frac{\Gamma(\beta-\alpha)}{\Gamma(\beta)}\left(\frac{1}{-j\omega}\frac{\alpha\beta}{A_0}\right)^{\alpha}\Phi\left(\alpha, 1+\alpha-\beta; \frac{1}{-j\omega}\frac{\alpha\beta}{A_0}\right) \\ &+ \frac{\Gamma(\alpha-\beta)}{\Gamma(\alpha)}\left(\frac{1}{-j\omega}\frac{\alpha\beta}{A_0}\right)^{\beta}\Phi\left(\beta, 1+\beta-\alpha; \frac{1}{-j\omega}\frac{\alpha\beta}{A_0}\right),\end{aligned} \tag{5-21}$$

where

$$\Phi(a,b;x) = 1 + \frac{a}{b}x + \frac{a(a+1)}{b(b+1)}\frac{x^2}{2!} + \frac{a(a+1)(a+2)}{b(b+1)(b+2)}\frac{x^3}{3!} + \dots \tag{5-22}$$

is the confluent hypergeometric function. Thus, the Poisson CF with gamma-gamma fading is

$$\begin{aligned}\phi_{p,g}(\omega) =& \exp\left[k_b(e^{j\omega}-1)\right]\left[\frac{\Gamma(\beta-\alpha)}{\Gamma(\beta)}\left(\frac{1}{1-e^{j\omega}}\frac{\alpha\beta}{k_sA_0}\right)^{\alpha}\right. \\ &\cdot \Phi\left(\alpha, 1+\alpha-\beta; \frac{1}{1-e^{j\omega}}\frac{\alpha\beta}{k_sA_0}\right) + \frac{\Gamma(\alpha-\beta)}{\Gamma(\alpha)} \\ &\left.\cdot\left(\frac{1}{1-e^{j\omega}}\frac{\alpha\beta}{k_sA_0}\right)^{\beta}\Phi\left(\beta, 1+\beta-\alpha; \frac{1}{1-e^{j\omega}}\frac{\alpha\beta}{k_sA_0}\right)\right],\end{aligned} \tag{5-23}$$

The CF of the exponential distribution is $\phi_e(\omega) = (1 - A_0 j\omega)^{-1}$ and the Poisson CF with exponential fading is

$$\phi_{p,e}(\omega) = \frac{\exp\left[k_b\left(e^{j\omega}-1\right)\right]}{1 - A_0k_s\left(e^{j\omega}-1\right)}. \tag{5-24}$$

In an APD exposed to constant intensity light the photoelectron count is approximated by the Webb distribution [**46**]. Using the same assumption of constant signal

fade for one signal interval, the conditional Webb PDF is

$$f_{w|\lambda}(k|\lambda) = \frac{1}{\sqrt{2\pi\lambda T_s g^2 F}\left(1+\dfrac{k-g\lambda T_s}{\lambda T_s g F/(F-1)}\right)^{3/2}} \cdot \exp\left[-\frac{(k-g\lambda T_s)^2}{2\lambda T_s g^2 F\left(1+\dfrac{k-g\lambda T_s}{\lambda T_s g F/(F-1)}\right)}\right], \tag{5-25}$$

where g is the mean photomultiplication gain, $F = \gamma g + (2-1/g)(1-\gamma)$ is the excess noise factor and γ is the ionization coefficient. The conditional CF for the Webb distribution is [**45**]

$$\phi_{w|I_s}(\omega|I_s) = \exp\left\{\frac{(I_s k_s + k_b)F}{(F-1)^2}\left[1-\sqrt{1-2(F-1)gj\omega}\right] - \frac{(I_s k_s + k_b)g}{F-1}j\omega\right\} \tag{5-26}$$

and the unconditional Webb CF is found by averaging over the gamma-gamma PDF as

$$\phi_w(\omega) = E\left[\phi_{w|I_s}(\omega|I_s)\right]. \tag{5-27}$$

5.3.2. Probability of Miss. In order to find the probability of miss, the CF of a single symbol integration must first be found. In the following development, the CF for the photoelectron count will be represented by $\phi_k(\omega)$ which will be equal to (5-19) for a p-i-n and (5-27) for an APD. Since the photoelectron count and thermal noise AWGN are independent, the single symbol CF is

$$\phi_s(\omega) = \phi_k(\omega)\phi_n(\omega), \tag{5-28}$$

where $\phi_n(\omega) = \exp(-\sigma_n^2\omega^2/2)$ is the zero-mean Gaussian CF. In order to compute the CF of the sum in (5-12), the assumption that each symbol integration is independent and identically distributed (IID) is used so that the sum CF is

$$\phi_v(\omega) = \left[\phi_k(\omega)\phi_n(\omega)\right]^{L'}. \tag{5-29}$$

Finally, (5-29) is inserted into the following inversion formula [**50**] to calculate the CDF:

$$P_M(v_T) = \frac{1}{2} + \frac{1}{\pi}\int_0^\infty \frac{\sin(\omega v_T)\mathrm{Re}\left\{\phi_v^{s+n}(\omega)\right\}}{\omega} - \frac{\cos(\omega v_T)\mathrm{Im}\left\{\phi_v^{s+n}(\omega)\right\}}{\omega} d\omega, \quad (5\text{-}30)$$

where $\mathrm{Re}\{\cdot\}$ and $\mathrm{Im}\{\cdot\}$ refer to the real and imaginary part of the argument, respectively.

5.3.3. Probability of False Alarm. In the event of a false alarm, no signal is present in the correlator and the photoelectron count CF is

$$\phi_k^n(\omega) = \phi_k(\omega; k_s = 0), \quad (5\text{-}31)$$

where the superscript n indicates that the count is only due to background noise. Inserting the sum CF given by

$$\phi_v^n(\omega) = \left[\phi_k^n(\omega)\phi_n(\omega)\right]^{L'} \quad (5\text{-}32)$$

into

$$P_F(v_T) = \frac{1}{2} - \frac{1}{\pi}\int_0^\infty \frac{\sin(\omega v_T)\mathrm{Re}\left\{\phi_v^{n}(\omega)\right\}}{\omega} - \frac{\cos(\omega v_T)\mathrm{Im}\left\{\phi_v^{n}(\omega)\right\}}{\omega} d\omega, \quad (5\text{-}33)$$

gives the probability of false alarm.

When the background noise is high, Gaussian approximations [**8**] can be used for photoelectron count in a p-i-n and APD resulting in simpler formulas for the probability of false alarm. The p-i-n formula is

$$P_F(v_T) = \frac{1}{2}\left[1 - \mathrm{erf}\left(\frac{v_T - eL'k_b}{\sqrt{2L'\left(\sigma_n^2 + e^2 k_b\right)}}\right)\right] \quad (5\text{-}34)$$

and the APD formula is

$$P_F(v_T) = \frac{1}{2}\left[1 - \mathrm{erf}\left(\frac{v_T - eL'gk_b}{\sqrt{2L'\left(\sigma_n^2 + e^2 F g k_b\right)}}\right)\right], \quad (5\text{-}35)$$

Table 5.1: OWC Link Parameters

Tx output power	1 mW
wavelength	850 nm
beam divergence	2 mrad
Rx FOV	2 mrad
bit rate	10 kb/s
Rx temperature	295 K
load resistance	50 Ω
spectral radiance	10^{-3} W/cm^2-μm-sr
background radiation BW	0.030 μm
aperture diameter	10 cm
quantum efficiency	0.1

where

$$\text{erf}(x) = \frac{2}{\sqrt{\pi}} \int_0^x e^{-t^2} dt \tag{5-36}$$

is the error function. The Gaussian approximations could also be used when calculating the probability of miss when the signal count is high, but this would not make the computation any simpler because the signal counts must be averaged over the PDF of the fading.

5.4. Examples

In this section, the probabilities of miss and false alarm are calculated and presented for various situations using the methods of the previous section. The parameters in Table 5.1 are held constant and the turbulence strength, path length and signal length are varied. In all situations, just for illustrative purposes, it is assumed that the probability of false alarm is set at 10^{-7} and it is required that the probability of miss be at least as good. Beam energy loss due to absorption and scattering (extinction coefficient) is not included in these calculations.

5.4.1. OWC Link with Varying Path Length. In the case where an optical link is established between a vehicle equipped with an optical wireless transceiver and

another vehicle or an immobile ground station, the link must maintain communications as the path length varies causing the scintillation strength to vary according to (5-5). For the following calculations, it is assumed that the transmission power is limited to 1 mW so that the probability of miss increases as path length increases not only because of the increasing scintillation strength, but also because less of the laser beam energy is captured by the receiver, lowering the SNR.

Figs. 5.1 and 5.2 depict the probability of miss for a p-i-n receiver operating in moderate and strong atmospheric turbulence characterized by $C_n^2 = 10^{-15}$ and 10^{-13}, respectively. The signal has Hamming weight $L' = 16$. Also plotted in these and all remaining figures is the probability of false alarm, which is the curve that always has negative slope. These two show that the goal of 10^{-7} for the probability of miss is achievable (in 0.5 km increments) up to 2.5 km for moderate turbulence and only up to 1.5 km for strong turbulence. Therefore, in the case of strong turbulence, to extend the range, the signal length must be increased beyond 16.

Another way to improve performance, other than increasing the signal length, is to use an APD instead of a p-i-n photodiode. Due to the internal gain of an APD, it is more sensitive than the p-i-n and, accordingly, the relative probabilities of miss and false alarm are smaller. Figs. 5.3 and 5.4 represent the same situation as the previous two figures except an APD is employed instead of a p-i-n. One obvious difference between the p-i-n and APD probability of miss curves is the p-i-n curves start to flatten out as the path length increases whereas the APD curves remain vertical. This is the result of thermal noise. In the p-i-n receiver, the strong turbulence probability of miss performance starts to become limited by thermal noise at 2.5 km for $P_M = 10^{-8}$. The APD receiver, however, is not affected by thermal noise at these signal levels.

5.4.2. Fixed-Length OWC Link with Varying Turbulence Strength. A fixed-length link, such as an urban building to building link, must handle fluctuating

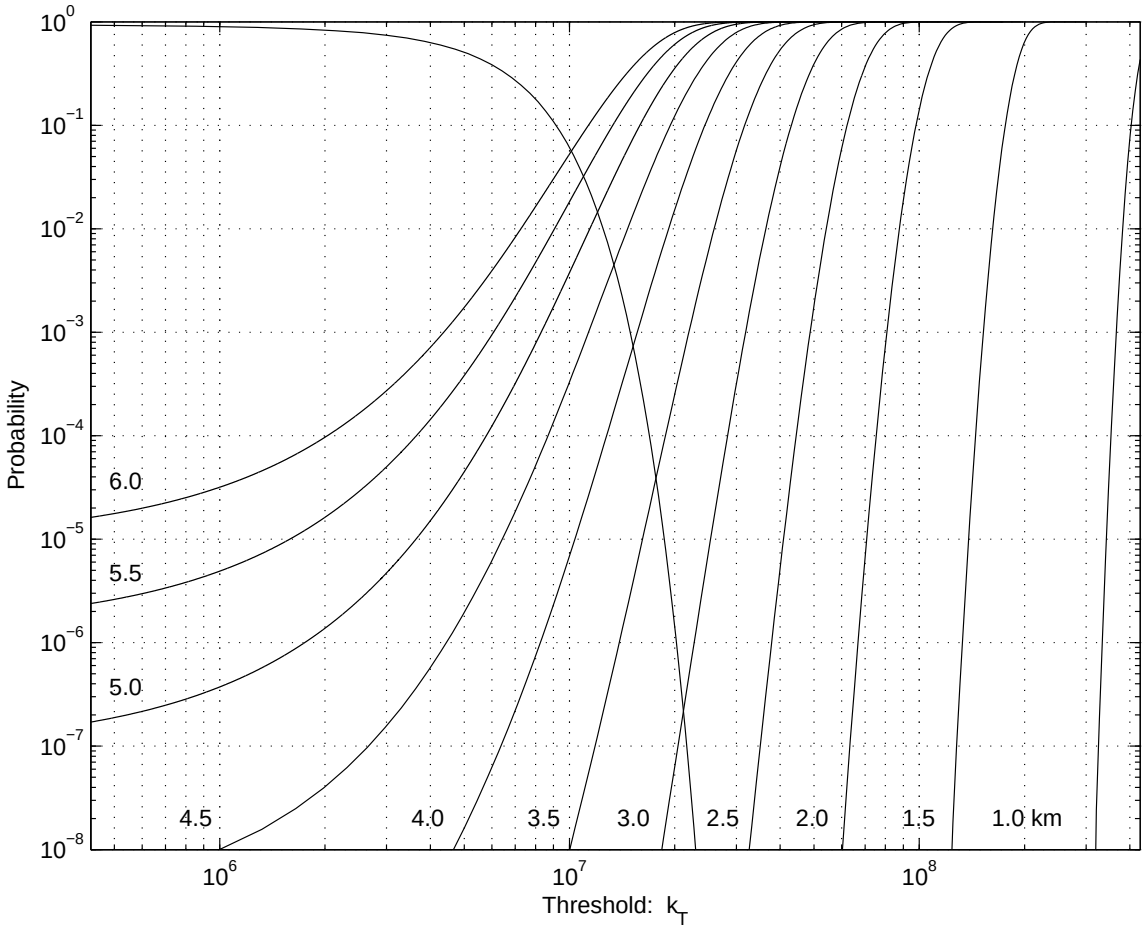

Figure 5.1: Probability of miss using using p-i-n photodiode in moderate atmospheric turbulence ($C_n^2 = 10^{-15}$). The optical transmit power is constant at $P_t = 1$ mW and the range of path lengths is 1 to 6 km.

scintillation power that results from changes in the turbulence strength caused by diurnal temperature variation. In Figs. 5.5 and 5.6, the probability of miss is plotted for path length $L_p = 2$ km, signal length $L' = 16$ and $C_n^2 \in \{10^{-15}, 10^{-14}, 10^{-13}\}$ for a p-i-n and APD receiver, respectively. The APD receiver is able to handle all levels of turbulence. The p-i-n receiver probability of miss, however, is too high at the highest level of turbulence ($C_n^2 = 10^{-13}$), and can not meet the required $P_M = 10^{-7}$.

From Fig. 5.5 it is evident that the signal length must be increased for the p-i-n receiver in order to mitigate strong turbulence. On the other hand, from Fig.

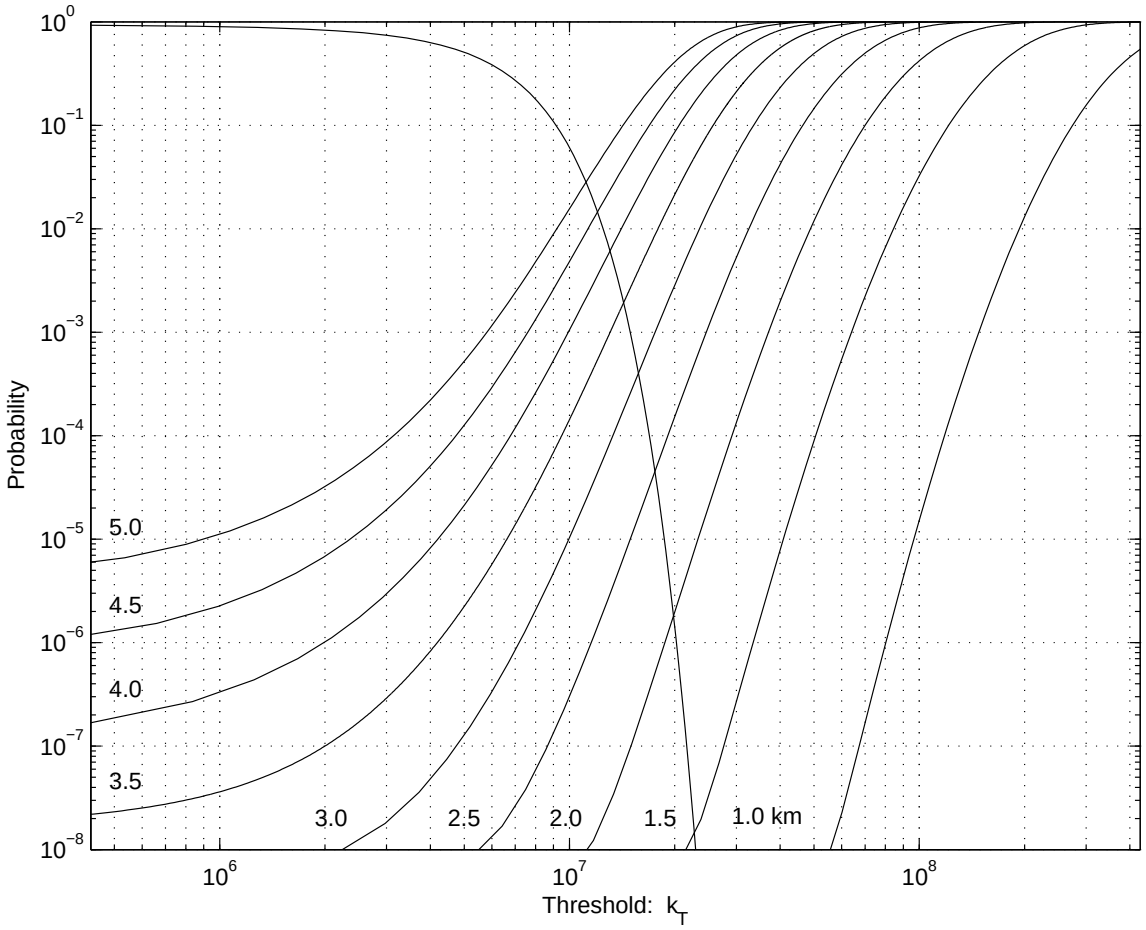

Figure 5.2: Probability of miss using using p-i-n photodiode in strong atmospheric turbulence ($C_n^2 = 10^{-13}$). The optical transmit power is constant at $P_t = 1$ mW and the range of path lengths is 1 to 5 km.

5.6 it seems it is possible to decrease the signal length and still gain the required performance. In consideration of this, the p-i-n and APD probability of miss are plotted versus the normalized threshold for five different signal lengths in Figs. 5.7 and 5.8, respectively. In this way, a signal length is determined by finding the intersection of the probability of miss and its corresponding probability of false alarm and if it's below 10^{-7}, then that signal length is sufficient. Fig. 5.7, for example, shows that the signal length $L' = 32$ is sufficient for a p-i-n receiver and Fig. 5.8 shows that $L' = 8$ is sufficient for an APD receiver.

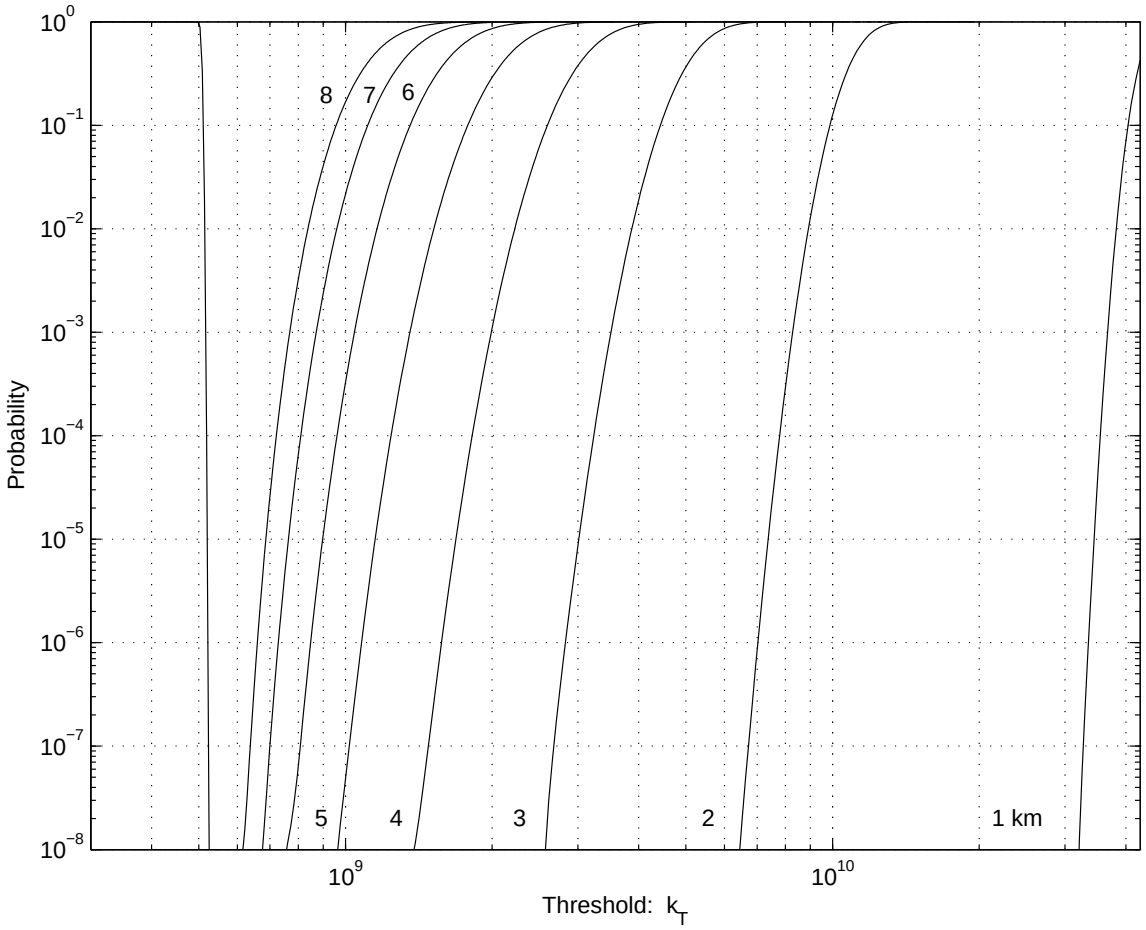

Figure 5.3: Probability of miss using using APD in moderate atmospheric turbulence ($C_n^2 = 10^{-15}$). The optical transmit power is constant at $P_t = 1$ mW and the range of path lengths is 1 to 8 km.

5.5. Concluding Remarks

Using the gamma-gamma distribution for optical signal intensity fluctuations caused by atmospheric turbulence, in this chapter it has been shown how to calculate the probability of miss for the signal detector of an optical receiver employing a p-i-n or avalanche photodiode. Since the gamma-gamma distribution is applicable to conditions representing from weak to strong turbulence, the methods used herein

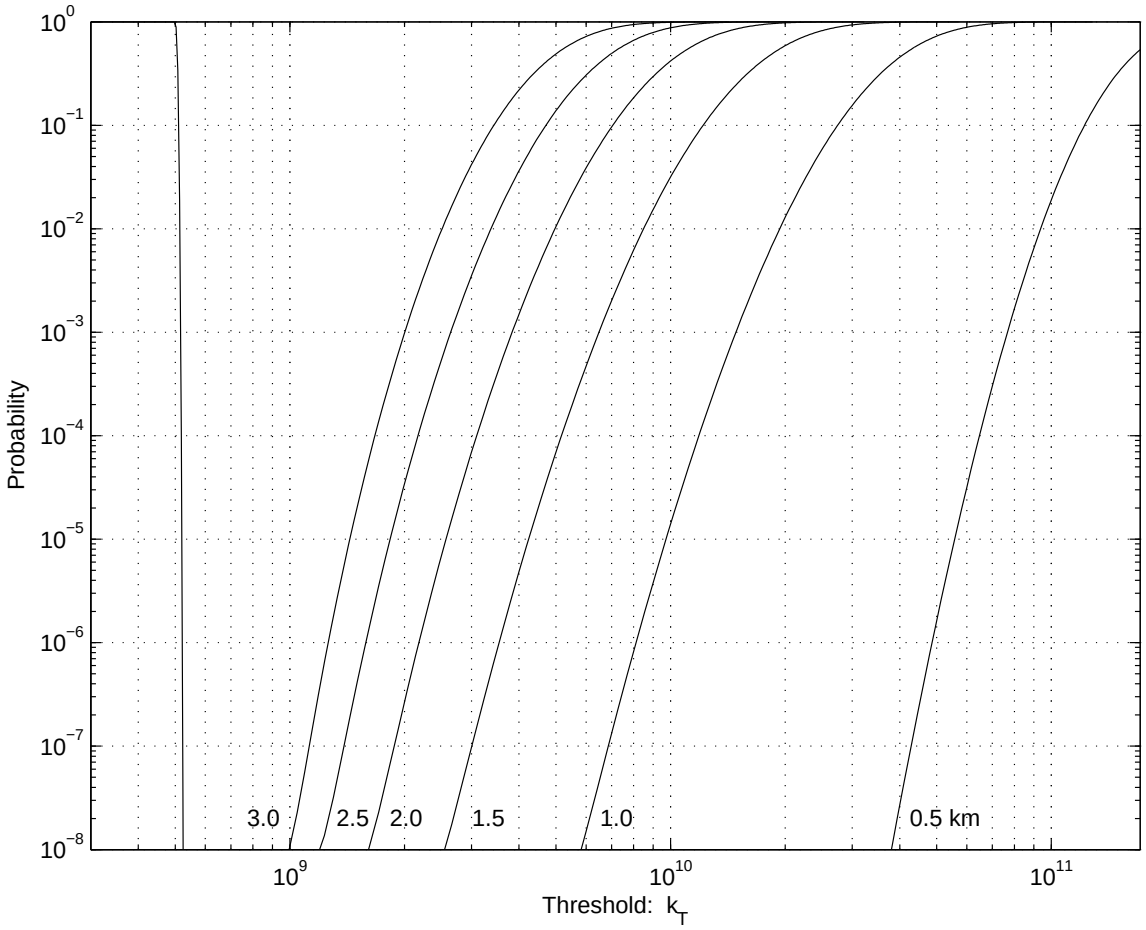

Figure 5.4: Probability of miss using using APD in strong atmospheric turbulence ($C_n^2 = 10^{-13}$). The optical transmit power is constant at $P_t = 1$ mW and the range of path lengths is 0.5 to 3 km.

are applicable to such conditions. However, since the channel was treated as memoryless and due to the relatively long temporal coherence of atmospheric turbulence, these results are valid for slow speed communications.

Upon observing Figs. 5.1-5.6, it is apparent that, as the scintillation strength increases, the greater probability of deep fades will significantly increase the probability of miss. Enough so that either the signal length or SNR must be increased to compensate for the deeper fades. For a fixed distance link, increasing the SNR

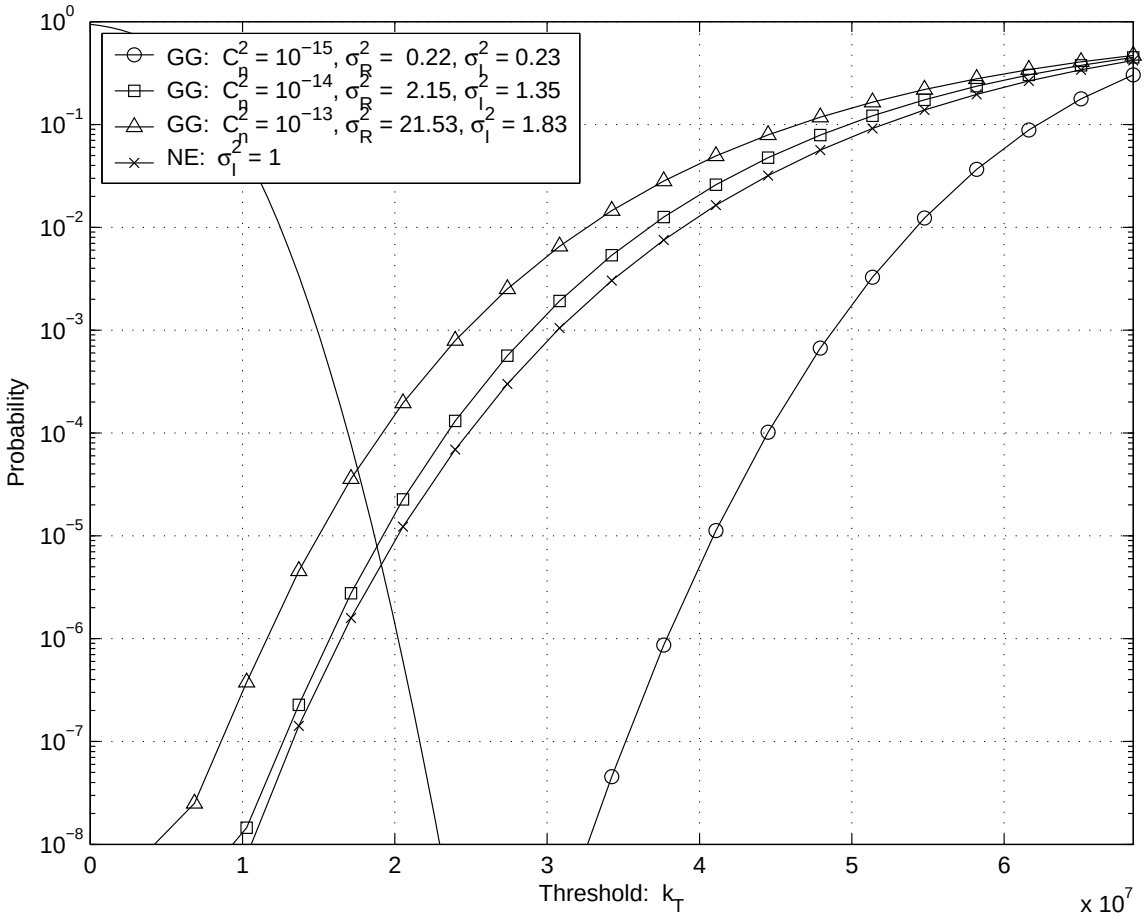

Figure 5.5: Probability of miss using using p-i-n for a constant path length $L_p = 2.5$ km and varying turbulence strength. The optical transmit power is constant at $P_t = 1$ mW.

requires increasing the transmitted power or the receiver sensitivity, which is not possible for a communications system designer using off-the-shelf transceivers. Therefore, in order to decrease the probability of miss, the signal length must be increased to an appropriate point, which can be determined using the methods described in this chapter.

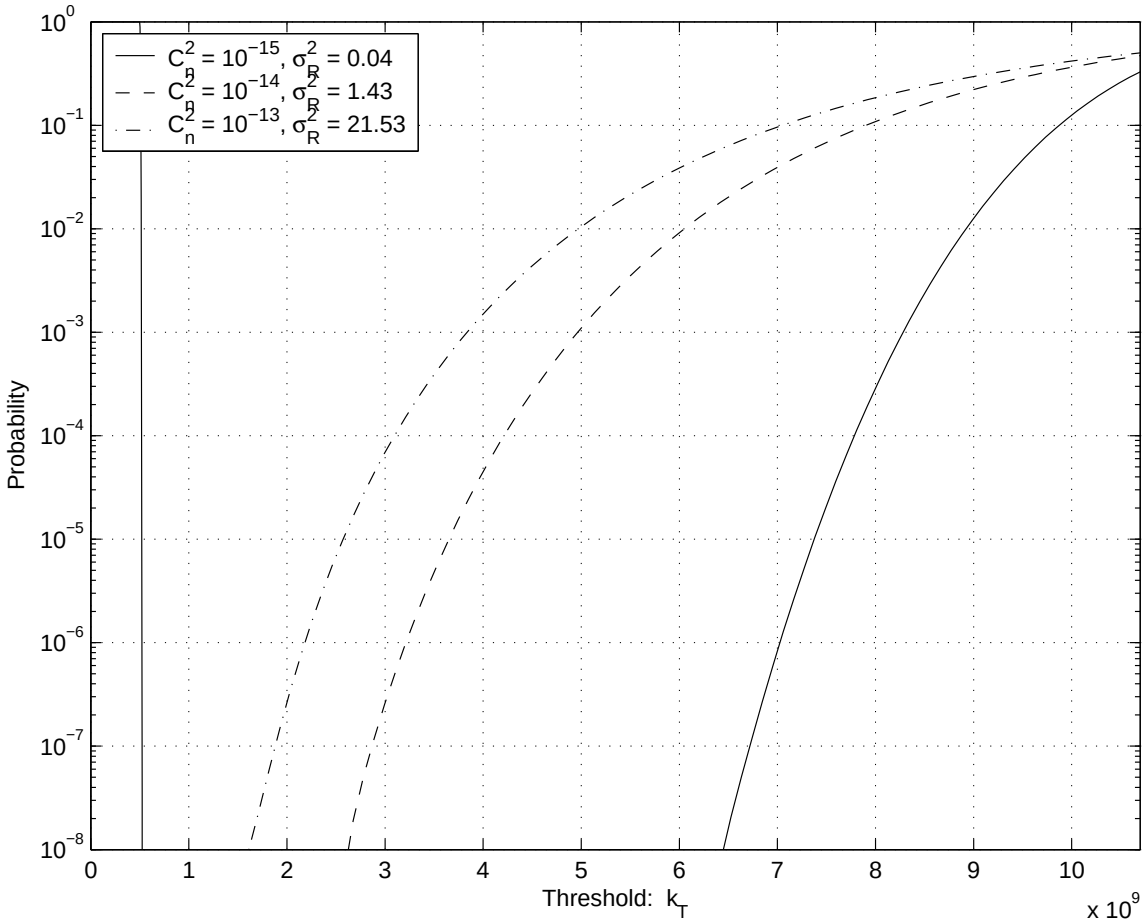

Figure 5.6: Probability of miss using using APD for a constant path length $L_p = 2$ km and varying turbulence strength. The optical transmit power is constant at $P_t = 1$ mW.

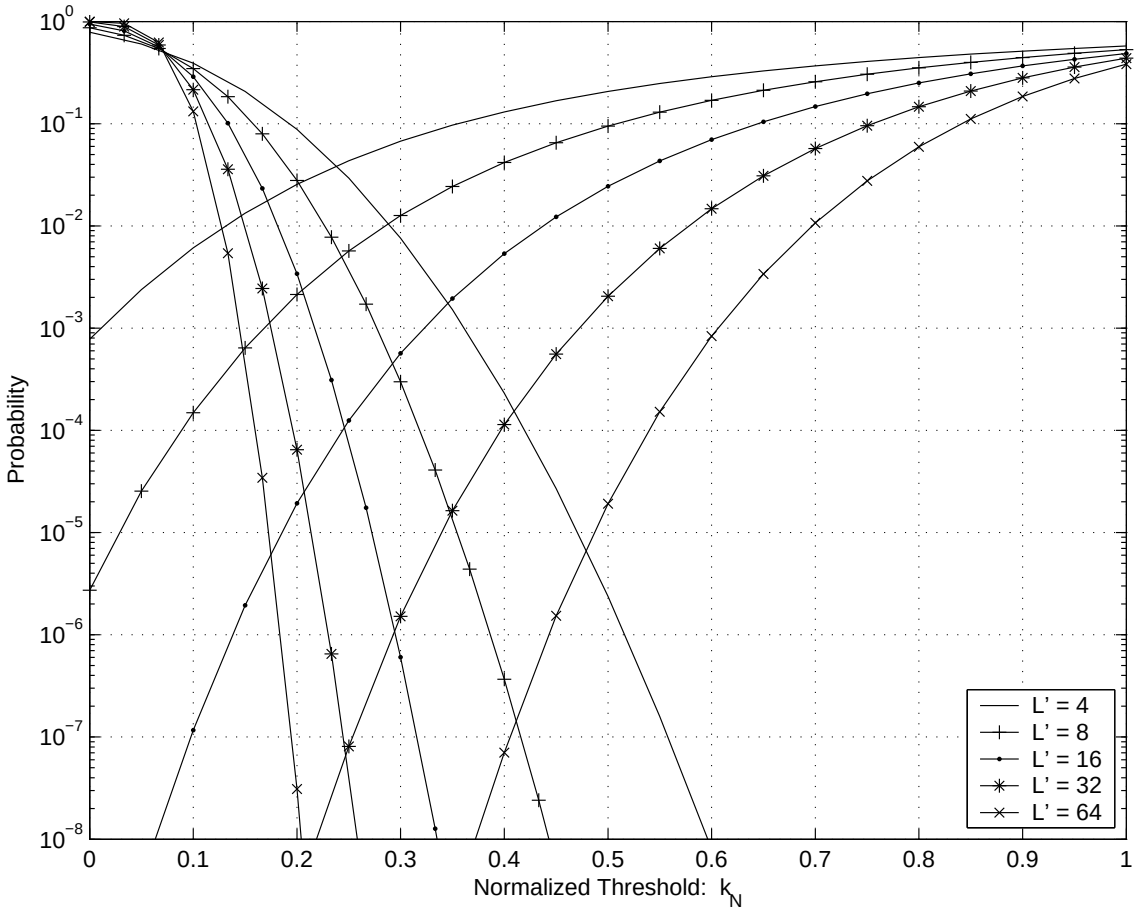

Figure 5.7: Probability of miss using using p-i-n for a constant path length $L_p = 2.5$ km, constant turbulence strength $C_n^2 = 10^{-13}$ and varying signal length. The optical transmit power is constant at $P_t = 1$ mW. In this case, $\sigma_R^2 = 21.53, \beta = 1.04, \alpha = 1.51$ and $\sigma_I^2 = 2.26$.

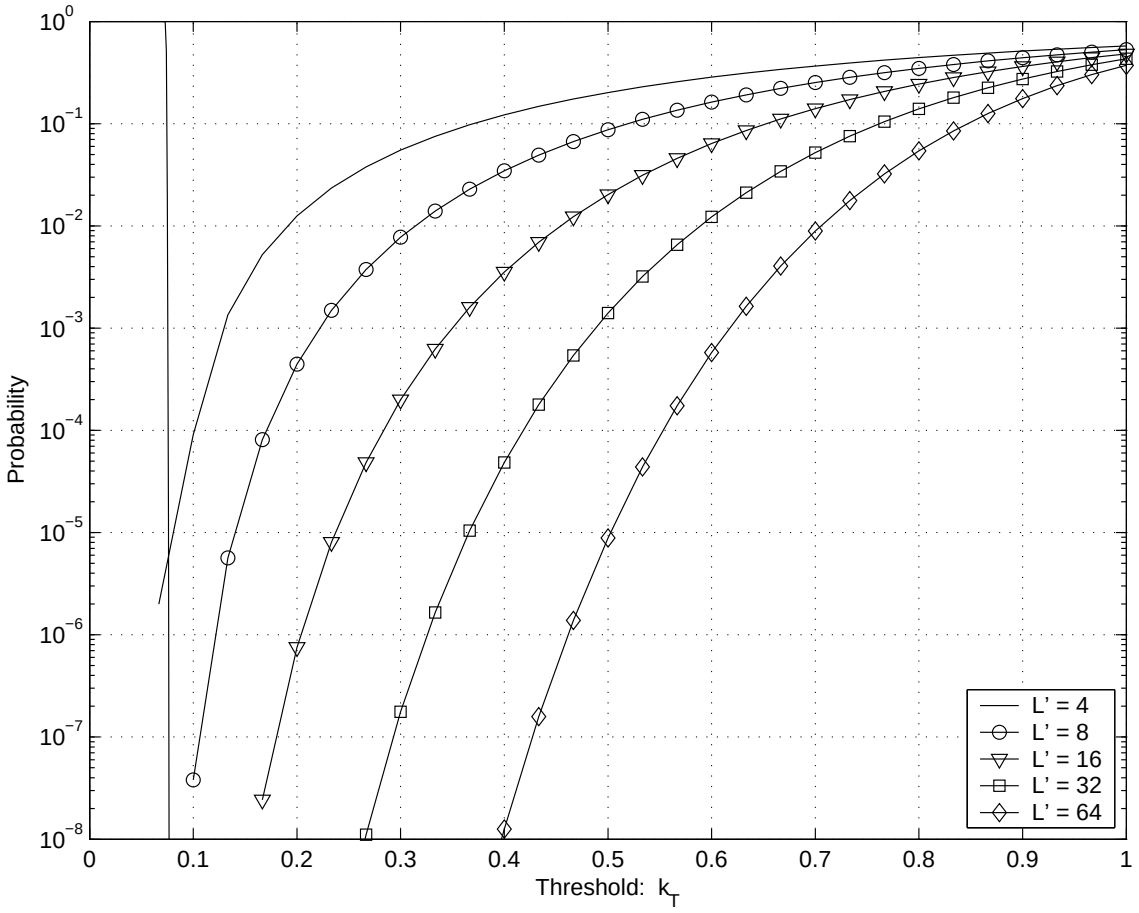

Figure 5.8: Probability of miss using using APD for a constant path length $L_p = 2.5$ km, constant turbulence strength $C_n^2 = 10^{-13}$ and varying signal length. The optical transmit power is constant at $P_t = 1$ mW. In this case, $\sigma_R^2 = 21.53, \beta = 1.04, \alpha = 1.51$ and $\sigma_I^2 = 2.26$.

Chapter 6

Conclusions

In this work, signal detection for intensity modulated, direct detection optical communications systems operating through the turbulent atmospheric channel has been studied. More specifically, using various system and channel models, the probability of miss has been theoretically derived in some cases and numerically calculated in others. Comparing the probabilities of miss and false alarm, it is then possible to determine the two signal detector parameters: signal length and detection threshold so that both the probabilities of miss and false alarm remain below a required level.

The systems were chosen to model those used in commercial and research devices, including the p-i-n and avalanche diode, and the atmospheric turbulence models used represent the whole range of scintillation strength from weak to strong to saturated. For the p-i-n and avalanche photodiodes, the photoelectron generation was modeled as Poisson and Webb stochastic process, respectively. In the range of weak turbulence, the lognormal model was employed and for saturated scintillation the exponential model. The gamma-gamma model was used to represent strong turbulence.

Future research topics in this area include: finding other, possibly more complex, signal detector structures, and determining their performance; investigating how the signal detector performance is affected if the transmitter, receiver or both are mobile and determining how to mitigate those effects; and, finally, experimentally measuring the probability of miss for an optical communication system operating through the atmosphere.

References

[1] E. Leitgeb, K. Zettl, S. S. Muhammad, N. Schmitt, and W. Rehm, "Investigation in free space optical communication links between unmanned aerial vehicles (UAVs)," in *ICTON '07*, Rome, Italy, Jul. 1-5 2007, pp. 152–155.

[2] G. Nykolak, P. F. Szajowski, A. Cashion, H. M. Presby, G. E. Tourgee, and J. J. Auborn, "40-gb/s DWDM free-space optical transmission link over 4.4 km," *Proc. SPIE, Free-Space Laser Communication Technologies XII*, vol. 3932, 2000.

[3] G. Lachs and M. C. Miner, "Detection statistics for laser radar in atmospheric turbulence with fluctuating targets," *IEEE Trans. Aerosp. Electron. Syst.*, vol. AES-11, no. 2, pp. 234–237, Mar. 1975.

[4] G. R. Osche, *Optical Detection Theory for Laser Applications.* Hoboken, NJ: Wiley, 2002.

[5] A. Acampora, "Last mile by laser," *Sci. Amer.*, vol. 287, pp. 48–53, Jul. 2002.

[6] R. A. Nichols and A. R. Hammons, Jr., "Performance of DTN-based free-space optical networks with mobility," in *Proc. IEEE Mil. Commun. Conf.*, Orlando, FL, Oct. 2007.

[7] Q. Liu, C. Qiao, G. Mitchell, and S. Stanton, "Optical wireless communication networks for first- and last-mile broadband access," *J. Optical Networking*, vol. 4, no. 12, pp. 807–828, Dec. 2005.

[8] R. M. Gagliardi and S. Karp, *Optical Communications.* Wiley, 1995.

[9] L. C. Andrews and R. L. Phillips, *Laser Beam Propagation through Random Media.* Bellingham, WA: SPIE, 1998.

[10] F. R. K. Chung, J. A. Salehi, and V. K. Wei, "Optical orthogonal codes: Design, analysis, and applications," *IEEE Trans. Inf. Theory*, vol. 35, no. 3, pp. 595–604, May 1989.

[11] B. Moran, "Mathematics of radar," in *Twentieth Century Harmonic Analysis - A Celebration*, J. S. Byrnes, Ed. Springer, 2001.

[12] D. L. Fried, G. E. Mevers, and M. P. Keister, Jr., "Measurements of laser-beam scintillation in the atmosphere," *J. Opt. Soc. Amer.*, vol. 57, no. 6, pp. 787–797, Jun. 1967.

[13] I. I. Kim, E. L. Woodbridge, V. J. Chan, and B. R. Strickland, "Scintillation measurements performed during the limited-visibility lasercom experiment," in *Proc. SPIE, Free-Space Laser Communication Technologies X*, G. S. Mecherle, Ed., vol. 3266, May 1998, pp. 209–220.

[14] P. H. Deitz and N. J. Wright, "Saturation of scintillation magnitude in near-earth optical propagation," *J. Opt. Soc. Amer.*, vol. 59, no. 5, pp. 527–535, May 1969.

[15] H. V. Poor, *An Introduction to Signal Detection and Estimation*. Springer, 1993.

[16] Q. Liu, *Applied Probability and Statistics in Engineering*. Pearson Education, 2004.

[17] R. L. Mitchell, "Permanence of the log-normal distribution," *J. Opt. Soc. Amer.*, vol. 58, no. 9, pp. 1267–1272, Sep. 1968.

[18] L. F. Fenton, "The sum of lognormal probability distributions in scatter transmission systems," *IRE Trans. Commun. Syst.*, vol. CS-8, pp. 57–67, Mar. 1960.

[19] S. C. Schwartz and Y. S. Yeh, "On the distribution function and moments of power sums with lognormal components," *Bell Syst. Tech. J.*, vol. 61, no. 7, pp. 1441–1462, Sep. 1982.

[20] N. C. Beaulieu, A. A. Abu-Dayya, and P. J. McLane, "Estimating the distribution of a sum of independent lognormal random variables," *IEEE Trans. Commun.*, vol. 43, no. 12, pp. 2869–2873, Dec. 1995.

[21] N. C. Beaulieu and Q. Xie, "An optimal lognormal approximation to lognormal sum distributions," *IEEE Trans. Veh. Technol.*, vol. 53, no. 2, pp. 479–489, Mar. 2004.

[22] R. Barakat, "Sums of independent lognormally distributed random variables," *J. Opt. Soc. Amer.*, vol. 66, no. 3, pp. 211–216, Mar. 1976.

[23] M. C. Jeong, J. S. Lee, S. Y. Kim, S. W. Namgung, J. H. Lee, M. Y. Cho, S. W. Huh, Y. S. Ahn, J. W. Cho, and J. S. Lee, "8×10-gb/s terrestrial optical free-space transmission over 3.4 km using an optical repeater," *IEEE Photonics Technol. Lett.*, vol. 15, pp. 171–173, Jan. 2003.

[24] T. J. Wolcott, J. M. Harris, and R. B. Ertel, "Airborne free space optical communication apparatus and method with subcarrier multiplexing," U.S. Patent 7,359,639, Apr., 2008.

[25] M. Aspelmeyer, T. Jennewein, M. Pfennigbauer, W. R. Leeb, and A. Zeilinger, "Long-distance quantum communication with entangled photons using satellites," *IEEE J. Sel. Topics Quantum Electron.*, vol. 9, no. 6, pp. 1541–1551, Nov./Dec. 2003.

[26] A. A. Farid and S. Hranilovic, "Outage capacity optimization for free-space optical links with pointing errors," *IEEE/OSA J. Lightw. Technol.*, vol. 25, no. 7, pp. 1702–1710, Jul. 2007.

[27] J. W. Goodman, *Statistical Optics*. New York: Wiley, 1985.

[28] D. A. DeWolf, "Are strong irradiance fluctuations log normal or rayleigh distributed?" *J. Opt. Soc. Amer.*, vol. 59, no. 11, pp. 1455–1460, Nov. 1969.

[29] X. Zhu, J. M. Kahn, and J. Wang, "Mitigation of turbulence-induced scintillation noise in free-space optical links using temporal-domain detection techniques," *IEEE Photonics Technol. Lett.*, vol. 15, no. 4, pp. 623–625, Apr. 2003.

[30] E. Jakeman and P. N. Pusey, "A model for non-rayleigh sea echo," *IEEE Trans. Antennas Propag.*, vol. AP-24, no. 6, pp. 806–814, Nov. 1976.

[31] L. C. Andrews, R. L. Phillips, C. Y. Hopen, and M. A. Al-Habash, "Theory of optical scintillation," *J. Opt. Soc. Amer. A*, vol. 16, no. 6, pp. 1417–1429, Jun. 1999.

[32] E. Jakeman and P. N. Pusey, "Significance of K distributions in scattering experiments," *Phys. Rev. Lett.*, vol. 40, no. 9, pp. 546–550, Feb. 1978.

[33] T. Kamalakis, T. Sphicopoulos, S. S. Muhammad, and E. Leitgeb, "Estimation of the power scintillation probability density function in free-space optical links by use of multicanonical Monte Carlo sampling," *Opt. Lett.*, vol. 31, no. 21, pp. 3077–3079, Nov. 2006.

[34] J. Q. Liu, J. Li, and G. S. Mitchell, "Packet detection in on-board switching broadband satellite IP networks," in *Proc. IEEE Mil. Commun. Conf.*, Washington, D. C., Oct. 23-25 2006.

[35] J. C. Brandenburg, J. Q. Liu, and M. P. Polis, "Effect of atmospheric turbulence on packet detection in optical communications," in *Proc. IEEE Mil. Commun. Conf.*, Orlando, FL, Oct. 2007.

[36] J. C. Brandenburg and J. Q. Liu, "Signal detection in optical communications through the atmospheric turbulence channel," in *Proc. IEEE Global Commun. Conf.*, New Orleans, LA, Dec. 2008.

[37] W. Feller, *An Introduction to Probability Theory and Its Applications*, 3rd ed. Wiley, 1968, vol. I.

[38] S. M. Ross, *Introduction to Probability Models*. Elsevier, 2007.

[39] S. Das, H. Henniger, B. Epple, C. I. Moore, W. Rabinovich, R. Sova, and D. Young, "Requirements and challenges for tactical free-space lasercomm," in *Proc. IEEE Military Commun. Conf.*, San Diego, CA, Nov. 16-19 2008.

[40] X. Sun, F. M. Davidson, L. Boutsikaris, and J. B. Abshire, "Receiver characteristics of laser altimeters with avalanche photodiodes," *IEEE Trans. Aerosp. Electron. Syst.*, vol. 28, no. 1, pp. 268–275, 1992.

[41] J. C. Brandenburg and J. Q. Liu, "Signal detection for optical communications through the turbulent atmosphere," *IEEE Trans. Commun.*, vol. 57, pp. 3425–3432, Nov. 2009.

[42] ——, "Optical signal detection in the turbulent atmosphere using p-i-n photodiodes," *IEEE J. Sel. Areas Commun.*, vol. 27, pp. 1564–1571, Dec. 2009.

[43] R. J. McIntyre, "The distribution of gains in uniformly multiplying avalanche photodiodes: Theory," *IEEE Trans. Electron Devices*, vol. ED-19, no. 6, pp. 703–713, Jun. 1972.

[44] J. Conradi, "The distribution of gains in uniformly multiplying avalanche photodiodes: Experimental," *IEEE Trans. Electron Devices*, vol. ED-19, no. 6, pp. 713–718, Jun. 1972.

[45] J. T. K. Tang and K. Ben Letaief, "The use of WMC distribution for performance evaluation of APD optical communication systems," *IEEE Trans. Commun.*, vol. 46, no. 2, pp. 279–285, Feb. 1998.

[46] P. P. Webb, R. J. McIntyre, and J. Conradi, "Properties of avalanche photodiodes," *RCA Review*, vol. 35, pp. 234–278, Jun. 1974.

[47] N. Sorenson and R. Gagliardi, "Performance of optical receivers with avalanche photodetection," *IEEE Trans. Commun.*, vol. COM-27, no. 9, pp. 1315–1321, Sep. 1979.

[48] K. R. Baker, "On the WMC density as an inverse gaussian probability density," *IEEE Trans. Commun.*, vol. 44, no. 1, pp. 15–17, Jan. 1996.

[49] M. C. K. Tweedie, "Statistical properties of inverse gaussian distributions. I," *Ann. Math. Statist.*, vol. 28, no. 2, pp. 362–377, 1957.

[50] A. H. Nuttall, "Numerical evaluation of cumulative probability distribution functions directly from characteristic functions," *Proc. IEEE*, vol. 57, no. 11, pp. 2071–2072, Nov. 1969.

[51] L. C. Andrews, R. L. Phillips, and C. Y. Hopen, *Laser Beam Scintillation with Applications*. SPIE, 2001.

[52] M. A. Al-Habash, L. C. Andrews, and R. L. Phillips, "Mathematical model for the irradiance probability density function of a laser beam propagating through turbulent media," *Opt. Eng.*, vol. 40, no. 8, pp. 1554–1562, Aug. 2001.

[53] M. Uysal, J. Li, and M. Yu, "Error rate performance analysis of coded free-space optical links over gamma-gamma atmospheric turbulence channels," *IEEE Trans. Wireless Commun.*, vol. 5, no. 6, pp. 1229–1233, Jun. 2006.

[54] W. Gappmair and S. S. Muhammad, "Error performance of PPM/Poisson channels in turbulent atmosphere with gamma-gamma distirbution," *Electron. Lett.*, vol. 43, no. 16, Aug. 2007.

[55] M. L. B. Riediger, R. Schober, and L. Lampe, "Fast multiple-symbol detection for free-space optical communications," *IEEE Trans. Commun.*, vol. 57, pp. 1119–1128, Apr. 2009.

[56] X. Zhu and J. M. Kahn, "Free-space optical communication through atmospheric turbulence channels," *IEEE Trans. Commun.*, vol. 50, no. 8, pp. 1293–1300, Aug. 2002.

[57] I. S. Gradshteyn and I. M. Ryzhik, *Table of Integrals, Series, and Products.* London: Academic Press, 1994.

Abstract

DETECTION STATISTICS OF MULTIPLE-PULSE OPTICAL SIGNALS THROUGH ATMOSPHERIC TURBULENCE

by

JACOB C. BRANDENBURG

December 2010

Advisor: Dr. John Q. Liu

Major: Electrical Engineering

Degree: Doctor of Philosophy

Statistics are studied for signal detection in optical communication systems operating through the atmosphere. Optical communication systems with which this study is concerned are those that employ intensity modulation and direct detection. Atmospheric turbulence, which is fluctuations in the atmosphere's optical index of refraction, is a hindrance to optical wireless communications because of the signal fades, called scintillation, it causes at the optical receiver. In order to mitigate the deteriorative effect of turbulence on the communications system, the signal length and detection threshold for the signal detector must be properly chosen.

In this study, mathematical models for photoelectron generation in the receiver's photodiode and for the atmospheric turbulence channel enable the derivation or numerical calculation of the probability of miss, which is crucial for determining the signal length and detection threshold. The two commonly used types of photodiodes are the p-i-n photodiode and the avalanche photodiode. A light source of constant intensity impinging upon a photodiode will generate a photoelectron count which is a Poisson process for a p-i-n and a follows the McIntyre-Conradi distribution for an avalanche photodiode. In this study, the Webb distribution will be used as an

approximation for the McIntyre-Conradi distribution. When the light intensity is itself a random process, as is the case for the received optical intensity after traveling through atmospheric turbulence, the photoelectron count will be a doubly (or conditional) stochastic process. To model the effect atmospheric turbulence, three different probability distributions are utilized to describe the received optical intensity. These are the lognormal distribution, valid for weak turbulence, the gamma-gamma distribution, valid for a range of turbulence strengths and the exponential distribution, valid for the saturation regime of signal scintillation.

With these models, the probability of miss is derived or numerically calculated. Simulations are provided to verify derived formulae for the probability of miss. Applying results in this study, a system designer can determine appropriate signal length and detection threshold settings in order to meet system specifications for signal detection.

Autobiographical Statement

Jacob C. Brandenburg received a B.S. degree in electrical engineering from the University of Michigan, Ann Arbor in 2002 and a M.S. degree in systems engineering from Oakland University, Rochester, MI in 2007. From 2004 to 2007 he worked as a controls engineer for Automated Production Systems in Sterling Heights, MI. His current research interests are signal detection and coding for optical communications through the atmosphere and signal detection and modulation for data communications through voice channels.